HT-PEM Fuel Cell System with Integrated Thermoelectric Exhaust Heat Recovery

Gao, Xin

Publication date:
2014

Document Version
Publisher's PDF, also known as Version of record

HT-PEM Fuel Cell System with Integrated Thermoelectric Exhaust Heat Recovery

AALBORG UNIVERSITY
DENMARK

Xin Gao

Dissertation submitted to the Faculty of Engineering and Science at Aalborg University in partial fulfillment of the requirements for the degree of

DOCTOR OF PHILOSOPHY

Aalborg University
Department of Energy Technology
Aalborg, Denmark

HT-PEM Fuel Cell System with Integrated Thermoelectric Exhaust Heat Recovery

ISBN: 978-87-92846-38-9

Printed in Denmark by UniPrint

Aalborg University
Department of Energy Technology
Pontoppidanstræde 101
9220 Aalborg
Denmark

Title: HT-PEM Fuel Cell System with Integrated Thermoelectric Exhaust Heat Recovery

PhD student: Xin Gao

Supervisor: Søren Knudsen Kær, Professor

Co-supervisor: Søren Juhl Andreasen, Associate Professor

List of Publications:

Paper 1: Gao, Xin; Chen, Min; Andreasen, Søren Juhl; Kær, Søren Knudsen: "Potential Usage of Thermoelectric Devices in a High-Temperature Polymer Electrolyte Membrane (PEM) Fuel Cell System: Two Case Studies". In *Journal of Electronic Materials*, 41(6), 2012, p. 1838-1844.

Paper 2: Gao, Xin; Andreasen, Søren Juhl; Chen, Min; Kær, Søren Knudsen: "Numerical Model of a Thermoelectric Generator with Compact Plate-Fin Heat Exchanger for High Temperature PEM Fuel Cell Exhaust Heat Recovery". In *International Journal of Hydrogen Energy*, 37(10), 2012, p. 8490-8498.

Paper 3: Gao, Xin; Andreasen, Søren Juhl; Kær, Søren Knudsen; Rosendahl, Lasse Aistrup: "Optimization of a Thermoelectric Generator Subsystem for High Temperature PEM Fuel Cell Exhaust Heat Recovery". In *International Journal of Hydrogen Energy*, 2014; Doi: 10.1016/j.ijhydene.2014.01.193.

Paper 4: Gao, Xin; Andreasen, Søren Juhl; Kær, Søren Knudsen; Rosendahl, Lasse Aistrup; Kolaei, Alireza Rezania: "Heat Exchanger Selection and Optimization of a Thermoelectric Generator Subsystem for HT-PEM Fuel Cell Exhaust Heat Recovery". Under review by *International Conference on Thermoelectrics*, July 2014.

Paper 5: Gao, Xin; Chen, Min; Snyder, G. Jeffrey; Andreasen, Søren Juhl; Kær, Søren Knudsen: "Thermal Management Optimization of a Thermoelectric-Integrated Methanol Evaporator Using a Compact CFD Modeling Approach". In *Journal of Electronic Materials*, 42(7), 2013, p. 2035-2042.

This present report combined with the above listed scientific papers has been submitted for assessment in partial fulfilment of the PhD degree. The scientific

papers are not included in this version due to copyright issues. Detailed publication information is provided above and the interested reader is referred to the original published papers. As part of the assessment, co-author statements have been made available to the assessment committee and are also available at the Faculty of Engineering and Science, Aalborg University.

Abstract

This thesis presents two case studies on improving the efficiency and the load-following capability of a high temperature polymer electrolyte membrane (HT-PEM) fuel cell system by the application of thermoelectric (TE) devices.

TE generators (TEGs) are harnessed to recover the system exhaust gas for electricity. For this aim, a heat exchanger based TEG heat recovery subsystem is designed. Instead of optimizing an ordinary rectangular heat exchanger, high efficient and commercialized compact plate-fin exchangers are applied. A library of types of them is also included to pinpoint the ideal heat exchanger type. Commercially available TEG modules are chosen for the subsystem.

To optimize the subsystem design, a numerical model was then built and validated. It is a model of several novel elements from the literature. To suit the desires of the subsystem design and operation studies, model precision, versatility and computational load are emphasized. Sensitivity analysis is introduced to master the characteristics of the subsystem and its major parameters for both design and operating considerations. The effects of a power conditioning method, such as Maximum Power Point Tracking (MPPT), of the subsystem power output on the subsystem design and performance were also systematically analyzed.

The TEG subsystem configuration is optimized. The usefulness and convenience of the model are proved.

TE coolers (TECs) are integrated into the methanol evaporator of the HT-PEM system for improving the whole system load-following capability. System efficiency can also be increased by reducing heat loss. Working modes of the integrated TEC modules are various and unique. They are redefined as TE heat flux regulators (TERs). The feasibility and merits of the TE-integrated evaporator are also identified by an own developed three-dimensional numerical model in ANSYS Fluent®.

This thesis introduces the progress of this project in a cognitive order. The first chapter initially prepares the theory and characteristics of the fuel cell system and TE devices. Project motivations are conceived. Then similar studies existing in literature are reviewed for their experiences. Afterwards, the project road map is identified by a list of project objectives. The detailed considerations and steps during carrying out the project are addressed in the second chapter. Major innovations out of this project are also highlighted. The third chapter presents the main results and discussions. Conclusions and future work are discussed in the last chapter.

Dansk Resumé

I denne afhandling præsenteres to studier, hvis formål det har været at forbedre effektiviteten og den dynamiske last-respons af et højtemperatur-polymer-elektrolyt-membran-brændselscelle-system (HT-PEM-system) ved hjælp af termoelektriskeenheder (TE-enheder).

Termoelektriskegeneratorer (TEG) kan blive brugt til at genvinde en del af den uudnyttede termiske energi i udstødningsgasser ved at omdanne denne til elektricitet. Til dette formål er der i dette projekt blevet designet et TEG-varmegenvindingsdelsystem baseret på en varmeveksler. I stedet for at optimere en ordinær rektangulær varmeveksler benyttes højeffektive og kommercielt tilgængelige kompaktpladevarmevekslere. Til at fastlægge den ideelle varmeveksler er et bibliotek af forskellige typer blevet benyttet i optimeringen af systemet.

Til at optimere delsystemets design er en numerisk model blevet opbygget og valideret. Modelen kombinerer forskellige nye elementer fra litteraturen. For at imødekomme delsystemets behov samt dem der er forbundet med driftsstudierne, er modelpræcisionen, alsidigheden og beregningsbelastningen blevet understreget. En sensitivitetsanalyse introduceres, som et værktøj til at klarlægge delsystemets karakteristik og dets primære design- og driftsparameter. Ligeledes analyseres systematisk koblingen mellem anvendelsen af effektomformningsmetode på delsystemet, så som Maximum Power Point Tracking (MPPT), og delsystemets design og drift.

Et optimalt TEG-delsystemskonfiguration bestemmes og modelens anvendelighed samt belejlighed bevises.

Termoelektriskekølere (TEK) er blevet integreret i HT-PEM-systemets metanolfordamper for at forbedre hele systemets dynamiske last-respons. Systemeffektiviteten kan også forhøjes ved at mindske varmetabene. De integrerede TEK-modulers driftsmønstre er forskellige og unikke. Styrkerne

ved den integrerede TE-fordamper er også blevet identificeret af en egenudviklet tredimensionel numerisk model i ANSYS Fluent.

Denne afhandling er opbygget således at den reflekterer den naturlige udviklingsproces hvorved projektet er forløbet. Det første kapitel beskriver indledningsvis teorien og den karakteristiske opførelse af brændselscellesystemet samt TE-enheder. Projektmotivationen beskrives i forlængelse heraf. Dernæst evalueres lignende studier i litteraturen med henblik på deres erfaringer, og en arbejdsplan for projektet identificeres igennem projektformål. I det andet kapitel bliver de detaljerede overvejelser, der blev gjort under projektforløbet, taget fat på. Disse omfatter de mest betydningsfulde innovationer. I tredje kapitel præsenteres og diskuteres hovedresultaterne. Endeligt afsluttes afhandlingen med en konklusion og perspektivering.

Acknowledgements

This thesis is submitted to The Faculty of Engineering and Science at Aalborg University, Denmark in partial fulfilment of the requirements of the PhD degree. The financial support from Aalborg University and China Scholarship Council is gratefully acknowledged.

Pursuing a PhD degree is no easy a journey. I am profoundly indebted to many people. Without you all, I just could not make it.

First and foremost, I offer my deepest gratitude to my supervisors, Professors Søren Knudsen Kær and Søren Juhl Andreasen: thank you for your understanding, patient guidance and encouragement; for the relaxing atmosphere during every discussion, the freedom given to carry out the project in my way, and the care taken not only for my work, but also for my feelings. I would also like to express my appreciation to Chungen Yin, Lasse Aistrup Rosendahl, Min Chen, Mads Pagh Nielsen, Kaiyuan Lu, Thomas Condra and Torsten Berning, for your valuable suggestions, kind help and time. You all, images of experienced researchers, are also invaluable examples to me.

Further, special thanks to my dear officemates, Alexandros Arsalis, Anders Christian Olesen, Vincenzo Liso, Jakob Rabjerg Vang, Haftor Örn Sigurdsson and Samuel Simon Araya, for selflessly helping me out whenever I was in need, your patience in improving my English, and so many fruitful and joyful discussions in the office. Your support is deeply appreciated! Thanks also go to John Kim Pedersen, all the secretaries and the rest people who have ever helped me in the Department of Energy Technology. Thank you all for providing such a smooth organization and such a friendly atmosphere.

Lastly, I am indebted to my parents, my brother and sisters, and my wife, for your unconditional love, encouragement, trust in me, bracing me from

whatever trouble and reminding me the meaning of life. Really nice to have you in my life.

Xin Gao
Aalborg, Denmark
March 2014

Thesis Outline

Guide to the Reader

This dissertation is prepared as a collection of scientific papers produced during my PhD period, which are composed of responses to the project objectives set at the beginning of the research work. Accordingly the thesis is primarily made up of 4 chapters, which are divided as follows:

Chapter 1 states the motivations of this project in the large background of the global energy concerns. It then describes the generalities of the main components investigated on, HT-PEM fuel cells and thermoelectric (TE) devices. After that, it summarizes representative studies in literature for experiences on TE applications and detailed design and operating concerns. During the literature review, the project objectives are gradually formulated and presented at the end of this chapter.

Chapter 2 shows the methodology for the work. Simulation is decided as the main research approach. Considerations on the architecture of the TEG subsystem are initially given herein. This chapter then notes the processes of modeling the fuel cell stack and the model development of the TEG subsystem. It also explains the analytical procedure, namely the sensitivity analysis. Ideas on modifying the design of the methanol evaporator are presented lastly.

Chapter 3 summarizes the main contributions of this project in relation to the available literature and the objectives of the project. For easy reading, the results are separated into two sections, which are distinguished by the working modes of TE modules.

Chapter 4 concludes the dissertation by giving the final remarks. Facing the limitations of the work, possible plans for future work are addressed.

Contents

List of Figures

List of Tables

Abbreviations

Acronyms	
AFC	Alkaline Fuel Cell
BoP	Balance of Plant
CCD	Charge-coupled device
CHP	Combined heat and power
CO	Carbon monoxide
COP	Coefficient of performance
CPL	Capillary pump loop
CV	Voltage-current
DMFC	Direct Methanol Fuel Cell
EES	Engineering equation solver
EGR	Exhaust gas recirculation
EIS	Electrochemical impedance spectroscopy
ESC	Extremum seeking control
GDL	Gas diffusion layer
GHG	Greenhouse gas
HFC	Hydro-fluorocarbon
HT-PEM	High temperature polymer electrolyte membrane
HVAC	Automotive heating, ventilation, and air-conditioning
ICEs	Internal combustion engines
LT-PEM	Low temperature PEM
MD	Methanol decomposition
MEA	Membrane Electrode Assembly
MPPT	Maximum Power Point Tracking
NOx	Nitric oxides
PAFC	Phosphoric Acid Fuel Cell
PBI	Polybenzimidazole
PEMFC	Polymer Electrolyte Membrane Fuel Cell
PM2.5	Soot particles less than 2.5 micrometers in diameter

PTFE	Polytetrafluoroethylene
P&O	Perturb and observe
SLCPs	Short-lived climate pollutants
SOFC	Solid Oxide Fuel Cell
SOx	Sulfur oxides
SMR	Steam methanol reformer
SR	Steam reforming
TE	Thermoelectric
TEC	Thermoelectric cooler
TEG	Thermoelectric generator
TER	Thermoelectric heat flux regulator
WGS	Water-gas shift
zT	Figure of merit of TE materials
ZT	Figure of merit of thermoelectric devices

1 Introduction

This chapter explains the motivations of this project and introduces the features of the main components investigated on. A literature review is then presented. Afterwards, the detailed project objectives and the supposed outcomes are conceived in the end of this chapter.

1.1 Project Motivations

Environmental deterioration and resource depletion are urging our whole human race to adopt a more environmentally friendly and sustainable lifestyle. Safety of energy supply concern further strengthens the eagerness. The key step here is finding cleaner and more efficient energy conversion technologies and renewable energy sources. Furthermore ensuring their successful market penetration is another vital factor. Among all possible novel solutions, high temperature polymer electrolyte membrane (HT-PEM) fuel cells and methanol seem a promising combination for approaching some of these challenges. HT-PEM fuel cell systems with on-board methanol steam reformers are clean, efficient, and compact-design. Methanol can be abounding from various renewable sources and is rather seamless with today's fossil fuel infrastructure. Harnessing all the above advantages makes these fuel cell systems an outstanding candidate, e.g., in the transport sector.

In a HT-PEM fuel cell system with on-board methanol steam reformer, every 1kW power output is accompanied by approximately 1kW exhaust heat [1], which is usually discharged unused. These systems need rechargeable lithium battery packs to supplement the parasitic losses under some occasions, such as system cold start. Recovering the exhaust heat for electricity to lower the battery power demand as well as boost the system efficiency is the first project motivation. Considering the magnitude and quality of the exhaust heat, thermoelectric generators (TEGs) are probably superb in this application. The other motivation is originated from the inherent agility of another system

component, the methanol evaporator, to fluctuations in operating parameters. Some designs can affect the system load-following capability significantly. Thermoelectric coolers (TECs) can be used as miniature heat regulators, moving heat back and forth swiftly under control. Hopefully, integrating them into the current chosen evaporator and driving them to regulate the inner heat flux can enhance the evaporator's controllability and the system dynamic performance. This project analyzes these two topics.

1.2 Background

1.2.1 Global Fossil Fuel Concerns

Global environmental pollution and climate change are already an undeniable presence. Behind these, the burning of fossil fuels, i.e., liquid fuels, natural gas and coal, is a major source. Combustion flue gas contains various hazardous pollutants, such as carbon monoxide (CO), sulfur oxides (SOx), and nitric oxides (NOx). Combustion yielded carbon dioxide takes the primary part of the world greenhouse gas (GHG) emissions and causes global warming. Incomplete combustion emits black carbon (soot). In recent years, the adverse health and environmental impacts of soot particles less than 2.5 micrometers in diameter (PM2.5) start drawing particular concern. It is estimated by the World Health Organization that annually over 1 million premature deaths are caused from exposure to outdoor fine particulate air pollution in urban areas [2]. Also after carbon dioxide, black carbon has the second strongest contribution to global warming [3], which is particularly evident in the Arctic. Besides black carbon, ground-level ozone (tropospheric ozone), methane and some hydro-fluorocarbons (HFCs) have similar short period environmental impacts. They are together labeled as the short-lived climate pollutants (SLCPs). Fast and sustainably reducing their emissions is considered as a key for a successful near-term environmental protection [4]. Despite the environmental issues, consumption of fossil fuels is still increased steadily and is expected to remain the largest source of energy through 2040, as shown in Fig. 1.1 [5]. To maintain this trend, it is reported that we may need the equivalent of two earths by the 2030s [6]. Fossil fuel depletion is just a matter of time. Another issue of fossil fuels is their uneven reserves around the world. It triggers the regional energy security concerns and is another important stimulant for countries to explore for alternative sources.

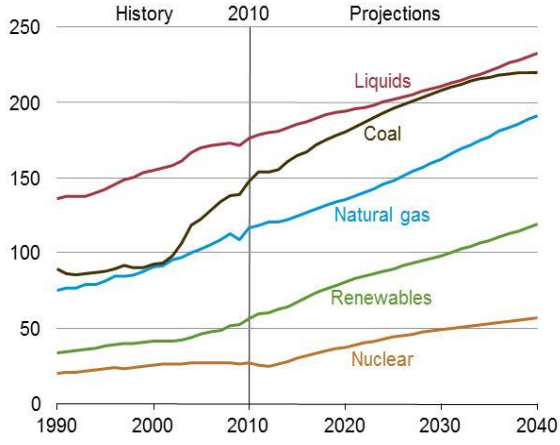

Fig. 1.1 - World energy consumption by fuel type, 1990-2040 (10^15 Btu) [5].

1.2.2 Sustainable Development

Facing the issues and concerns, the world comes to the commitment of "sustainable development". It is often defined as "development that meets the needs of the present without compromising of future generations to meet their own needs" [7]. Under this framework, alternative renewable energy sources and innovative clean energy technologies are being subject to intensive R&D. This can be roughly reflected by the global new investment in renewable energy in Fig. 1.2 [8]. Clearly, solar power and wind power dominate the investment. They are clean, ubiquitous and naturally replenished. However, large-scale use of these energies requires efficient energy concentration and storage solutions [9,10]. Herein, renewable and carbon-neutral fuels derived from these powers are prime energy carriers, such as hydrogen, methanol and octane [11,12]. To convert these fuels for electricity and heat, fuel cells are an ideal choice. They are efficient, simple, compact in design, versatile, and clean [13,14]. All in all, this combination can probably heal the world, to some extent.

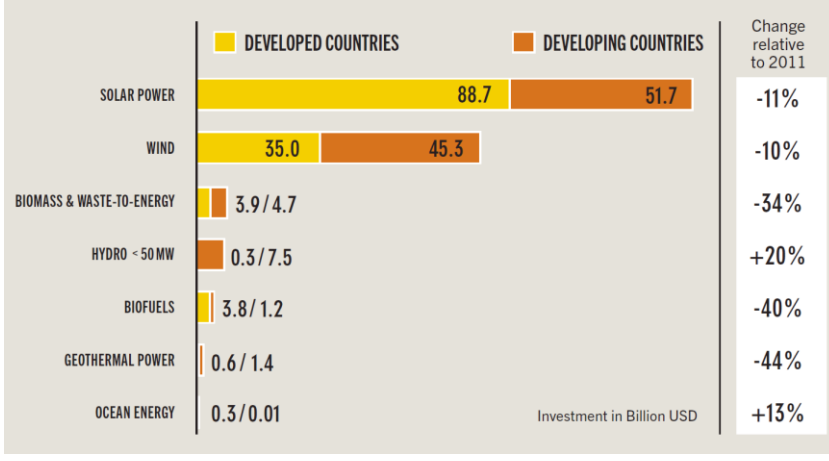

Fig. 1.2 - Global new investment in renewable energy by technology, developed and developing countries, 2012 [8].

1.3 Fuel Cells

1.3.1 Fuel Cell Fundamentals

Fuel cells are a category of electrochemical converters that directly converts chemical energy of fuels into DC electricity [14]. Similar as batteries, fuel cells are another important type of galvanic cells. The main difference between them lies in that, of a battery, the chemical reactants are an inherent and inner part; whereas fuels must be supplied from external reservoirs to a fuel cell [15]. Unlike a battery, a fuel cell will keep generating electricity as long as fuels are supplied; it cannot 'go flat'. This feature is in common with internal combustion engines. However, fuel cells have no intermediate step of heat or mechanical energy production before electric power output. They can be solid state energy conversion devices without any moving parts [13]. Fig. 1.3 illustrates their architecture and operating principles. A fuel cell typically has two electrodes, namely anode and cathode, in between of which is the electrolyte. Anode electrode is where fuel oxidation happens and electrons flow out; cathode is where oxidant reduction takes place and electrons flow in. The function of the electrolyte, simply speaking, is to conduct ions between the electrodes and stop electrons and fuels from crossing over [16].

Depending on the material of the electrolyte used, there are several types of fuel cells. As also shown in Fig. 1.3, the main five types of fuel cells are: a) Alkaline Fuel Cell (AFC), b) Polymer Electrolyte Membrane Fuel Cell (PEMFC), c) Phosphoric Acid Fuel Cell (PAFC), d) Molten Carbonate Fuel

Cell (MCFC), and e) Solid Oxide Fuel Cell (SOFC). Their characteristics are summarized in Table 1.1. Sometimes, a Direct Methanol Fuel Cell (DMFC) is also classified as yet another type of fuel cell; however based on its electrolyte, it is essentially a PEMFC that uses methanol other than hydrogen as a fuel.

Like batteries, fuel cell performance is quantitatively described by voltage-current (CV) curves (polarization curves). A CV curve also illustrates the main four irreversibilities in a fuel cell: a) activation losses, b) fuel crossover and internal currents, c) ohmic losses, and d) mass transport or concentration losses. However, a Nyquist plot from an electrochemical impedance spectroscopy (EIS) test can give a much more detailed and insightful understanding of these phenomena [17].

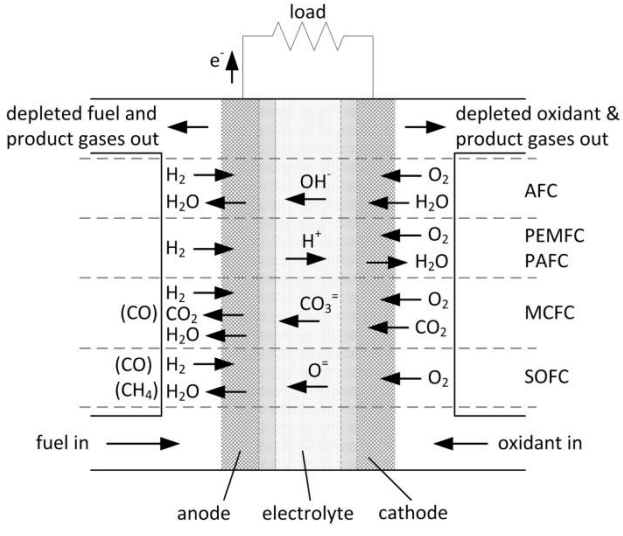

Fig. 1.3 - Schematic diagram and operating principles of various fuel cells [14].

Table 1.1 - Summary of major fuel cell types [14,16,18].

	AFC	PEMFC	PAFC	MCFC	SOFC
Electrolyte	Liquid KOH in a matrix	H^+ conductive polymer membrane	Liquid H3PO4 in SiC matrix	Molten carbonates in LiAlO2 matrix	Ceramic
Mobile ion	OH^-	H^+	H^+	CO_3^{2-}	O^{2-}
Operating temperature	50-250℃	60-200℃	150-200℃	600-700℃	800-1000℃
Typical catalyst	Ni, Ag, metal oxides	Platinum	Platinum	Nickel	Nickel

Fuel intake	H_2	H_2, CH_3OH	H_2	H_2, CH_4	H_2, CO, CH_4
Electrical efficiency	45-60%	40-60%	35-40%	45-60%	50-65%
Typical kWe	>20kW	<250kW	200kW	>200kW	<200kW
Applications	Submarines, spacecraft	Vehicles, small stationary	Stationary	Stationary	Stationary

To sum up, fuel cells have many advantages. Since there is no combustion involved in the energy conversion, they are clean, silent, potentially more durable and efficient. Unlike batteries, they have more scalability in power (determined by the fuel cell size) and capacity (limited by the fuel reservoir size). Fuel cells can easily scale from 1-W range (portable electronics) to megawatt range (power plants). They can also be quickly recharged by simply refueling. Their fuel flexibility is another advantage; especially these fuels mostly are renewable and carbon-neutral. Although they currently still need breakthroughs in material development, system design, and infrastructure construction, fuel cells are still a quite promising candidate for powering a sustainable future.

1.3.2 Proton Exchange Membrane Fuel Cells

The PEMFC, also called the low temperature PEM (LT-PEM) fuel cell, was initially developed by the American company General Electric in 1960s for NASA's first manned space vehicles.

A PEMFC usually consumes hydrogen and oxygen to produce electricity. The following electrochemical half reactions take place simultaneously in the two electrodes.

$$\begin{aligned} &H_2 \rightarrow 2H^+ + 2e^- \text{ (anode)} \\ &\frac{1}{2}O_2 + 2H^+ + 2e^- \rightarrow H_2O \text{ (cathode)} \end{aligned} \tag{1.1}$$

Protons H^+ are the mobile ions that go through the electrolyte. The electrolyte deployed is famous with its name Nafion, a registered trademark of Dupont. It is a sulphonated polytetrafluoroethylene (PTFE) membrane. The PTFE base, which is also sold as Teflon, makes the electrolyte membrane mechanically strong, highly durable, particularly hydrophobic, and resistant to chemical attack. It separates the two electrodes. The sulphonation then forms H^+ pathways through the PTFE polymer via adding side chains ending with HSO_3

to PTFE molecules. Now the sulphonated PTFE membrane is ready as the remarkable electrolyte for a PEMFC. The mechanism of H^+ pathways determines that the membrane is H^+ conductive only when soaked in water. This limits PEMFC operating temperatures to ≤80℃ [19].

In this temperature range, Platinum is the best catalyst for both the anode and the cathode. The basic structure of the two electrodes is usually identical. Platinum catalyst is treated into very fine particles and bound on the surface of larger particles of carbon powder. To prevent the electrodes from being flooded by the product water, Nafion ionomer is also added using its highly hydrophobic feature. It also helps H^+ transportation in the electrodes and improves their performance [20]. Then the Nafion/carbon-supported catalyst particles are either hot pressed or sprayed or 'printed' onto the two surfaces of the electrolyte [21,22,23]. The method chosen depends on whether the catalyst is immersed in the gas diffusion layer (GDL) or not. The GDL is generally a carbon paper or carbon cloth. Its function is to diffuse gases, discharge product water, form an electrical connection, and protect the very thin layer of catalyst. The two GDLs are labeled 'anode' and 'cathode' in Fig. 1.3. Between them and the electrolyte membrane are the two catalyst layers. Binding the five layers together forms the sandwich-structure Membrane Electrode Assembly (MEA). The remaining structures in Fig. 1.3 are two bipolar plates. Flow fields for fuels and products are carved in them. Bipolar plates are also collectors of electrons for the external circuit. Force is applied on them to clamp the MEA tightly and reduce the electrical contact resistance in between.

Compared with other fuel cell types, PEMFCs are more compact and efficient thanks to their very thin MEAs and the outstanding performance of Nafion® membrane. In other words, their power densities are higher than other types, ranging from 300 to 1000 mWe/cm^2 [13]. Working at relative low temperatures also guarantees that PEMFCs have swifter on-off operations and startups than other fuel cells, such as SOFCs and MCFCs. For the above reasons, PEMFCs are a prime candidate to replace today's vehicular internal combustion engines (ICEs) and a promising substitute to batteries in portable applications [24]. However, low operating temperatures make PEMFCs have very limited options of catalysts. Platinum is still the most practical but costly choice. Besides, under these low temperatures, Platinum catalyst is rather vulnerable to and easily deactivated by fuel impurities, e.g., CO, SOx, NOx, H2S, and NH3 [25]. Hydrogen purification adds a further cost burden. Costly hydrogen storage and lack of refueling infrastructure are another two barriers to bring PEMFC systems into market. On-board producing and decontaminating

hydrogen from hydrocarbons is a good solution. However, this also raises the PEMFC system complexity and cost. PEMFC thermal management then consumes extra space and power. The relatively small temperature gap between PEMFC system and environment results in a sluggish heat rejection and in turn a large radiator. Furthermore, water management of a PEMFC is complicated, due to the characteristics of Nafion membrane and the liquid-phase product water.

1.3.3 High Temperature PEM Fuel Cells

HT-PEM fuel cells can be considered as the technical off-springs of LT-PEM fuel cells. They make use of Phosphoric acid doped Polybenzimidazole (PBI) membrane as the electrolyte. Unlike the PAFC electrolyte, most acid molecules herein are immobilized. These membranes were first invented by Wang et al. in 1995 [26,27]. Since then, they have drawn much attention as their excellent characteristics versus Nafion membranes.

PBI base films have excellent oxidative and thermal stability [28]. Their operational temperature can reach up to 200℃ without affecting the mechanical flexibility. PBI films themselves are also good vapor, electron and ion barriers and exhibits low gas permeability. Proton H^+ conductivity thereof is added by the doped Phosphoric acid and is comparable to Nafion. The acid doped membrane also possesses an almost zero electro-osmotic drag number, compared to the drag number of 0.6-2.0 for Nafion [29,30,31]. These features make the doped PBI membrane an ideal electrolyte. This membrane allows HT-PEM fuel cells operating above 100℃, since no membrane hydration is needed for the proton pathways. The recommended operating range is from 140℃ to 170℃ [32]. Benefits from the elevated operating temperature are threefold: a) thermal management is eased; heat rejection to the ambient is facilitated; b) water management is barely an issue anymore, since membrane hydration is of no need and product water is now steam; c) the Platinum catalyst can tolerate fuel contaminations (CO is the main concern) at much higher concentrations. It can withstand up to 5% CO without any performance loss at 180℃ [33]. Regarding Nafion, the number is 10ppm (0.001%) [16,34,35].

In practice, the above advantages can translate into much simpler and more compact system design, higher system efficiency, and more flexibility in fuels. Fuel humidifiers can be safely ruled out of a HT-PEM fuel cell system now. Taking advantage of the enhanced heat rejection, much smaller radiator and coolant circulation pump are required.

At present, the use of pure hydrogen as a fuel source still has quite a few formidable limitations [34]. Especially in transportation applications, a major one is on-board hydrogen storage. To refuel a fuel cell vehicle using hydrogen would be time-consuming; the major storage schemes, i.e., cryogenic liquid hydrogen, compressed hydrogen gas, and metal hydride adsorption, each have significant drawbacks [36]. Then the lack of infrastructure for hydrogen distribution further exacerbates these on-board storage issues. Another fact is that hydrogen is nearly not available in natural form on earth. Thus, the method of on-board reforming liquid hydrocarbon or alcohol fuels to generate hydrogen comes into focus, among which fuels the most likely candidate is methanol [37,38]. As analyzed by Lindström et al. [38], its reforming processes have a superior hydrogen yield on both weight and volume basis than other fuels; the reforming processes are rather easily achieved at relatively low temperatures; methanol is abundant as a chemical material and already bulk-produced in industry; and the present network for distributing gasoline only needs minor changes to be 'methanol-ready'. In addition, the reformate gas mixture of methanol contains about 74% hydrogen, 25% carbon dioxide and 1-2% CO [39]. The CO concentration is far below the 5% criterion mentioned above. HT-PEM fuel cells can directly consume the on-board product hydrogen without significant performance loss. Fuel purification devices are simply unnecessary for a HT-PEM fuel cell system. All the above save considerable space and parasitic losses. The fuel flexibility and convenience further notably enhance the competitiveness of HT-PEM fuel cells. In a word, the commercialization barriers of fuel cells can possibly be greatly mitigated by the HT-PEM fuel cell.

On the other hand, HT-PEM fuel cells still have some obstacles to their full commercialization. Their efficiency is still slightly low. It is reported that they require cell voltages over 0.7V to achieve higher system efficiencies than LT-PEM fuel cells, which target has not been reached [40]. Durability is the second concern. Under higher operating temperatures, the corrosion of the catalyst carbon support becomes notable. This decreases the number of sites available to anchor the Platinum particles and degrade the catalyst performance [41,42]. Agglomeration or dissolution of Platinum particles on the carbon support is also more evident. Cost is another challenge in several aspects. Decreasing the Platinum catalyst loading and developing non-noble metals as catalyst materials are the two main answers. Last but not least, Phosphoric acid leaching is concerned as a main degradation factor to the PBI MEA. But it is analyzed that this phenomenon is negligible during normal operation [40]. Liquid water is another threat to dilute the Phosphoric acid and cause the

leaching during startup, this can be handled by heating up the MEA to above 100℃ before operating.

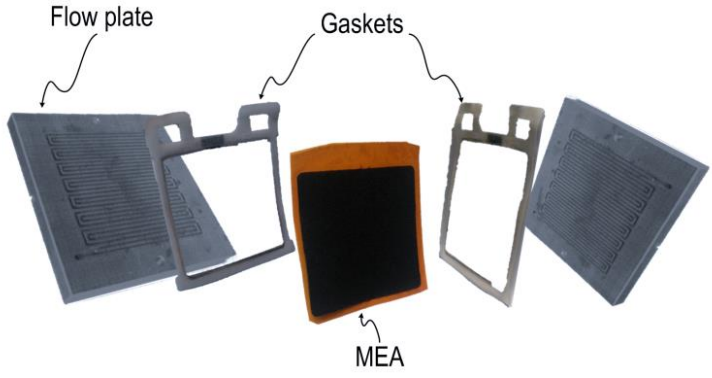

Fig. 1.4 - The central part of a HT-PEM single cell [43].

Fig. 1.4 shows a picture of the key parts of a single HT-PEM fuel cell [43]. MEA is the core part of a cell. It is where all the reactions take place. Similar as a Nafion MEA, it usually also has 5 layers. GDLs stay the same; the electrolyte is different. The two catalyst layers are almost the same, except that the Nafion ionomer is replaced by PBI saturated with Phosphoric acid. The bipolar plates (flow plates) are quite similar as those in LT-PEM fuel cells, which also shape the anode and cathode flow fields and collect electrons. The single cell shown is just a prototype. Bipolar plates are made of reinforced graphite bricks. In practices, these plates are much thinner. The thickness of a packed single cell can be less than 5mm. Its typical performance is given by the following CV curve, Fig. 1.5 [44,45]. In practice, in order to magnify the system power output, these single cells are usually series-connected in a stack. Then, the whole assembly of the cells is called a stack, as shown in Fig. 1.6.

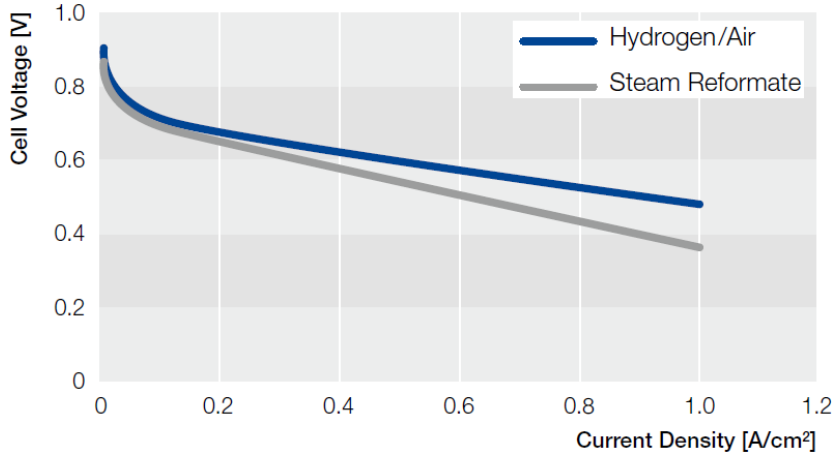

Fig. 1.5 - HT-PEM fuel cell typical performance CV curve [44,45].

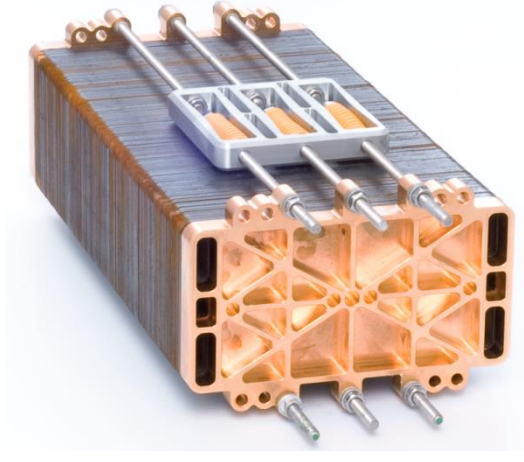

Fig. 1.6 - Picture of a HT-PEM fuel cell stack [46].

1.3.4 The HT-PEM Fuel Cell Power System

The HT-PEM fuel cell power system studied in this project is from the previous work by Andreasen et al. [1]. Its nominal electric power output is 1kWe. The system configuration and elementary components are illustrated in Fig. 1.7. It is methanol fueled, of which the advantages are abovementioned. The fuel, liquid methanol/water mixture, is stored in the fuel tank. When the system is running, the fuel is pumped to the evaporator and gets evaporated and superheated. Then the evaporated methanol/water steam is delivered into the steam methanol reformer (SMR) whereat it is converted mainly to

hydrogen and carbon dioxide. Afterwards, the product gas is supplied to the stack (FC in Fig. 1.7) anode side to generate electricity; oxygen is consumed as the oxidant and supplied by air blower to the cathode side. Excess air is also aerated through the cathode flow field to remove the exothermic reaction heat and prevent the stack from over-temperature. It is also of the function to avoid oxidant starvation occurring on the cathode electrode considering that oxygen is diluted by nitrogen in atmospheric air, and as a result, it is sluggish in reaching the catalytic sites especially when high current is drawn by the electric load. The ratio between the total supplied amount and the reacted is termed stoichiometry. In this system, the cathode stoichiometry can be as high as 20. On the other hand, the anode stoichiometry is only about 1.2. This is benefited from the much smaller molecules of hydrogen. The remaining hydrogen after the stack is reacted with oxygen in the SMR burner side to provide heat. In case of heat shortage, the anode stoichiometry can be increased. In the end, both the flue gases from the SMR burner side and the stack cathode side are ventilated through the evaporator for the fuel evaporation and then rejected to the environment.

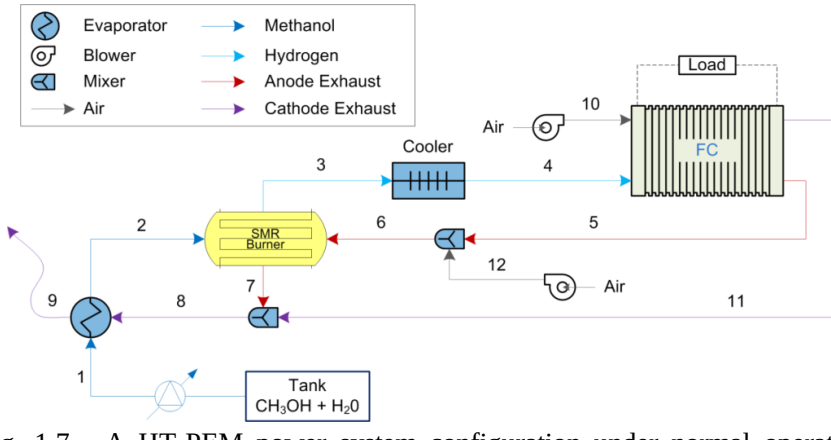

Fig. 1.7 - A HT-PEM power system configuration under normal operation [1,47].

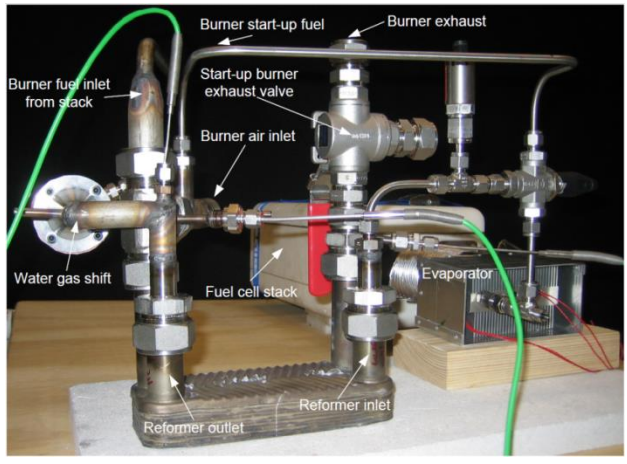

Fig. 1.8 - Picture of the integrated HT-PEM power system [1].

Fig. 1.8 gives a picture of the integrated HT-PEM power system although with a slightly different configuration. The fuel cell stack is in the white box in the back. The stack is wrapped in the foam insulation to avoid insufficient temperatures during operation. Under the standard working condition $i \approx 0.6 A/cm^2$, the stack can produce 1kWe electricity and approximate 1kW reaction heat. This is more clearly shown by the system energy flow Sankey diagram, Fig. 1.9 [1,48]. As explained above, the 1kW reaction heat is carried out of the stack by the cathode flue gas in the form of exhaust heat and is then reused by the evaporator. It can be noticed that there is still nearly 70% of the exhaust heat rejected into the environment unutilized, even if the 329W heat for the evaporator is entirely supplied by the exhaust gas. However, in reality it is not this supposed condition and the evaporator is rather inefficient. This can be explained by Fig. 1.10 [1]. $P_{Evap,Convection}$ in the figure is the heat that the evaporator harvests from the exhaust heat. In most time, $P_{Evap,Convection}$ is negative, which means the evaporator actually is losing heat to the exhaust gas, i.e., the exhaust gas is being heated up. This is exactly opposite of the design purpose. It can also be noticed that no matter if the evaporator is gaining or losing heat from or to the exhaust gas, the evaporator cannot work independently without the auxiliary electric heat. All these issues can be traced back to the evaporator design and operating set points.

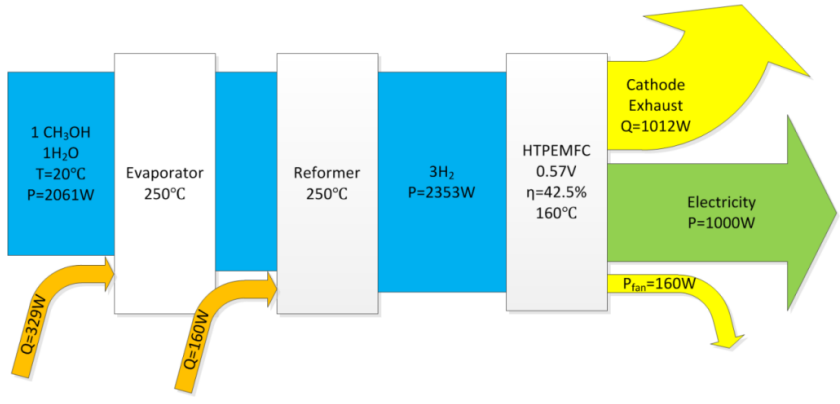

Fig. 1.9 - Energy flow Sankey diagram [1,48].

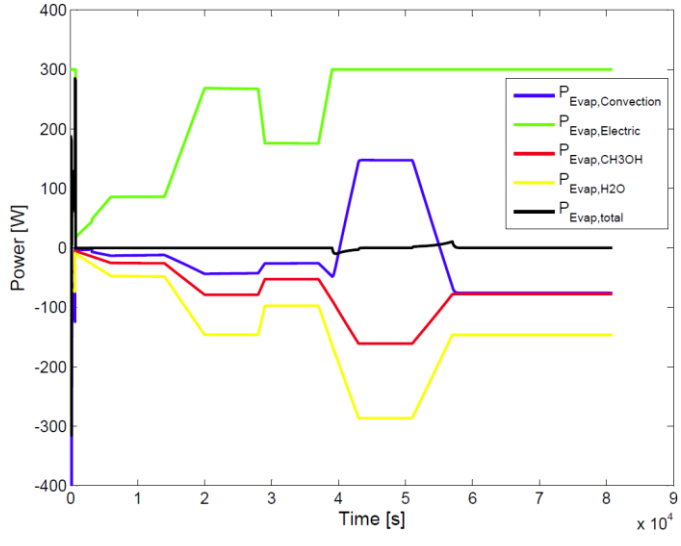

Fig. 1.10 - General energy flow in the evaporator with adjustable auxiliary electric heat (maximum 300W) [1].

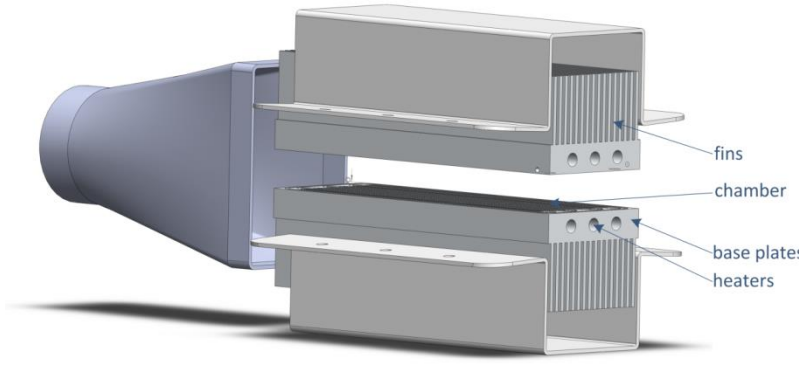

Fig. 1.11 - Design of the evaporator [47].

The design of the evaporator is illustrated in Fig. 1.11 and shown in the bottom right part of the picture Fig. 1.8. Basically, it is a plain plate-fin heat exchanger. The evaporation chamber (the flow fields) for the liquid methanol/water mixture is carved in the base plates. Here are also mounted the cartridge heaters. The evaporator is supposed to work like this: during normal operation, the liquid methanol/water mixture is pumped into the evaporation chamber and gets evaporated then superheated, using the heat recovered from the exhaust gas by the plain plate fins. Occasionally, when heat shortage happens, e.g., during system startup, the cartridge heaters will be turned on to supplement with electric heat. Regarding that, the methanol/water mixture boiling point is about 72℃ [49] and the exhaust heat temperature is around 160℃ [1], this design is feasible; the evaporation and superheating can be accomplished.

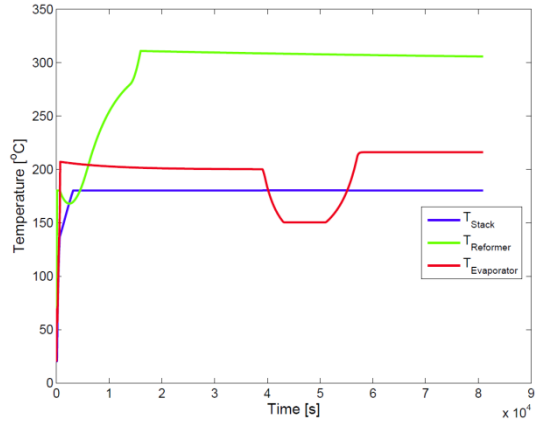

Fig. 1.12 - System temperatures during simulation using adjustable electric heat to evaporator [1].

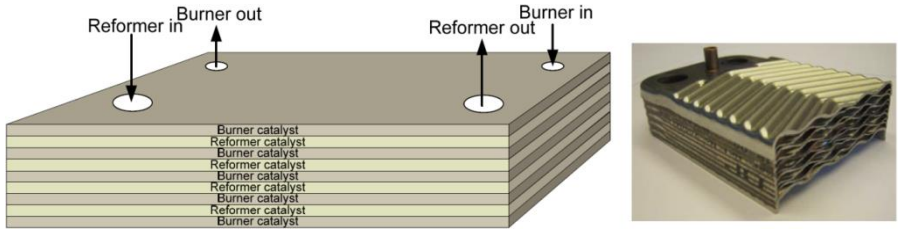

Fig. 1.13 - Illustration and picture of the SMR [1].

It is apparent that the more exhaust heat it recovers and the less electric heat it consumes the more efficient the evaporator is, which is directly correlated to the evaporator operating set point. According to Fig. 1.12 from [1], the set points were, however, too high and beyond the exhaust heat temperature, which explains the negative $P_{Evap,Convection}$. There are two reasons for these high set points.

The first one is to match the SMR and avoid using part of the SMR to evaporate the methanol/water mixture. As shown in Fig. 1.13, the SMR is a catalyst-coated plate heat exchanger taking the thermal advantages of the optimized heat transfer, compact design and fast temperature dynamics of the heat exchanger. It is also advantageous in its simple rigid structure and excellent scalability from its layer structure. The catalyst coated is Pt-based. Superheated methanol and water react on it and produce hydrogen. This process is called the methanol steam reforming (SR) reaction, as shown in Equation (1.2).

$$SR:\ CH_3OH + H_2O \leftrightarrow 3H_2 + CO_2 (+49.5 kJ/mol) \tag{1.2}$$

Which can be further split into two simpler reactions: methanol decomposition (MD) and water-gas shift (WGS).

$$MD:\ CH_3OH \leftrightarrow 2H_2 + CO (+90.7 kJ/mol) \tag{1.3}$$

$$WGS:\ CO + H_2O \leftrightarrow H_2 + CO_2 (-41 kJ/mol) \tag{1.4}$$

The methanol SR reaction is endothermic and set to run at about 300℃. Therefore, the SMR requires a heat input. This is from the catalytic oxidation of hydrogen on the burner side of the SMR. Referring to Fig. 1.7, the hydrogen is the remaining unreacted hydrogen from the HT-PEM stack. Obviously, if the fuel evaporation and/or superheating happened in the SMR, more hydrogen will be needed and in turn the whole system efficiency will be lowered.

The second reason of the high set points is to keep a safe distance from the fuel boiling point for the evaporator to handle load fluctuations. This is because of its limited dynamic performance, which can be noticed in Fig. 1.12. To sum up, the fuel evaporation and superheating in the current system will either cause heat loss to the exhaust gas or drain heat from the SMR. Either condition will compromise the system efficiency.

Despite the above issue, the dynamic performance, i.e., the load-following capability, of the whole HT-PEM power system possibly still needs improvement [48]. From Fig. 1.7, it can be predicted that as soon as the electric load increases, the stack will consume more hydrogen immediately to fulfil the need and demand more hydrogen from the SMR. So the SMR needs more heat to produce the additional hydrogen. Contrarily, less hydrogen at the moment is left from the stack for the catalytic oxidation in the SMR to generate heat as more has already been reacted in the stack. If the system is more efficient, i.e., the stoichiometry is more precisely controlled, the consequences of this countermove will be even worse. When the electric load decreases, the above behaviors are vice versa. Surplus hydrogen now will cause SMR temperature overshoot, more CO in the reformate hydrogen risking poisoning the stack and lower system efficiency.

To deal with the above issues, the first scenario is to keep the HT-PEM power system working in steady state as a range extender (basically a battery charger). Second scenario can be a new design of the evaporator that has improved heat management and dynamic performance [47]. Nevertheless, a simple calculation can reveal that an ideal evaporator only needs around 100W exhaust heat to evaporate and superheat enough methanol/water mixture. The rest exhaust heat, which still contains almost 1kW, will remain ejected unused to the ambient. Therefore, another more direct choice is to cut the loop and try out some other compact devices to recover the exhaust heat for electricity to boost the whole system efficiency. Most likely, the generated electricity can also mitigate the load-following issues.

All the above analyses explain the motivations of this project.

1.4 Thermoelectric Devices

Thermoelectric (TE) devices are solid-state energy converters. They are both heat engines and heat pumps [50]. Their combination of thermal, electrical and semiconducting properties allows them to directly generate electricity from

waste heat or convert electrical power directly into cooling and heating. They are superb in their miniature outline, excellent scalability, outstanding reliability and long lifetime, yet still suffering from their low efficiency. Fig. 1.14 below shows a typical TE device.

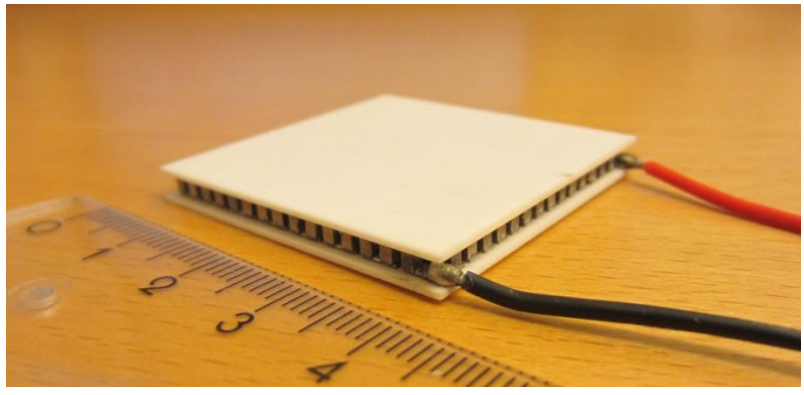

Fig. 1.14 - Picture of a typical TE module.

1.4.1 Thermoelectrics

As shown in the above picture, a TE module includes multiple semiconductor legs. They are either p- or n- type and alternately arranged. Each pair of the p- and n-legs is electrically connected in series by a conducting strip (usually copper) and forms the basic unit a TE module, a 'thermocouple'. All the thermocouples in a module are then connected together electrically in series and thermally in parallel. Finally, all the connected thermocouples are sandwiched by two ceramic substrates on top and bottom and a TE module is complete.

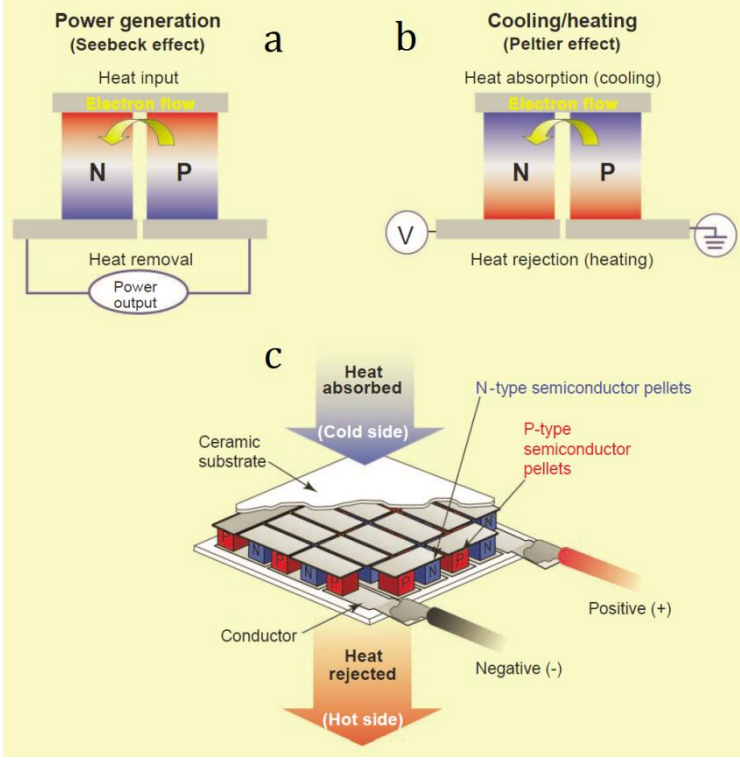

Fig. 1.15 - How a TE module works [51]. a) Seebeck effect makes TE generators. b) Peltier effect makes TE heat pumps. c) Thermocouples packed into a module.

The thermoelectric effects which underlie thermoelectric energy conversion are called Seebeck effect, Peltier effect and Thomson effect. As illustrated by a thermocouple in Fig. 1.15a, if the junction at the top are heated and the two feet at the bottom are cooled, a voltage potential, the Seebeck voltage, which drives the hole/electron flow in the two semiconductor legs, is created by the temperature difference between the junction and the feet. If connected to an external circuit, the voltage source can then output power. Observed by Seebeck in 1821, this effect is named after him and is the basis for TE power generation [52]. The voltage across the two feet can be expressed as:

$$U_{pn} = \alpha_{pn}(T_h - T_c) \tag{1.5}$$

Where α_{pn} is the difference of the Seebeck coefficients between two legs and $T_h - T_c$ is the temperature difference falls on the two legs. This equation also defines the Seebeck coefficient.

Thirteen years after Seebeck's discovery, Peltier published an article on his observation of temperature anomalies in the boundary vicinity between two different conductors when an electric current is flowing through them [52]. This phenomenon is then called Peltier effect after his name. It is the reverse situation of Seebeck effect. As shown in Fig. 1.15b, when an external power source is applied on the two feet of the thermocouple and a current I flows in a clockwise sense in the legs, a rate of heat $\dot{q}$ is absorbed at the junction and ejected from the two feet. When the current I direction reverses, the heat flow will also be instantly changed into the opposite direction. This is the Peltier effect and describes the capability of heating and cooling of a TE module when a current is applied on it. Quantitatively, it is given by Kelvin's Law using the following equation. π_{pn} is the thermocouple's Peltier coefficient.

$$\dot{q} = \pi_{pn} I \tag{1.6}$$

The above two effects, Seebeck and Peltier, are the two main thermoelectric effects. The last one, the Thomson effect, consists of reversible heating or cooling $\dot{q}_\beta$. It is induced when there is both a flow of electric current I and a temperature gradient ΔT existing through a single homogeneous conductor. Compared to this, it should be clear that Seebeck and Peltier effects are not interfacial phenomena although they only take place at junctions between dissimilar conductors [53]. The reason is that all three effects depend on the bulk properties of the materials involved. Thomson coefficient β is given as:

$$\dot{q}_\beta = \beta I \Delta T \tag{1.7}$$

The discovery of Thomson effect actually unveils the interdependency of the Seebeck and Peltier phenomena. All these three coefficients are convertible to each other by the Kelvin relationships:

$$\alpha_{pn} \cdot T = \pi_{pn},\ d\alpha_{pn}/dT = \left(\beta_p - \beta_n\right)/T \tag{1.8}$$

These relationships are deduced by irreversible thermodynamics [54]. In practice, especially in applications with moderate temperature gradients, Thomson effect is of much less significance than the other two and usually just neglected [55]. Besides the above three thermoelectric phenomena, other effects, such as volumetric Joule heating, contact resistance etc., also affect TE device performances significantly and should be carefully considered.

In principle, a single thermocouple can be adapted to fulfil the required power generation capability or heating/cooling capacity by altering its ratio of length to cross-sectional area. However, such a uni-couple device would operate

under a very small voltage and a very large current unless the request is minimal [53]. For practical reasons, hundreds of them are typically electrically connected in series and packed as a TE module, as shown in Fig. 1.14 and Fig. 1.15c.

1.4.2 Thermoelectric Generators

A thermoelectric generator (TEG) is a TE module working on Seebeck effect to generate power from heat. In principle, since Seebeck and Peltier effects are reversible, TEG is a definition of a working mode of a TE device; Thermoelectric Cooler (TEC) is the other. To describe a TEG's performances, the following characteristic parameters are employed.

1.4.2.1 Characteristic Parameters

1) Figure of merit of TE materials (zT)

The dimensionless figure of merit of materials (zT) determines the maximum efficiency of a thermoelectric material for both power generation and cooling. It is defined as:

$$zT = \frac{\alpha^2 \sigma}{k} T \tag{1.9}$$

where α is the Seebeck coefficient, σ is the material electrical conductivity, k is the thermal conductivity, and temperature T in the unit of Kelvin, is used to make this parameter dimensionless.

2) Figure of merit of thermoelectric devices (ZT)

The device figure of merit (ZT) indicates the efficiency of a thermoelectric device. It depends on some other factors other than the zT of materials. One thing needs to be clearly distinguished is that ZT (uppercase) has different meaning from the lower-case zT, the material's figure of merit. For a TE generator, the maximum device efficiency ($\eta_{\max}$) is used to determine ZT:

$$\eta_{\max} = \frac{\Delta T}{T_h} \cdot \frac{\sqrt{1+Z\bar{T}}-1}{\sqrt{1+Z\bar{T}}+\frac{T_c}{T_h}}, \bar{T} = (T_h + T_c)/2 \tag{1.10}$$

In the equation, T_h is the temperature of heat source (heat input), T_c is the temperature of heat sink (heat removal), ΔT is the temperature difference between T_h and T_c. $Z\bar{T}$ is the device figure of merit at temperature $\bar{T}$. Of a typical TE module as in Fig. 1.14, Z can be calculated from

$$Z = (\alpha_p - \alpha_n)^2 / R_e K_t,$$
$$\mathrm{K}_t = k_p A_p / L_p + k_n A_n / L_n,\ \mathrm{R}_e = \mathrm{L}_p / \sigma_p A_p + L_n / \sigma_n A_n \tag{1.11}$$

There are two conditions, under which Z (uppercase) equals z. The first one is that one leg of a thermocouple is superconductor. The other condition is that the n- and p-leg material properties are assumed independent from temperature and equivalent to each other, i.e., α, σ and k of the two legs have nearly the same values. Although the second two assumptions are believed inaccurate in many cases [56], they are a widely used simplification in literatures with satisfactory accuracy (within 10% accuracy [54] and better in lower temperature applications). If the above assumptions are true, there is

$$Z = z = \frac{\alpha^2 \sigma}{k} \tag{1.12}$$

Where $\alpha^2\sigma$ is termed as the electrical power factor.

3) Efficiency of a TEG module

The efficiency of a TEG module is given by

$$h_{TEG} = \frac{energy\ supplied\ to\ the\ load}{heat\ energy\ absorbed\ at\ the\ hot\ \ junction} \tag{1.13}$$

Assume that a TEG module is ideally insulated from the ambient, α, σ and k of two legs of every thermocouple are the same and constant under temperature changes, and the contact resistances at the junctions are negligible, then the efficiency can be expressed as

$$\eta_{TEG} = \frac{I^2 R_{load}}{n_{tc} k_{tc} (\mathrm{T}_h - \mathrm{T}_c) + n_{tc} \alpha_{pn} T_h I - n_{tc} I^2 R_e^{tc} / 2} \tag{1.14}$$

Where R_{load} is the external circuit, k_{tc} is the thermal conductance of a single thermocouple, R_e^{tc} is the electrical resistance of every thermocouple in a TEG module, and n_{tc} is their total number. Based on the above assumptions, equations describing the maximum power output point and peak efficiency point of a typical TEG module are listed in Table 1.2 [54,57].

Table 1.2 - Power output and efficiency equations of a typical TEG module.

	$P_{\max}$	$\eta_{\max}$
I	$\alpha_{TEG} \Delta T / 2R_e^{TEG}$	$\alpha_{TEG} \Delta T / (\mathrm{M}+1) R_e^{TEG}$
R_{load}	R_e^{TEG}	$R_e^{TEG} M$

P	$\alpha_{TEG}^2 \Delta T^2 / 4R_e^{TEG}$	$M\alpha_{TEG}^2 \Delta T^2 / (\mathrm{M}+1)^2 R_e^{TEG}$
η	$Z\Delta T / \left(4 + ZT_h + Z\bar{T}\right)$	$(M-1)\Delta T / \left[(M+1)T_h - \Delta T\right]$

$M = \sqrt{1+Z\bar{T}}$, $\alpha_{TEG} = n_{tc}\alpha_{pn}$, $\Delta T = T_h - T_c$, $\bar{T} = (\mathrm{T}_h + \mathrm{T}_c)/2$

4) Thermoelectric compatibility factor

Thermoelectric compatibility factor explains the phenomenon that the real electric current needed for a TE module to reach its peak efficiency point $\eta_{\max}^s$ is smaller than the value predicted by Z as shown in Table 1.2. $\eta_{\max}^s$ is also lower than the theoretical value $\eta_{\max}$ in the table. This effect is most important for segmented TEGs, which are designed for applications under large temperature gradients, e.g., cases with ΔT > 600℃ in [56, 58, 59]. If not considered, the device ZT of a segmented TEG module can be significantly lower than the average zT of materials. However, in calculating the exact performances for all other types of TE modules, this factor also affects [54]. The thermoelectric compatibility factor for a TE material is expressed as:

$$s = \left(\sqrt{1+zT} - 1\right) / \alpha T \tag{1.15}$$

For small zT , this approximately equals to

$$s \approx \frac{z}{2\alpha} \tag{1.16}$$

Then it can be derived that the reduced peak efficiency point $\eta_{\max}^s$ is

$$\eta_{\max}^s = \frac{\sqrt{1+zT} - 1}{\sqrt{1+zT} + 1} \tag{1.17}$$

In a TEG module, if the compatibility factor of one part is significantly different from another part, no current match will possibly be set up between them for each part to operate nearby to its $\eta_{\max}^s$. For higher efficiency, as a rule of thumb, this factor of different TE materials in a TE module should be within about a factor of two across the different temperature ranges [54].

The compatibility factor is an intrinsic property of thermoelectric materials. It must be counted for segmented TEGs in high temperature applications, since it always affects the device efficiency largely. In similar applications for cascaded TEGs, however, efforts could be done to avoid the compatibility influences on device performance, which is one advantage of this kind of TEGs.

1.4.2.2 TEG Categories

TEG types and materials discussed here are those commercialized, i.e., only mature TEG modules and materials are discussed in this section. Sorted by operational temperature intervals as shown in Fig. 1.16 and determined by the properties of TE materials employed, generally speaking, there are three categories of TEGs: a) low-temperature (<200℃), b) medium-temperature (200 - 600℃), and c) high-temperature (600 - 1000℃).

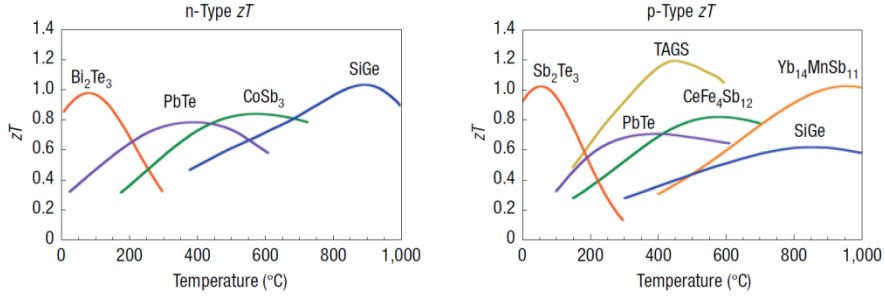

Fig. 1.16 - zT of commercial TE materials.

Fig. 1.16 also gives the material zT values of most commercial available materials [60]. These are believed the 'Best Practice' materials [61]. Bi_2Te_3 based materials (n-leg composition close to $Bi_2(Te_{0.8}Se_{0.2})_3$, typical p-leg composition $(Sb_{0.8}Bi_{0.2})_2Te_3$) dominate the applications around room temperature (<200℃) [62]. Peak zT value for these materials usually falls in the range 0.8-1.1.

For TEGs applied in temperature range from 200 to 600℃, group-IV tellurides, such as PbTe, GeTe and SnTe, are typically employed as n-leg materials with peak zT at about 0.8. In these medium-temperature applications, $AgSbTe_2$ -based alloys can be used both in n-legs and p-legs. These materials are reported several times with peak zT>1. Among them, p-type TAGS, $(GeTe)_{0.85}(AgSbTe_2)_{0.15}$, has been successfully applied in long-life TEGs for a long time, of which the maximum zT>1.2. For TEGs working in this 200 - 600℃ range, there are some more material choices for both p-legs and n-legs, e.g., skutterudite-based compounds, complex oxides and silicide-based materials. Silicide-based materials in [63] (n-type Mg_2Si and p-type $MnSi_{1.73}$) and [58,64] (n-type Mg_2SiSn with $zT_{max}=1.1$ and p-type Zn_4Sb_3 with $zT_{max}=1.3$) were deployed other than lead alloys, which are restricted according to environment regulations. There are

still some other novel materials reported with higher zT values, most of which are bulk nanostructured materials. However, none has been yet reproduced by other laboratories, not to mention their industrialization [65,66].

For applications from 600℃ up to 1000℃, SiGe alloys are one of the only a few ideal choices for both n-legs and p-legs [67]. TEGs operational in these applications are usually Radioisotope Thermoelectric Generators (RTGs) for the reason that they consume the released heat from the nuclear decay of radioactive isotopes (typically Plutonium-238) to generate electrical power.

It should be noticed that there is another interesting property for all the TE materials. By changing their carrier concentration, their zT could reach its peak values at different temperatures in their operational ranges [56,65,68,69]. This brings the convenience that it can be assumed TEGs are working at their max zT points during TEG system design and optimization, as long as their operating temperatures are constant or only fluctuate in relatively narrow intervals.

Despite distinguishing TEGs by their working temperature ranges, they can also be sorted by the ways how the thermocouples in a module are arranged. TEG modules can then be labelled either conventional (theoretical) or segmented or cascaded. Actually these differences in module design are also with the purpose to suit different operating temperatures. Applications around room temperature are suitable for the conventional TEG modules. Segmented TEG modules are typically used in automotive applications with temperatures up to about 500℃. The operational temperature range of cascaded TEGs is partially overlapped with segmented TEGs. Theoretically, their operating temperatures can go much higher. Another advantage of cascaded TEGs is that their design can avoid the material compatibility issues.

1) Conventional (theoretical)

Thermocouples in this category are connected thermally in parallel and electrically in series, as illustrated in Fig. 1.15c. Each leg of a thermocouple is casted by one homogeneous composition. This module configuration is still the most widely used by far, because of the structure's simplicity and durability. Its detailed pros and cons are:

- Simplest structure; easiest to manufacture.
- Convenient and direct to calculate out the performances of the TE materials.

- Easier to optimize their working conditions.
- TEG modules in this category have the longest lifetime.
- Lower efficiency, since only a few layers of TE materials in legs work on the ideal temperature points; inner temperature gradients are not included; carrier concentration is not tuned.
- Heterogeneous thermal expansion of legs can easily happen; it affects the module lifetime especially when temperature gradients are large.

2) Segmented

Segmented TEGs are for large temperature differences (typical $\Delta T > 600$). Thermocouples in this category are still thermally in parallel between legs, and electrically in series. The only difference now is that p- and n- legs are combinations of TE material segments and segments in each leg are thermally and electrically both in series. Alternative configurations of segmented TEG modules are shown in Fig. 1.17 [70]. The motivation of this segmented arrangement is to optimize TE materials along the temperature gradients in legs. Operational temperature ranges and peak zT temperature points are different between various thermoelectric materials. In case a TEG device working between extremely large temperature differences, one homogeneous TE leg, e.g., the legs in a conventional TEG module, will probably sinter on the hot side and work far below optimal zT regions on the cold side. These phenomena have negative effects on device efficiency or even can unfit a TEG module from these applications. Using different materials in series in each leg, each segment can be adapted near to its maximum zT point. As a total, the device efficiency is improved and operational temperature range is extended. Material compatibility within each leg and between legs is very important, as explained in the above section. In order to handle this, each material segment may have different aspect ratios (cross-sectional area to segment thickness) [71]. The advantages and disadvantages of these segmented TEGs are:

- Improved efficiency; easier to get the maximum zT.
- Higher total contact resistance.
- Higher design complexity and lower manufacturability, affected by the compatibility and the thermal expansion.
- Bad device stability because of the segment connections.

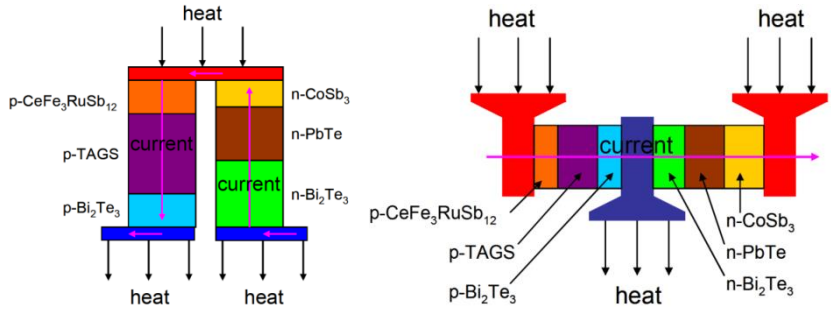

Fig. 1.17 - Alternative segmented TEG modules.

3) Cascaded

Similar as the segmented style, cascaded arrangement is also for high temperature applications. Their structures are compared in Fig. 1.18 [54]. Besides the aim to improve the working temperature of every material spot, the invention of cascaded arrangement is mainly to get rid of the material compatibility issue. In a cascaded module, each stage has an independent circuit comparable with each thermocouple in a conventional module. By nature, the compatibility issue is ruled out. Cascaded TEG modules have the following pros and cons:

- Improved efficiency; easier to get the peak zT.
- Higher total contact resistance.
- Higher design complexity than conventional modules, although simpler than the segmented.
- Bad device stability from the stage connections.

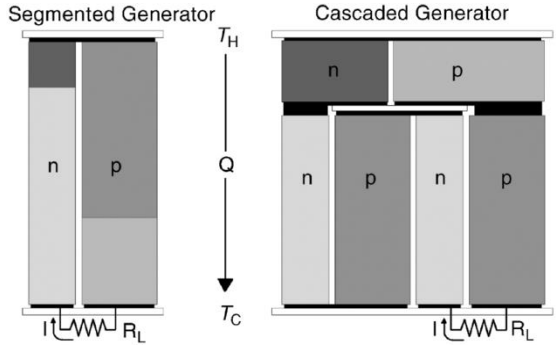

Fig. 1.18 - Schematic diagram comparing segmented and cascaded TEGs.

To summarize, it can be noticed that all the above module designs are plate-like. Thickness of the modules is mainly in the range from millimeters (the thin-film TE devices [72]) to centimeters. Except for the plate-like modules, some other module styles have also been proposed, such as ring-structured module design for heat flows in radial direction [73]. It is concluded that this configuration is advantageous in that the thermoelectric converter is at the same time working as conductor and generator. In addition, the efficiency could be improved because it enhances its heat sink capabilities and depresses the reverse heat transfer inside the converter, which usually are the two main factors downgrading a TEG's performance. However, this configuration dramatically increases manufacturing complexity and still remains as lab demonstration setups. An mW-level module, a 'thermoelectric tube', was exposed in [73] and is shown here in Fig. 1.19. Two years after, a report from DOE by Bell and Crane referred that a similar cylindrical TEG system was being under construction by BSST [74]. But no further details could be identified and no further reports have come out afterwards. Recently, another tubular module is fabricated by Schmitz et al. [75]. It has an updated design to [73] that can better release thermal stress. A picture of the module is given in Fig. 1.20. There are also some other types of TEGs, such as flexible polymer based micro TEGs for wearable electronics, of which details can be found in [76,77].

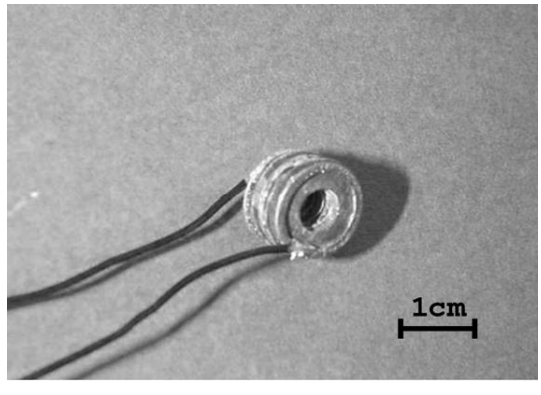

Fig. 1.19 - Photo of a 'thermoelectric tube'.

Fig. 1.20 - Tubular PbTe module consisting of four thermocouples connected with nickel bridges.

1.4.3 Thermoelectric Coolers

Thermoelectric coolers (TECs) are heat pumps utilizing the Peltier effect. They harness electrical power to accelerate heat transfer from hot to cold or force heat to flow from cold to hot [78]. As the other working mode of a TE device, TECs share most characteristics with TEGs. They are connected through the Kelvin relationship by Equation (1.8). The performance of any refrigerator is generally described quantitatively by its coefficient of performance (COP). This is given by the heat flux being pumped by the device, $\dot{Q}_c^{TEC}$, divided by the rate at which electrical energy is supplied, P_e^{TEC}.

$$COP = \frac{heat\ \ flux\ being\ \ pumped}{electrical\ \ power\ input} = \frac{\dot{Q}_c^{TEC}}{P_e^{TEC}} \tag{1.18}$$

$$\dot{Q}_c^{TEC} = n_{tc}\alpha_{pn}T_1 I - n_{tc}I^2 R_e^{tc}/2 - n_{tc}k_{tc}(\mathrm{T}_2 - \mathrm{T}_1) \tag{1.19}$$

$$P_e^{TEC} = n_{tc}\alpha_{pn}I(\mathrm{T}_2 - \mathrm{T}_1) + n_{tc}I^2 R_e^{tc} \tag{1.20}$$

In the above equations, T_1 is the temperature of the surface the pumped heat is removed from. T_2 is the surface end of the pumped heat flux. All the other variables can refer to the previous section for detailed definitions. Correspondingly, based on the previous assumptions, equations describing the maximum pumping capability $\dot{Q}_{\max}$, peak COP point $COP_{\max}$, and achievable highest temperature difference between the two substrate surfaces $\Delta T_{\max}$ of a conventional TEC module are listed in Table 1.3 [54,57].

Table 1.3 - Peak performances of a typical TEC module.

$\dot{Q}_{\max}$	$COP_{\max}$	$\Delta T_{\max}$
ΔT		$Z(T_1)^2/2$

I	$\alpha_{TEC}T_1/R_e^{TEC}$	$\alpha_{TEC}\Delta T/\left[(M-1)R_e^{TEC}\right]$	$\alpha_{TEC}T_1/R_e^{TEC}$
V	$\alpha_{TEC}T_2$	$M\alpha_{TEC}\Delta T/(M-1)$	$\alpha_{TEC}T_2$
$\dot{Q}_c^{TEC}$	$K_{TEC}\Delta T\left[\frac{Z(T_1)^2}{2\Delta T}-1\right]$	$K_{TEC}\Delta T\left[ZT_1-\frac{\Delta T(\mathrm{M}+1)}{T_2+T_1}-1\right]$	0

$M=\sqrt{1+Z\bar{T}}$, $\alpha_{TEC}=n_{tc}\alpha_{pn}$, $\Delta T=T_2-T_1$, $\bar{T}=(\mathrm{T}_2+\mathrm{T}_1)/2$, $K_{TEC}=n_{tc}k_{tc}$

As TEGs, segmented TEC modules also have the material compatibility concerns. But different from TEGs, the compatibility factor of TECs is expressed as [79]:

$$s=\left(\sqrt{1+zT}+1\right)/\alpha T \tag{1.21}$$

Similar to TEGs, TECs can also be sorted into categories. In applications, if a TEC module has to operate between widely different temperature differences, it is unlikely that a single conventional module will suffice. Segmented or Cascaded TEC modules may be adequate. The problem of segmented modules is that their achievable maximum temperature difference is still limited by $Z(T_1)^2/2$; cascaded modules are just complicated to design and manufacture. Instead, conventional modules are stacked together and named multi-stage modules [53]. It should be clear that these multi-stage TECs do not belong to another category of TE devices. They are just another way of building cascaded modules, except that cascaded modules are usually for TEGs and multi-stage modules are typically used to call these TECs. Fig. 1.25 gives a schematic illustration of a two-stage TEC module.

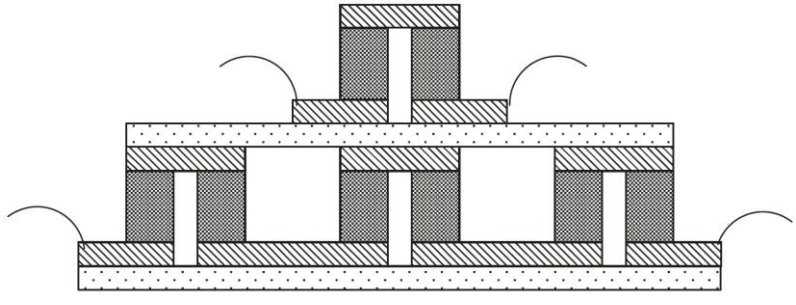

Fig. 1.21 - Schematic arrangement of a two-stage TEC module [53].

TECs are unique miniature heat pumps and coolers. As TEGs, TECs have excellent scalability. An ordinary module as shown in Fig. 1.14 has a size of around 5mm x 40 mm x 40 mm. There are also mass-produced modules in larger sizes and they can be stacked to be multi-stage. Smaller modules can be

in several cubic millimeters; thin-film modules can be thin as a piece of paper. Some pictures of these modules are given below in Fig. 1.22 and Fig. 1.23.

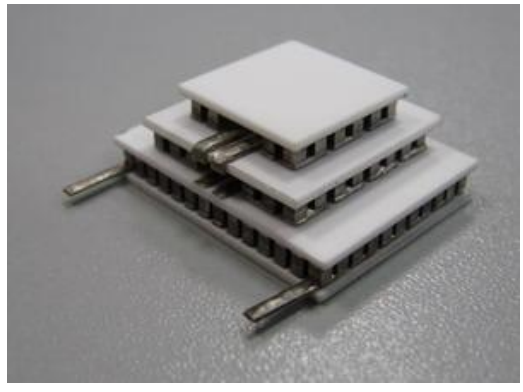

Fig. 1.22 - A three-stage TEC module [80].

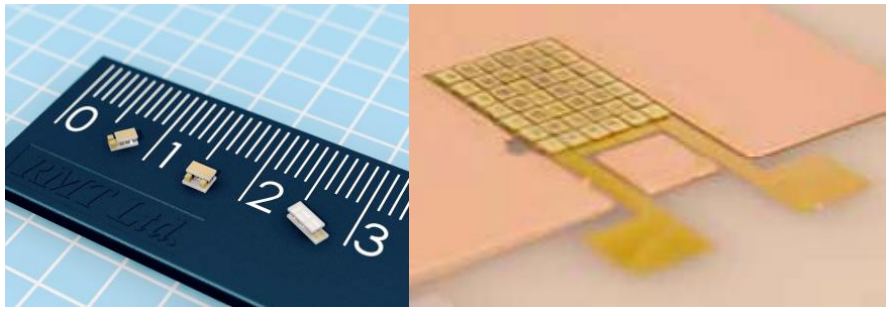

Fig. 1.23 - Pictures of a) a mini TEC module [81], b) a thin-film TEC module in 0.1 mm x 3.0 mm x 3.5 mm [82].

1.5 Literature Review

In short, the motivations of this project are trying to harness thermal energy using TEGs in the HT-PEM power system to improve its system efficiency and to deploy TECs to improve the load-following capability of the HT-PEM system. Since this project is application-oriented, literature review is carried out covering three main aspects.

1.5.1 Thermoelectric Materials

Over the past decades, the exploration of high-efficient thermoelectric materials has been under intensive research from both an academic perspective and with a view to industrial applications. It is the mainstream in the whole

thermoelectric community. The focus is on increasing the TE material figure of merit, zT, aiming for more energy-efficient and cost-effective systems.

Referring to Equation (1.9) and (1.12), to maximize zT, the following approaches are required: to maximize the Seeback coefficient α, to increase the material electrical conductivity σ, and to minimize the thermal conductivity k. However, these three properties are typically conflicting to each other. Lower carrier concentration insulators and semiconductors have larger Seebeck coefficient. By the same token, it results in poorer material electrical conductivity. Fig. 1.24 shows the compromise between the three properties changing with carrier concentration [56]. It can be noticed that the optimum carrier concentrations for peak zT are between 10^{19} and 10^{21} carriers per cm^3. In this range, typical materials are heavily doped semiconductors. Compared to them, electrical and thermal properties of metals are directly related by electrons. On the other extreme, non-metals just have too low electrical and thermal conductivities.

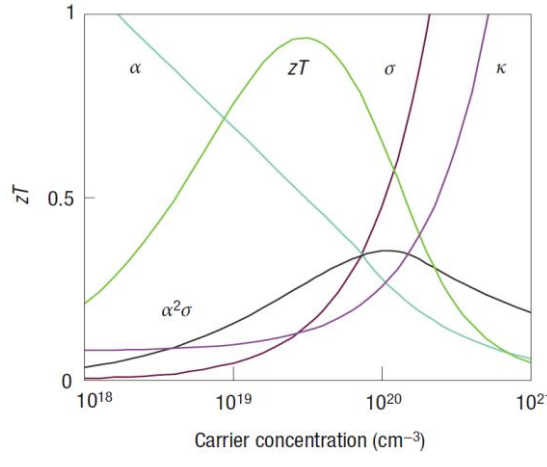

Fig. 1.24 - Compromise of material properties to maximize zT [56].

In the past several decades, laboratory zT values have been increased several fold. Thermoelectric materials being intensively studied include bismuth and bismuth-antimony, lead telluride and related compounds, silicon-germanium alloys, skutterudites and clathrates, oxides, and some other types, e.g., zinc antimonide, half-heusler compounds, metal silicides, and boron carbide [53,83]. To achieve higher zT values on these materials, typical material treatment methods include nanotechnology [84], reducing device dimensionality [85,86,87], engineering the band structure by doping [88,89], and exploring

new materials with complex crystalline structure [56,90]. Fig. 1.25 presents the history of zT and some recent achievements in labs [65,91]. Yet most of these materials or devices have not been available in market by today. So far as actual applications are concerned, bismuth telluride is still the most common thermoelectric material with $zT \approx 1$ [65,68,92]. Unfortunately, zT must have values of two or higher to enable thermoelectrics from niche applications into the mainstream of energy technologies.

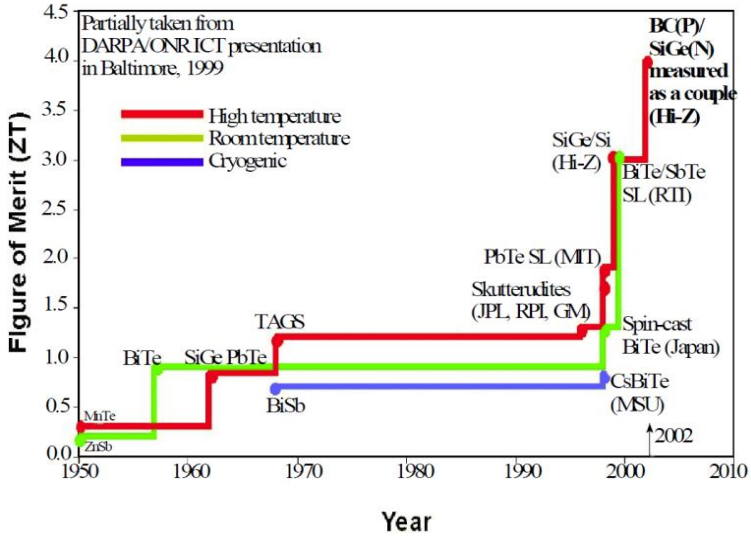

Fig. 1.25 - History of Thermoelectric Figure of Merit, ZT.

Until now, most efforts are being done on the reduction of the thermal conductivity for higher zT value from various scattering sources to block the phonon propagation [88]. It is believed that further reduction in the thermal conductivity alone may be sufficient to raise zT up to 2. For zT values of 3 or even higher, it is becoming essential to enhance both the Seeback coefficient and the electrical conductivity steadily. In order to realize these breakthroughs, a clear challenge for the thermoelectric research community is to understand exactly the physics behind the reported high zT values [65,78,88].

It should be mentioned that, besides the theoretical immaturity, there are also some other factors hampering the progress for higher zT. They are the measurement inaccuracy and material sensitivity [54]. The temperature gradients, particularly larger ones, induce considerable systematic inaccuracies, which could easily make the zT uncertainty reach 50%. Moreover, the material sensitivity to its impurity, dopant concentration variation and inhomogeneity

makes the measurement accuracy far worse. These factors are also the reasons that many materials reported with remarkable high zT values, but few have been confirmed by others.

TE material developing is under so intensive research that many novel materials come out every day in literature. Since this project is application-oriented, it is not in this project's scope to go too deep into thermoelectric material science. For more detailed reviews, these books [53,54,93,94], review papers [56,92,95,96,97] and some other papers cited above are excellent references.

1.5.2 Module Design and Operating Concerns

Module-level (also called device-level) researches on thermoelectrics have been done on [98]:

- The geometric parameters of thermocouple legs (ratio of length to cross-sectional area and non-uniform shape) [99],
- The combination optimization of n- and p- type legs [100],
- The thermal and electrical contact resistances [101],
- The Joule heat effects due to the material electric resistance [102,103],
- Heat and its induced thermal stress from Thomson effect [104,105,106,107],
- The effects of futile heat transfer forms (e.g., the inner reverse heat convection and heat losses to the ambient) [108],
- The dynamic behaviors of TE device [109,110],
- The effects of thermocouple arrangements in segmented and cascaded/multi-stage TE devices [111,112].

These studies not only cover the design, modeling, optimization and fabrication of the hardware (the concrete thermocouple and module), but also include some operating strategy considerations, such as the proposed "pulse mode" operation of TEG modules for higher efficiency in [109]. Of TECs, transient cooling effect for improved performances has been extensively investigated [113,114,115]. Working mode switch between TEG and TEC is also considered by Buist and Lau in [116]. They concluded that TECs can be safely used as TEGs and vice versa. Working as TEGs, TEC modules provide the highest conversion efficiency, since TEC modules are fabricated from the highest performance material available for that temperature range. In other words, material requirements of TECs are more rigorous. Admasu et al. [117]

analyzed the effects of temperature non-uniformity on a module and concluded that uniform temperature distribution delivered better module power output.

TECs can carry out bidirectional heating and cooling and they act fast. A conventional single-stage TEC module can achieve a cooling target in several seconds; novel thin-film TEC modules are even faster and on the order of milliseconds [82]! Whether it is heating or cooling depends on the direction of the electric current put on the module. They are also capable: a conventional TEC module can generate a temperature difference up to 70℃ between its two substrate surfaces, or can drive a heat flux at a rate of 125W [118]. As Yang and Stabler concluded in [119], TEC characteristics have not been fully harnessed in applications.

In [120], Gao and Rowe concluded that inner electrical and thermal contact resistances will probably have no substantial effect on module performances as long as leg length of thermocouples not short than 1mm. Later in [99], they theoretically and experimentally proved that a reduction in thermocouple leg length can significantly enhance the module power output by about 75% but slightly lower the module efficiency by 8%. This conclusion also has important economic benefits and can save nearly 50% of the module cost, based on the assumption that these modules have at least 20-year lifetime. Xuan [121] draws similar conclusions. Besides the module cost, heat exchanger and operating costs were also considered in the report.

As mentioned previously, Thomson effect is typically neglected in applications under the condition that temperature gradients or fluctuations are relatively modest and no large electric current is drawn out [55,122,123]. However, as proved in experiments [124,125,126], Thomson coefficient can be on the same order of magnitude of Seebeck coefficient. Thomson heat affects the module performances evidently and brings extra thermal stress onto thermocouples aside from the Joule's heat [107].

1.5.3 Thermoelectric Applications

1.5.3.1 TEG Applications

TEGs are competitive in waste-heat recovery, but rarely used as primary power suppliers due to their low heat to electricity ratio [127]. Major waste-heat sources could be industrial processing heat, cogeneration system, waste heat from the transportation sector, and municipal solid waste. In contrast with conventional energy conversion systems, TEG systems can be more suitable to

these energy sources because of the desirable merits, such as no moving parts, simple configuration, long-run unattended operation for thousands of hours, adaptability for any temperature range or energy level, no scaling effect from mW to several hundred kW, and so on [54].

In applications, a practical TEG system basically consists of four parts [119,139]:

- **A support structure**, a heat exchanger housing, which works as a heat source, and on which surfaces the thermoelectric modules are located. It generally looks like a tube with modified inner faces to benefit the heat absorption from the exhaust media (gases or liquids). It can also include a fuel combustion unit to provide heat, if sufficiently efficient TEG modules can be designed [119].
- **TEG modules**, the heat-power convertors, the materials of which need tuned accordingly to the operating temperature range (the exhaust media temperature), as mentioned above.
- **A heat rejection system**, a heat sink. The function is to maintain temperature gradients through the TE modules by drawing heat from them and rejecting the heat out of the TEG system.
- **An electrical power conditioning and interface unit**, to bridge the TEG system and external electric load and to keep the TEG system working around its maximum power point.

The whole TEG system should be studied as an integrated solution, because TE material properties and heat exchanging performance are closely linked [128]. There are also other auxiliary parts, such as valves, pumps, fans, sensors and controllers to make sure the TEG system working properly. Due to the present low efficiency of TEGs, the power consumption of these balance of plant (BoP) needs to be elaborately reduced for higher net power output of a TEG system.

1) TEG and fuel cells

Exhaust heat from various fuel cells is low-grade in general for TEGs. The application of TEGs in recovering this exhaust heat is relatively novel. In 2004, Huston et al. finished a report named: Application of Thermoelectric Devices to Fuel Cell Power Generation: Demonstration and Evaluation [129]. It is the first project that has systematically studied applying TEGs in a fuel cell system for increased electrical generation efficiency and reduced environmental impacts. This feasibility study was carried out on a UTC 200kW Phosphoric

Acid Fuel Cell Power Plant (PC25C) and TEG modules manufactured by Leonardo Technologies, Inc. (LTI). Tasks were conducted on TEG potential contribution assessment, site assessment, installation and initial operation and supplementary TE wafer (single thermocouple) study. Precious experiences and lessons were gained. TE Device test stands (Control & Data Acquisition System) and procedures were developed. Cost estimations were accomplished. However, system optimization was not carried out in this project.

Chen et al. [130] proposed a PEMFC-TEG system. In the system, TEGs were used to recover the exhaust heat from a HT-PEM fuel cell stack. A module-level three dimensional full-geometry physical TEG model in ANSYS FLUENT® was prepared for the convenience of the co-design and co-optimization of the system. A prototype PEMFC-TEG setup was also demonstrated in the lab. The TEG system developed is an aluminum exhaust pipe with hexagonal cross-sectional shape and un-finned bare inner surface. TEG modules are anchored on the pipe external surface. In this work, model was prepared; experiments were carried out to validate the TEG model. However, optimization was neither done on the TEG system nor its operational scenarios.

A solid oxide fuel cell and TEG (SOFC-TEG) hybrid system was studied in [131] using a zero-dimensional system model. Heat recovery through a regenerative heat exchanger was assumed ideal. SOFC and TEG were supposed working under the same current density. The main parameters and the optimally operating regions of the hybrid system, SOFC and thermoelectric generator were determined. More recently, the application potential of TEGs in a SOFC micro combined heat and power (CHP) system was assessed by Rosendahl et al. [132]. Results proved that with TEG application it is possible to increase the micro-CHP system power output by more than 15%, or system efficiency by some 4 to 5 percentage points. However, the tested hybrid micro-CHP did not gain those percentage points as inefficient commercially available TEG modules were applied. Energy flow analysis and new designs of TEG systems were also prepared for future work.

Kuo et al. [133] designed and built a LT-PEM fuel cell thermoelectric cogeneration system in the lab. It is a sophisticated system that provides both high-quality electric power and heated water. Key components include the fuel cell stack, hydrogen feeding subsystem, air supply subsystem, humidifier subsystem, and TEG heat recovery subsystem. System dynamic simulation and a comprehensive analysis were conducted both theoretically and

experimentally. The concurrent simulation was carried out in MATLAB/Simulink to guide the system design beforehand and facilitate operation analysis afterwards. The model accuracy was proved >95%. Experiments showed that the combined efficiency was higher than 92%. However, almost no details on design and optimization of the TEG subsystem were addressed in the report. Results also indicated that the TEG heat recovery contribution to the cogeneration system efficiency seemed limited, which was only about 1%. Still, this work is a detailed reference of the design and operation of a fuel cell-TEG cogeneration system.

An idea of employing a cylindrical TE p-leg as the cathode material of a SOFC single cell for an additional electric potential was explained in [134]. It is a novel way of applying TEGs in a SOFC system. Results showed that the open circuit voltage of the cell increased, ascribed to the additional TE voltage.

2) TEGs in automotives

TEG applications on waste-heat recovery from the transportation sector (especially in vehicles) have been thoroughly studied for decades. The motivations of integrating TEGs into automotives are stimulated by the pursuit for high system efficiency, the emission regulations (especially CO2) and the advantages of TEGs.

Birkholz et al, in collaboration with Porsche studied the installation of a TEG system into Porsche 944 in the 1980s [135]. Nissan Research Centre has also developed TEGs for different temperature ranges and tested them under different working conditions of ICEs [136,137]. In Japan, there was another a national project launched from 2002 by the New Energy and Industrial Technology Development Organization (NEDO), named “The Development for Advanced Thermoelectric Conversion Systems” [138].

Vázquez et al. reviewed most of the past automotive projects (Porsche, Nissan, Hi-Z projects), which had reported relatively low efficiencies [139]. In this paper, he concluded that the following factors should be considered in constructing an efficient TEG system:

- The space and weight of a whole TEG system are constrained and the support structure takes the major part.
- The inner part of a support structure is often finned and/or hole-plate to enhance heat convection. The optimization of its geometry is vital, since: proper turbulence needs to be generated for better heat convection;

pressure drop caused by the inner structure should be controlled; its size should be appropriately tuned to enable all TEG modules to keep working near their peak performance points; its material is also important covering both performance and lifetime aspects. The heat exchanger degradation mechanisms should also be counted.

- Different TEG module materials and configurations may need to be chosen for various temperature ranges. In some cases, the shape, size and configuration of the thermocouples are also taken into account for higher efficiency, space taken, mechanical strength and so on.
- The heat sink design and its integration. Heat sinks reported in most automotive applications are designed as liquid coolant jackets in aluminum and integrated as part of the ICE coolant circulation system. Few are air-cooled radiator. The integration method is also quite important to improve for the efficiency.
- TEG mounting methods. The mounting methods should guarantee lower contact resistance on both surfaces of a module and be elastic to compensate thermal stress.
- Thermal and electrical insulation of TEGs. Thermal insulations done on modules should be both inner-module and external between the ambient. Inner heat bypasses between thermocouples and heat loss to the ambient can both affect the module performance significantly. It needs to be sure that most heat passes through thermocouple legs instead of the bypasses. Electrical insulation is an important part of all electrical systems and also important to eliminate safety hazards.

Later, Saqr et al. has done a more detailed and theoretical analysis on these factors [140]. After a theoretical analysis on TEG system energy balance, this paper reviewed the following TEG systems reported in literature: a 1kW system from Hi-Z Inc., a 35.6W system from Nissan and a 300W HZ-20 system jointly built by Clarkson University, Delphi Systems and General Motors (GM). He summarized that the following four main factors controls the efficiency of a TEG system:

- Heat exchanger geometry
- Heat exchanger materials
- The installation site of the TEG
- The coolant system of the TEG

In recent years, several companies in vehicle industry, BMW/Ford, GM, General Electric, and Cummins, have accomplished a few vehicle-TEG

cogeneration projects funded by the US Department of Energy Freedom Car Office, in the scope of the "Advanced combustion Engines" research plan [141,142]. In these projects, TE materials and material-related supports were provided by Marlow Industries. G. Jeffrey Snyder from Jet Propulsion Laboratory was consulted on material theory and segmenting technology. Crane et al. from Gentherm subsidiary BSST proposed the integration architectures and assisted the above companies to bring into practice [143]. They have done detailed systematic researches on TEG integration and optimization. Most of the results are already published and patented. As part of the fruits, GM has developed a TEG exhaust heat recovery system and tested on a Chevrolet Suburban. Some experiences and results can be found in [144,145].

Another project also funded by DOE was on TEG waste-heat recovery from stationary diesel generators [146]. TEG system architectures were evaluated and analyzed. Fuel diversity effects were also studied. An economic analysis was carried out and coded in Visual Basic to facilitate other similar projects.

In addition, there are also some other teams who have done a great amount of research examining vehicle exhaust heat recovery. Hendricks et al. [128,147,148,149] has created a generic generator model and subsequently optimized the system under various conditions and TEG materials. Thacher et al. [150,151,152] concentrates on testing and optimizing TEGs in vehicle exhaust heat recovery applications. Instead of most other studies focusing barely on TEG systems, they paid much attention to their impacts on whole vehicle systems. Full of details, their studies are valuable and practical samples.

Espinosa et al. from European vehicle companies AB Volvo and Renault Trucks SAS also undertook a numerical investigation on the feasibility of applying TEGs to recover the exhaust heat from a truck diesel engine [69]. TEG modules they used are uni-couples, i.e., a single module contains a single thermocouple. Temperature unevenness among TEG modules and its effects on TE material properties were considered. The whole TEG assembly was divided into two parts: high temperature portion and low temperature portion. TEG modules composed of Mg_2Si/Zn_4Sb_3 were for high temperatures followed by Bi_2Te_3 for the low temperature portion. Compact plate-fin heat exchanger 'Strip-fin plate-fin, surface 1/4(s)-11.1', which was used here for the diesel engine exhaust gas, was directly taken from a mass-produced exhaust gas recirculation (EGR) unit. It was composed of five plates, each of which included a hot-side heat exchanger housing, a cold side and an intermediate

wall. Water coolant from the engine at 90℃ was circulated in the cold side as the heat sink. TEG modules were supposed mounted in the walls. The whole TEG system was then numerically discretized by the size of modules through the finite-difference method in engineering equation solver (EES) software. After model validated, the number of modules along the exhaust gas flow direction was optimized under two conditions: a) all the modules were electrically in series; b) all of them were in parallel. These are also the only two electrical connection styles of all the TEG modules considered in this work. In the above analysis, the number of modules perpendicular to the exhaust gas was fixed to 100. Afterwards, it was variable and studied for a fixed total number of modules, 10000, all of which were assumed electrically in parallel. System pressure drop and power output were plotted. In the end, the optimum ratio between the two TE module portions has been addressed. This study is an entire piece of work with plenty of practical and detailed considerations.

In recent few years, there are also some other studies on vehicle-TEG cogeneration. Andersson from Scania AB studied different power conditioning techniques for TEGs in vehicle waste heat recovery [153]. Two different Maximum Power Point Tracking (MPPT) technologies were compared. It was concluded that for the tens of watts TEG-rig worked on, a switching network with two states seems more efficient than a DC/DC converter. Phillip et al. [154] investigated two MPPT algorithms for TEGs: the perturb and observe (P&O) algorithm and extremum seeking control (ESC). The study was carried out in MATLAB/Simulink. The results showed that an ESC MPPT algorithm in combination with a buck-boost DC-DC converter was more favorable for TEG systems. Various MPPT algorithms for TEGs were also reviewed and compared by Chatzidakis et al. in [155]. It was concluded that, compared to short circuit current method (Isc), open-circuit voltage (Voc) method is more practical for TEG systems with power output less than 1kW. For over 1kW TEG systems, P&O method and Incremental Conductance method (InC) are more competitive, although they are more complex. Transient behaviors of a TEG-EGR system was simulated using a 3D CFD model by Högblom et al. [156]. They concluded that the greatest heat transfer resistance was identified in the gas phase and it was a tricky tradeoff between the heat convection performance and the maximum allowable pressure drop. A thermal buffering device was developed by Mizuno et al. to cope with temperature fluctuations for a TE power generator [157]. There are also some other studies on these similar topics [158,159,160,161].

Besides all the aforementioned TEG application studies, some other application potentials, e.g., in wearable electronics [162], in furnaces or stoves [163], on ships [164], as sensors [165], in wireless sensor or telecom networks [166], in photovoltaic-TEG hybrid systems [167] etc., have also been analyzed. Compared to them, researches on vehicle-TEG cogeneration are more systematic and thorough. Publications from these researches are the main references in relation to this project.

1.5.3.2 TEC Applications

TECs, which are also well known as Peltier coolers, have been successfully commercialized for decades. The merits of them are that they are unique miniature heat pumps and can manipulate high heat-flux transfer swiftly and precisely. In contrast, conventional fluid-refrigerant systems may be more efficient in kW-level applications or above. They are just too bulky to suit high-performance, compact cooling systems, from milliwatts to hundreds watts. In addition, characteristics like system simplicity, maintenance-free, noiseless, rugged, highly scalable, and low cost in mass production, make TECs more competitive [54]. Although there are still some other future miniature refrigeration cooling technologies, such as MEMS vapor compression and capillary pump loop (CPL), none of them are yet commercialized [168]. In applications, TEC systems usually have quite similar elements and design and operation concerns as the abovementioned TEG systems.

In electronic or optoelectronic cooling applications, TECs have been widely deployed to remove heat from the surfaces of microchips and other component, to cool down infrared detectors and charge-coupled devices (CCDs), and to stabilize the temperature of laser diodes etc. [168,169,170]. The purposes are to maintain a safe temperature for, to increase the working frequency of and reduce electromagnetic noise in integrated circuits.

TE dehumidification has been examined by several researchers. Vian et al. developed a small dehumidifier prototype made up of three TEC modules and optimized its design and performance by a homemade computational model (AERO) [171]. Their system COP was proved much lower than the vapor-compression devices. Another study was conducted by Jradi et al. [172] who constructed an integrated TE-photovoltaic renewable system to dehumidify air and produce fresh water. A system model was also built and validated by experiments. They determined that the air flow rate, air inlet conditions and electric current input to the TEC modules were the controlling parameters. The system was considered practical for stand-alone remote areas applications.

Automotive applications of TECs are believed of great interest [119]. TECs have the potential to bring revolution into automotive heating, ventilation, and air-conditioning (HVAC) systems, as the forthcoming TE-HVAC systems have many desirable features. They can be more silent and compact, potentially lighter, faster, more reliable and durable than today's conventional systems. Actually, some mature products are already available in the market, such as climate seats from Gentherm [173].

There are still many other applications of TECs, e.g., in mug rugs, in cup holders, in picnic baskets, in mobile freezers, as sensors, in reformers and in medical instruments [118,174,175]. As Yang and Stabler commented in [119], the entire potentials of TECs, especially their quick response and bidirectional heating/cooling capabilities, are not yet fully appreciated or utilized.

1.6 Project Objectives

The general motivation of this PhD study is to improve the performances of a methanol-fueled HT-PEM power system by virtue of TE device integration. In particular, TEGs are introduced with the purpose of increasing the system efficiency through recovering the exhaust heat; system dynamic performance, the load-following capability, is also hopefully to be enhanced by applying TECs for a better heat management of components, in turn, improved system efficiency can also be envisaged.

In previous sections, the theories and features of the components being worked on and experiences of similar projects in literature have been studied and surveyed. To form the detailed tasks and to draw the roadmap of this project, the present study comprises the answers of the following questions:

1) What are the application potentials of TE devices in the HT-PEM system?
2) How to optimize the performance of the TEG subsystem?
3) What are the controlling parameters of the design and operation of the TEG subsystem?
4) What is the optimal design of the TEG subsystem?
5) Can TECs improve the performances of the methanol evaporator in the HT-PEM system?

The initial question is with the purpose to draw a blueprint of the whole project. Answers to it have embodied Paper 1, in which question 5 is also partially consisted. Question 2-4 are then formulated to examine TEG contributions to

the HT-PEM fuel cell system in details. Answers to these questions are the main body of this study and contribute the major improvement to current state-of-the-art studies on TEG applications. These answers are presented successively in Paper 2, 3 and 4. The last question is meant to assess the roles of TECs in a TE-integrated methanol evaporator. Feasibility of the new evaporator design is proved by simulation results elaborated in Paper 5. In this paper, contributions to the research community on exploring novel applications of TECs are embodied by a new concept as well.

2 Methodology

In this chapter, the methodology employed in this research is described in detail. Overall, it consists of four parts: modeling of the HT-PEM fuel cell stack, design and modeling of the TEG subsystem, overview of TEG subsystem characteristics, and modification of the methanol evaporator.

2.1 Modeling of the HT-PEM Fuel Cell Stack

The scheme, energy flow, operating principles and main issues of the current HT-PEM fuel cell power system have been introduced in section 1.3.4. Since the fuel cell stack is the main exhaust heat source [48], modeling of it is of first priority. A short literature survey has picked out several major research groups working on HT-PEM fuel cell modeling. They are listed in Table 2.1.

Table 2.1- Some research groups on HT-PEM fuel cell modelling.

Authors	Model features	Publications	Solvers
Cheddie, Munroe et al.	2D, 3D; single-phase, multi-phase; isothermal, non-isothermal; pure-numerical, semi-empirical	[176,177,178,179, 180,181,182]	COMSOL Multiphysics®
Sousa, Mamlouk, Scott et al.	2D, single phase, isothermal	[183,184]	COMSOL Multiphysics®
Peng, Lee et al.	3D, single-phase, non-isothermal and isothermal	[185]	ANSYS Fluent®
lobato, Cañizares, Rodrigo et al.	3D, single-phase, isothermal, half-cell	[186,187]	COMSOL Multiphysics®
Korsgaard, Bang, Andreasen, Kær et al.	0D, semi-empirical, cell and lumped stack	[188,189,190,191, 192]	EES and Matlab Simulink®
Zenith et al.	0D, empirical, cell and lumped stack	[193,194,195,196, 197]	Matlab Simulink®/C++

These models can be roughly divided into two categories by the modeling purposes. First three groups are all about in-situ electrochemical modeling of phenomena happening in part of a single cell. Their models are more theoretical exhaustive and cell-design-oriented compared to the second category, the remaining two groups.

In the second category, the dynamic HT-PEM fuel cell model from Zenith et al. is specific for control purposes. Not like other models, this model uses the external load characteristic as the cell operating input, such as MOSFET transient. All the modeling and parameter regression were done at fuel cell working at 150℃. This study and the model created are exclusively focused on different time constants of various phenomena taking place in a fuel cell and scenarios handling them. In a word, they are all control-oriented, which are not so desirable to this project.

The HT-PEM fuel cell model composed by Korsgaard et al. uses a series of semi-empirical equations to express the fuel cell voltage versus current density, anode CO impurity, cathode stoichiometry and cell temperature. It is operating-oriented. This model shows excellent accordance with experiments on PEMEAS P1000 MEAs operated between 120℃ and 200℃, which gives the probability of carrying out an accurate heat-balance calculation on a HT-PEM fuel cell stack. Furthermore, taking into account of fuel contamination effects on the fuel cell performance offers more versatility for future work. Since this model is also on hand, it is chosen to describe the electrochemical reactions of the fuel cell stack in this work.

All the equations were written in EES, a general-purpose numerical solver. Another reason for choosing this software is that a sophisticated database of substance thermodynamic and kinetic properties is contained, which means higher accuracy of calculations, such as on the heat balance.

2.2 Design and Modeling of the TEG Subsystem

The TEG subsystem is designed for the cathode exhaust gas of the HT-PEM fuel cell stack. It is the main exhaust heat source, which conclusion is from the tentative assessment done in Paper 1 and shown below. In practice, it can be concluded from section 1.5.3 that a concrete TEG system is always composed of an assembly of numbers of TEG modules with efficient heat exchanging structures. They are together scaled properly to account for the magnitude of the exhaust heat sources.

Table 2.2 - Tentative assessment of all the possible TEG installation positions.

Position	T_H (℃)/T_C (℃)	Heat flux (W)	Representative materials	P_{peak}
Cathode exhaust	145/25	1012	Bi_2Te_3 & $(Bi,Sb)_2Te_3$	58W
Evaporator	250/70	329	Mg_2SiSn & Zn_4Sb_3	24W
Reformer	400*/250	160	Mg_2SiSn & Zn_4Sb_3	7W*
Cooler	205/25	39	Bi_2Te_3 & $(Bi,Sb)_2Te_3$	3.1W
Burner exhaust	137.5/25	34.5	Bi_2Te_3 & $(Bi,Sb)_2Te_3$	2W

*The temperature of hydrogen catalytic combustion is in the range 100 - 2210℃. Here a typical temperature is used.

2.2.1 The TEG Modules

First of all, the type of the TEG modules needs to be decided. Since the cathode exhaust gas temperature is below 200℃ and this project is application-oriented, conventional TEG modules made from bismuth telluride (Bi_2Te_3) are the prime choice. There will be certain amount of these modules in the TEG subsystem.

The next question is how to model all these Bi_2Te_3 TEG modules, the whole TEG assembly. In all those researches reviewed above, module models applied can be sorted into lumped models, one-dimensional models and multi-dimensional models. All these models are based on or derived from the classical analytical model from Ioffe, the Figure of Merit theory [52].

Lumped models are usually the direct use of Ioffe's theory. If material properties are independent from temperature and all the contact resistances are neglected, main equations for TEG modules are

$$\dot{Q}_h = \left(k_{tc}(T_h - T_c) + \alpha_{pn} T_h I - I^2 R_e^{tc}/2\right) n_{tc} n_{TEM} \tag{2.1}$$

$$\dot{Q}_c = \left(k_{tc}(T_h - T_c) + \alpha_{pn} T_c I + I^2 R_e^{tc}/2\right) n_{tc} n_{TEM} \tag{2.2}$$

$$P_e = Q_h - Q_c = \left(\alpha_{pn}(T_h - T_c) I - I^2 R_e^{tc}\right) n_{tc} n_{TEM} \tag{2.3}$$

Where $\dot{Q}_h$ means heat energy absorbed at the hot side and $\dot{Q}_c$ is the rejected heat from the cold side. n_{TEM} is the total number of TE modules in a system. P_e is the system power output. Similar as the above, control equations for TEC modules can also be derived from Equation (1.19) and (1.20).

TE devices described by these models can be a uni-couple module ($n_{tc} = 1$), a multi-thermocouple module ($n_{tc} > 1$), and multi-modules (a whole TE assembly, $n_{TEM} > 1$) [69,131,198,199]. Lumped models are scarcely applied in module-

level studies, because inner phenomena of a module cannot be described. They are more operating- or application- oriented. In other words, they are more system-level suitable. Though they seem all over-simplified, these models are handy tools to preliminarily assess performances of a TE system with satisfactory accuracy and help identify some key features. The tentative assessment conducted in Paper 1 is based on these lumped models.

One-dimensional (1D) and two-dimensional (2D) device models can be available for either module-level or system-level studies. Inner structure optimizations, i.e., module-level studies, assisted by 1D or 2D device models are numerous [99,108,120,200]. In system-level studies, representative device models are from Crane and Jackson [201], Espinosa et al. [69], Yu and Zhao [202], and Karri et al. [152]. TEG assemblies considered in their works consist of multi-modules. Dealing with uneven temperature and heat flux distributions, TEG assemblies in these models are typically discretized into control-volumes. Control volumes can be single thermocouples [202], uni-couple modules [69,201], and multi-thermocouple modules [152]. TEG performance in each control volume is calculated by the above lumped model. In general, these models can be expressed as:

$$\dot{Q}_h = \sum_{n_{TEM}} \sum_{n_{tc}} \left(k_{tc} (\mathrm{T}_h - \mathrm{T}_c) + \alpha_{pn} T_h I - I^2 R_e^{tc} / 2 \right) \tag{2.4}$$

$$\dot{Q}_c = \sum_{n_{TEM}} \sum_{n_{tc}} \left(k_{tc} (\mathrm{T}_h - \mathrm{T}_c) + \alpha_{pn} T_c I + I^2 R_e^{tc} / 2 \right) \tag{2.5}$$

$$P_e = Q_h - Q_c = \sum_{n_{TEM}} \sum_{n_{tc}} \left(\alpha_{pn} (T_h - T_c) I - I^2 R_e^{tc} \right) \tag{2.6}$$

α_{pn}, k_{tc} and R_e^{tc} can either be constant or varying with temperature. Most values of these variables in the above studies are directly substituted by material properties. Due to model simplifications, e.g., neglecting contact resistances, module performances deduced in this way are higher than tested. A simple solution is to adapt these values to fit [152]. Moreover, these studies usually involve module design optimizations, such as leg length, feature ratios and so on. For system-level studies, modules should be mature; they should have been optimized beforehand. Therefore, modules are just treated as black boxes in this work. Numerical discretization of them is also reconsidered. Our simulation results show that discretizing modules by thermocouples is unnecessarily fine; treating each module lumped is contrarily too coarse and module performance is overestimated in this way. Module parameters in our studies, α, k and R_e, are directly from workbench [203]. A typical test stand is shown as follows; test procedures can also be found in [203]. These empirical

module parameters are believed easier reproducible in real-life applications. Overall, modeling modules in such way has two advantages: a) mitigating the model complexity and b) keeping the model precision from vulnerable to simplifications.

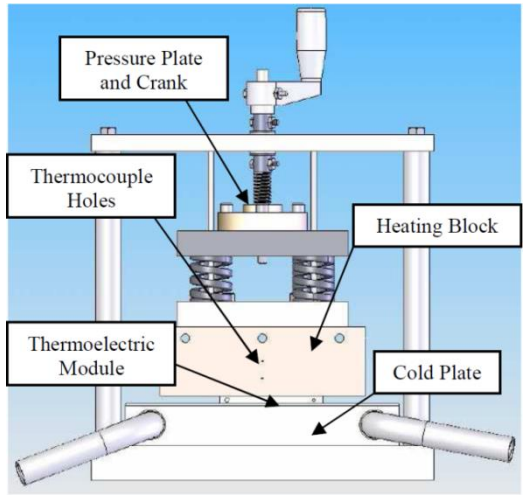

Fig. 2.1 - A test stand for module parameters [203].

Phenomena inside and outside of TE devices are not always uni-dimensional or bi-dimensional. TE device design and optimization are complicated. To count in all these phenomena and design and optimization aspects thoroughly and unconstrainedly, only three dimensional (3D) TE device models are capable. For the same reasons, these models are cumbersome to solve and numerical solvers, e.g., ANSYS Fluent® and COMSOL Multiphasic®, are used in most cases. These features further inherently determine that these models are powerful tools for module-level studies but difficult to use when up to system-level [98,106,107,117,130]. Representative models in this category are from Antonova and Looman [204] and Jaegle [205]. It is believed that a lot of work still needs to be done in this area especially after the thermoelectric mechanisms are understood more deeply in the future. In our work, TEC modules are modeled in 3D. The abovementioned two models combined with a simplified model from Chen and Snyder [206] were referred as literature input.

2.2.2 Heat exchangers

Heat exchangers are key components of a TE system and affect its performance significantly. Investigations under way in literature on heat exchanger performances include: fin geometry design, configuration

optimization, more precise simulation, and operation assessment. In the open literature, fin geometries widely used in TE applications are basic straight-base rectangular fins (illustrated in Fig. 2.2) and optimization of them has been scarcely addressed [152,201,202,203]. Discussions on different fin geometries and optimal heat exchanger configuration, i.e., mainly on optimal heat exchanger housing size, are even fewer [69,207,208,209,210,211].

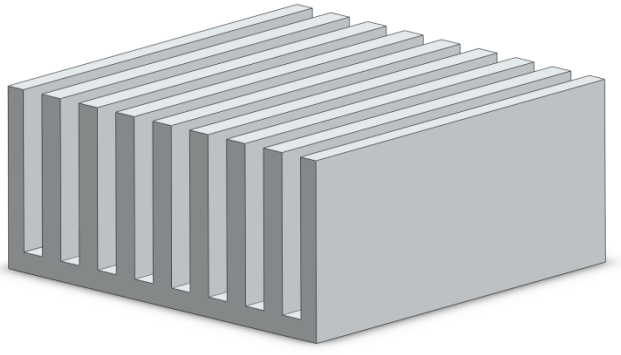

Fig. 2.2 - Illustration of straight-base rectangular fins.

In our work, the cold side of the designed TEG subsystem for the HT-PEM fuel cell stack is two blocks of water jacket, as shown in Fig. 2.3. Flowing inside these water jackets is the liquid coolant, liquid methanol/water fuel stored in the tank (shown in Fig. 1.7). The hot side heat exchanger of the TEG subsystem is for the exhaust gas from the fuel cell stack. Instead of the basic rectangular fin heat exchangers, compact plate-fin heat exchangers are chosen. Similar choice was made in [69]. Since in a gas-to-liquid heat exchanger, the heat transfer coefficient of the liquid side is ordinarily orders of magnitude larger than the gas side [212]. Following a broadly used simplification in literature, the two water jackets were represented by the ambient temperature in our studies.

The main effort was invested on optimizing the hot side. Compact heat exchangers, by their very nature, lead to high performance [213]. There are kinds of compact plate-fin heat exchangers [213], such as plain rectangular, plain trapezoidal, wavy, serrated or offset strip fin, louvered, perforated, and pin fin. Some are presented in Fig. 2.4. Which of them is more suitable in the current TEG subsystem yet needs to be answered. In [69], compact plate-fin

heat exchanger 'Strip-fin plate-fin, surface 1/4(s)-11.1'was directly from an optimized EGR unit. In our case, there is just no direct reference.

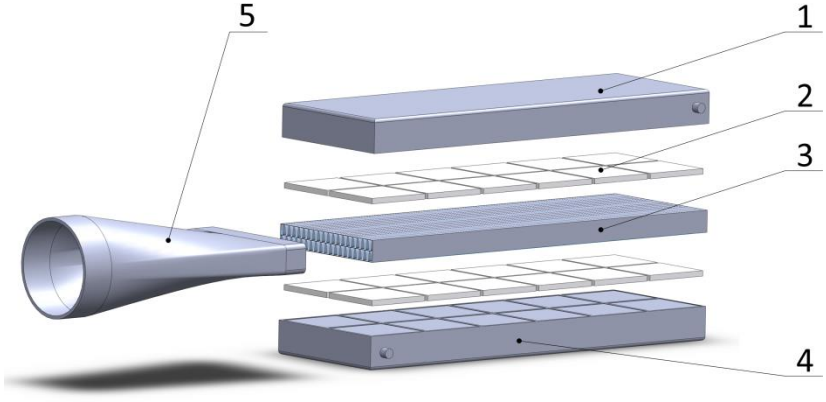

Fig. 2.3 - Design of the TEG subsystem (1,4 - Water jackets; 2 - TEG module assembly; 3 - Compact heat exchanger housing; 5 - Diffuser).

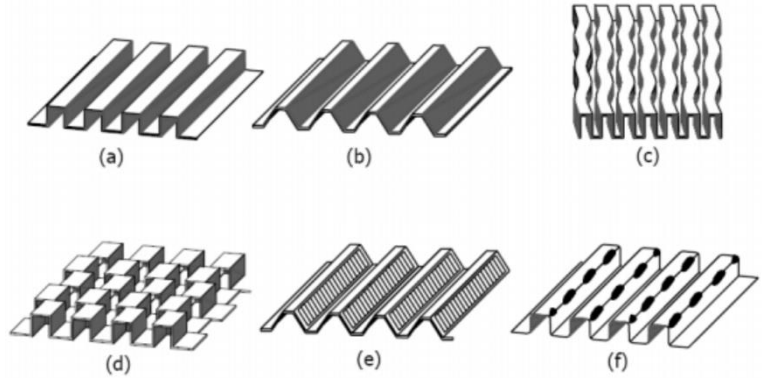

Fig. 2.4 - Types of fin geometries [214]: a) plain rectangular, b) plain trapezoidal, c) wavy, d) serrated or offset strip fin, e) louvered, and f) perforated.

The basic characteristics of a compact heat exchanger surface are its heat transfer and flow friction characteristics. They are commonly presented in terms of the Colburn factor j and Friction factor f versus Reynolds number Re. j can be defined as [212]:

$$j = StPr^{(2/3)}, St = \frac{\bar{h}_{out}}{Gc}, G = \frac{\dot{m}}{A_{min}}, Pr = \frac{c\mu}{k}, Re = \frac{GD_h}{\mu}. \quad (2.7)$$

In the above equations, St is the Stanton number and Pr is the Prandtl number. $\bar{h}_{out}$ is the fluid-heat exchanger heat convection coefficient. c is the fluid specific heat. G is the fluid mass flux. $\dot{m}$ is the mass flow rate. A_{min} is the minimum free flow cross section area of the heat exchanger. μ is the kinetic viscosity and k is the thermal conductivity of the fluid. D_h is the hydraulic diameter of the flow channels. After $\bar{h}_{out}$ is calculated from j, thermal conductance UA (the heat exchanging performance of the heat exchanger) can finally be identified. On the other hand, f determines the pressure drop of a heat exchanger, in turn the parasitic loss and net heat recovery benefit, through the following equation. Detailed definitions of variables in the equation can be found in Paper 2.

$$\Delta p_{hx} = \frac{u_{gas}^2}{2\rho_{gas,in}}\left[\frac{4 f_{hx} L_{hx} \rho_{gas,in}}{D_h \bar{\rho}_{gas}} + \left(1+\sigma^2\right)\left(\left(\rho_{gas,in}/\rho_{gas,out}\right)-1\right)\right] \quad (2.8)$$

For compact heat exchangers, the relationships between j, f and Re are unfortunately different for different surfaces and are hard to describe accurately by equations, although there are some correlations for less-critical design purposes in literature [215], such as Magahanic correlation, Wieting correlation and Joshi & Webb correlation. In other words, these characteristic data of compact heat exchangers are all empirical and screening as many kinds of compact heat exchangers as available is becoming the only choice for our purposes. Hereon, the database from Kays and London on compact heat exchangers [213] is becoming a handy tool and was referred to in our simulations. It includes a wide range of fin geometries and for which j and f are directly gained from series of experiments. The database has been extensively applied in industry for decades. For our studies, the other way, numerical predictions, is just again too cumbersome and easily mismatching from experimental data.

Optimizing a heat exchanger is always an art of compromise between heat exchanging performance and its pressure drop. Besides the fin geometry, the dimensions of the heat exchanger housing also matter. The reasons are that the cross section area of the heat exchanger housing determines Re of the fluid and the length of it decides the pressure drop. Nowadays, another factor, the MPPT power conditioning, is becoming an increasingly popular after treatment method of a TEG system. Whether it affects the heat exchanger design has

never been answered clearly in literature. All these uncertainties have been systematically analyzed in Paper 2 and 3.

2.3 Overview of TEG Subsystem Characteristics

A multiple parameter sensitivity analysis approach was performed on the TEG subsystem model to grab a whole picture of the subsystem characteristics. Structural and operating parameters that affect the subsystem performances most were helped identified. This approach was originally designed to assess the effects of measurement inaccuracy in experiments on calculated variables [216]. The assumption supporting this calculation is that all the input variables are uncorrelated and random. It means the covariance between them is assumed to be zero. Then the uncertainty in a system's performance can be expressed by the following equation. In our studies, this approach was imported through an uncertainty propagation tool in EES. Details can be found in Paper 2 and the main references [217,218,219].

$$U_\eta = \sqrt{\sum_i \left(\partial \eta / \partial X_i\right)^2 U_{X_i}^2}, \eta = f\left(X_1, X_2, \ldots, X_n\right). \tag{2.9}$$

2.4 Modification of the Methanol Evaporator

Modification of the methanol evaporator is with the purposes to benefit the whole HT-PEM system efficiency and its load-following capability from the merits of integrated TE modules. The integration takes place between the evaporator fins and the evaporation chamber through replacing the cartridge heaters in the original design with TE modules. The modification is illustrated in the following figure.

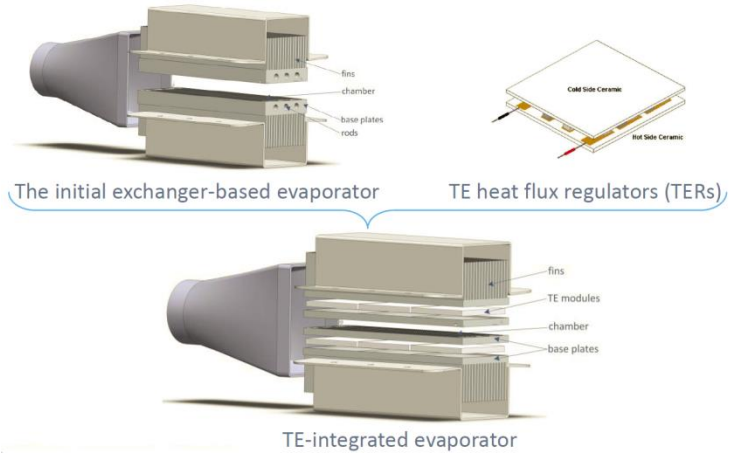

Fig. 2.5 - Modification of the methanol evaporator.

The feasibility and the advantages of the TE-integrated evaporator have been elaborated in Paper 5 by simulation. From energy balance standpoint, this modification reduces the heat loss of the original evaporator, in turn increases the efficiency.

Instead of uni-directionally heating or cooling, these integrated TE modules will alternately enhance and suppress the heat flux from the fins to the chamber and shift between the two modes frequently. That is to say, they regulate the heat flux. Moreover, the magnitude of the enhancement and suppression can be simply and instantly manipulated by the electric current supplied to the modules. All in all, these features will result in much more precise and swifter heat flux control inside the evaporator and a superheated methanol/water gaseous mixture with more accurately controlled temperature and flow rate. In short, the TE-integrated evaporator can be more efficient and with enhanced dynamic performance.

TEC modules herein are typically under rather small temperature gaps. They control the heat flux other than temperature. Their working modes are various and their dynamic performance is vital. To emphasize the specialties of this application, TE modules are named thermoelectric heat flux regulators (TERs).

Aside from the above TE-modification, there are already some other designs of the evaporator available in practice, for example, attaching the evaporation chamber directly to the surface of the fuel cell stack. However, this TE-

integrated evaporator has more control freedom and is of more theoretical and practical potentials.

3 Principal Results and Discussion

In this chapter, principle discoveries throughout the progress of this research project are summarized. They are organized by the working modes of the TE modules. Detailed results and discussions have been elaborated in all the papers.

3.1 TEG Exhaust Heat Recovery

A numerical model of the TEG heat recovery system is developed in EES and validated. It is a finite-element model with higher precision on fluid properties and heat transfer. It is also of higher flexibility for both design-type and simulation-type problems. In detail, its versatility is enhanced by integrating a database of 59-type compact plate-fin heat exchangers. A discretized ε-NTU solution method is additionally of great help.

Sensitivity analysis is conducted on the model and proves its value in understanding the characteristics of the subsystem. Main parameters affecting the design and operation of the subsystem are identified in descending priorities.

Through simulation, the optimal configuration of the current TEG exhaust heat recovery subsystem is confirmed. There are 48 TEG modules in the final configuration. As arranged in the following Fig. 3.1, 2 blocks, each with 2 rows of 12 modules are installed. They together decide the dimensions of the subsystem including the attached heat exchanger housing. The ideal type of the heat exchanger is 'Pin-fin plate-fin, surface PF-4(F)'. TEG module type was temporarily selected to be Melcor HT8, of which the performance data are from [203]. Taking into account of the MPPT power conditioning, all the modules are electrically divided in 3 branches along the exhaust gas flow, as represented in different colors in the figure. This configuration is optimized for

both on-design and off-design operating conditions. The methodology of optimizing the TEG subsystem is also concluded.

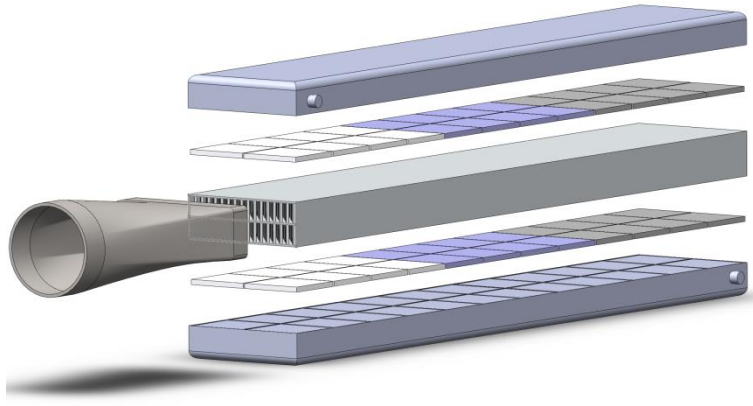

Fig. 3.1 - The final optimal architecture of the TEG subsystem.

The electrical connection style and the MPPT power conditioning of the TEG assembly affects the subsystem design in various aspects: the optimal size, the reliability and the performance, both on-design and especially off-design. Balanced between the subsystem performance and complexity, 3-branch scenario is currently the final decision. This can boost the subsystem power output by 12.9% versus the in-series configuration.

According to the module performance data from [203], these TEG modules only have a $ZT = 0.50$ in practice. As a result, the subsystem gives a 3.5% boost in the fuel cell system power output. However, it is generally accepted by the TE research community that $zT = 2$ is an informer of the beginning of massive commercialization of TEGs [119], which seems soon achievable [65,91]. After this commercialization barrier $zT = 2$ crossed, at least 10% increase in the power output can be expected. The results are shown in Fig. 3.2 and Fig. 3.3.

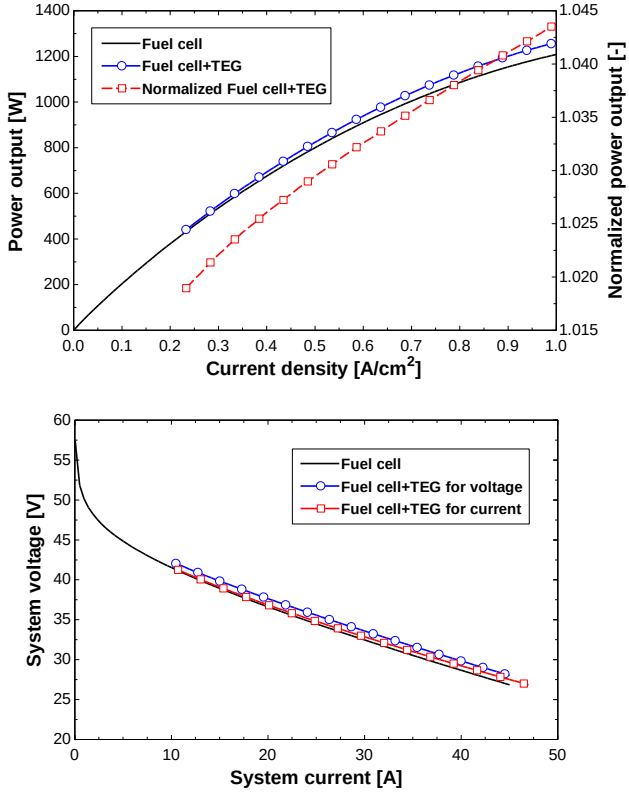

Fig. 3.2 - Contribution of TE heat recovery to the fuel cell system, ZT=0.50.

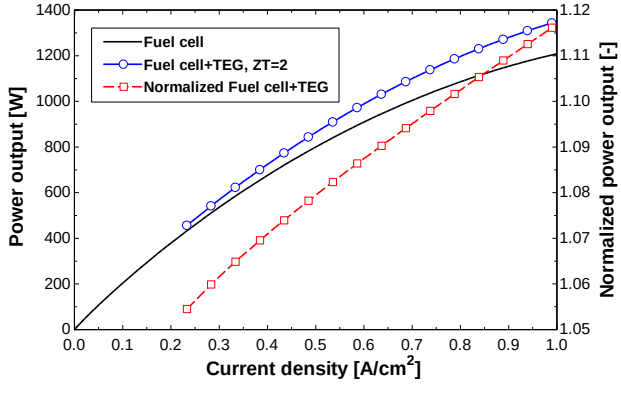

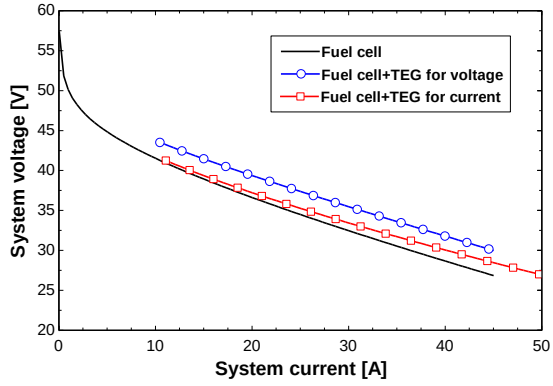

Fig. 3.3 - Expected contribution of TE heat recovery to the fuel cell system, ZT=2.

3.2 TE-integration in the Evaporator

TE-integration in the Evaporator is proved of mutual benefits. The evaporator in the initial design can only constantly produce 50.1W heat or above if with the supplementary electric heat from the cartridge heaters. As compared in Fig. 3.4, the TE-integrated evaporator can provide the chamber of 15.0-124.4W heat actively. Besides, the characteristics of TE devices can be more fully utilized when working as TERs. The TE-integrated evaporator furthermore losses less heat to the ambient and supplies electric heat more efficiently to the chamber during the system cold start.

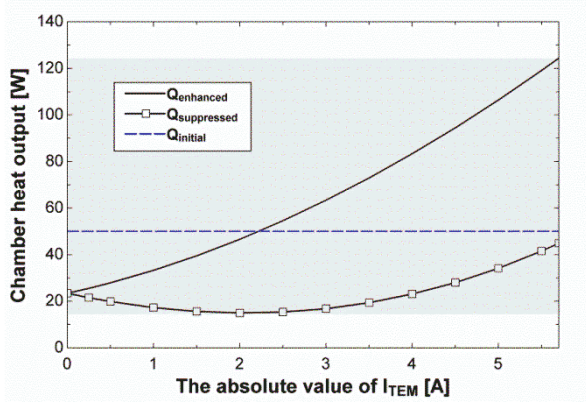

Fig. 3.4 - Differences in chamber heat output versus electric current between two designs of the evaporator.

A 3-dimentional evaporator model is set up in ANSYS FLUENT®. With the help of it, the heat output range of the TE-integrated evaporator has later been extended to 2.5W to 152.2W. This is achieved by finer rectangular fins of increased heat exchange surface area. However, the evaporator pressure drop is also increased simultaneously. As always, there is tradeoff between them. The numerical simulation also clarifies that axial conduction penalty is insignificant in the heat exchanger of the TE-modified evaporator.

4 Conclusions and Future Work

Two case studies on modifying a HT-PEM fuel cell system with TE devices have been carried out in this work. A TEG heat recovery subsystem was designed for recovering heat for electricity from the exhaust gas ejected out of the fuel cell stack. A numerical model was prepared and applied in optimizing the subsystem configuration for various working conditions of the fuel cell stack. Practices are carried out on identifying the optimal heat exchanger type, its proper dimensions for the subsystem and power conditioning effects on the subsystem design. Characteristics of the TEG subsystem are also analyzed through simulations. TECs are integrated into the methanol evaporator of the current fuel cell system to improve the load-following capability of the evaporator and the whole system. A numerical model for the TE-integrated evaporator is built and has assisted in all the analyses carried out and published. The feasibility of this TE-integration is presented. It is also proven that the whole system efficiency can be increased by the improved heat management of the TE-integrated methanol evaporator. This work has broadened the application of TE devices. The characteristics of TE devices have been more thoroughly explored and better utilized. All these add up to the scientific contributions of this work.

Throughout this work, it is shown that modifying the HT-PEM fuel cell system with TE devices exhibits several benefits and potentials. It is proven that the TEG recovered power can improve the fuel cell system efficiency during normal operation. However, more potential values of the TEG application in the current fuel cell system remain to be assessed by future work. Because of its simplicity of operation, the TEG subsystem can potentially assist the fuel cell system in some special occasions and supplement with some useful features to the fuel cell system. For example, the TEG power can kick in much earlier before the fuel cell stack temperature reaches 100 or 140℃, which can be utilized to drive the BoP components and prepare the stack startup. This whole idea has been introduced as ‘assist the system cold start’ in

Paper 1. The TEG power can also assist the fuel cell stack shutdown process and prepare it into standby mode. When the whole system is in standby mode, the TEG subsystem can treat the system as a heat capacitor and use the ambient temperature fluctuations to power up essential sensors and auxiliaries to monitor and maintain the fuel cell stack condition. Potentially, these 'special' applications can prolong the fuel cell lifetime and lower cost.

Up to this point, the TEG subsystem for HT-PEM fuel cell exhaust heat recovery has been optimized through simulations. Results show that the conducted optimization has increased the TEG subsystem power output by 12.9% through solely choosing an optimum power conditioning method. The power output improvement then goes up to 40.6%, when the performance differences between types of heat exchangers are also considered. Although it turns out that the current optimized subsystem takes approximately the same space of the fuel cell stack, it can only recover less than 100W power from the exhaust gas. This improvement is relatively small especially regarding that the fuel cell system is potentially for vehicle applications, of which power density is crucial.

However, the methodology of applying compact heat exchangers, modeling the subsystem and optimizing its configuration can be projected into various projects including the fuel cell system design and optimization itself. The design optimization of the TEG subsystem individually is an entire piece of knowledge preparation before TEGs are successfully commercialized.

For future work, practical concerns and the feasibility of deploying this TEG subsystem to increase the fuel cell system efficiency still need further experimental assessments. Larger scale system-level modeling and simulation study would also be beneficial. In detail, work can be carried out on the following topics:

1) Concrete system build and assessment in the lab. The more variables included the better. They can be:
    - heat exchanger type, size, material and fin geometry,
    - updated TEG modules of different materials, for example, quantum-well thermoelectric material or oxides [152],
    - electrical connection styles,
    - power conditioning technologies.
2) Modeling and simulation studies can be on:

- TEG subsystem water jacket design,
- TEG subsystem diffuser design, experimental work can also be included,
- dynamic performance study,
- HT-PEM-TEG whole system modeling and operation strategy study,
- A rigorous thermo-economic optimization.

3) TEG power output power conditioning, integration into the whole system, management and utilization can also be interesting.

TEC applications in the current fuel cell system, on the other hand, are already practical. The simulation work in Paper 5 has revealed that the integration of TE devices into the methanol evaporator can most likely make it work more efficiently and improves its controllability. Possible further work can be:

1) A new evaporator model in EES, as the current 3D finite-element model only describes part of the evaporator and will be cumbersome for study of the whole evaporator;
2) Thermal and fluid dynamic optimization;
3) The transient performance of the TE-integrated evaporator;
4) Control scenario study and corresponding control circuit consideration and buildup;
5) Experiments.

TECs have been widely applied in industry for a long time, because they are unique miniature and capable. Applications as TERs have the potential to redefine the device and have the possibility to let the device become epic.

References

[1] S.J. Andreasen. Design and Control of High Temperature PEM Fuel Cell System. PhD dissertation, Aalborg University, 2009; ISBN: 87-89179-78-1.

[2] WHO/UNICEF (World Health Organization/The United Nations Children's Fund). Joint Monitoring Programme (JMP) for Water Supply and Sanitation. 2011. http:// www.wssinfo.org/data-estimates/introduction.

[3] V. Ramanathan, G. Carmichael. Global and regional climate changes due to black carbon. Nature Geoscience 1, 221-227 (2008).

[4] United Nations Environment Programme (UNEP) Year Book 2013.

[5] U.S. Energy Information Administration (EIA), International Energy Outlook 2013, July 2013.

[6] GFN (Global Footprint Network) (2012). Annual report 2011. http://www.footprintnetwork.org/en/index.php/GFN/page/world_footprint/

[7] United Nations. 1987."Report of the World Commission on Environment and Development." General Assembly Resolution 42/187, 11 December 1987.

[8] Renewable Energy Policy Network for the 21st Century (REN21), Renewables 2013 Global Status Report.

[9] George A. Olah, Alain Goeppert, and G. K. Surya Prakash. Beyond Oil and Gas: The Methanol Economy, 2nd ed.; Wiley-VCH: Weinheim, Germany, 2009.

[10] Vincenzo Balzani, Alberto Credi, and Margherita Venturi.Photochemical Conversion of Solar Energy. ChemSusChem 1(1-2), 26-58, 2008.

[11] George W. Crabtree, Mildred S. Dresselhaus, and Michelle V. Buchanan. The hydrogen economy. Physics Today 57(12), 39 (2004); doi: 10.1063/1.1878333.

[12] George A. Olah. Beyond oil and gas: the methanol economy. Angewandte Chemie International Edition 44(18), 2636-2639, (2005); doi: 10.1002/anie.200462121.

[13] Ryan O'Hayre, Suk Won Cha, Whitney Colella, and Fritz B. Prinz. Fuel Cell Fundamentals. John Wiley & Sons, Inc., 2nd edition, 2009. ISBN 978-0-470-25843-9.

[14] F Barbir. PEM Fuel Cells: Theory and Practice. Academic Press. Elsevier / Academic Press, 2012. ISBN 9780123877109. URL http://books.google.dk/books?id=elO7n4Z6uLoC.

[15] Wolf Vielstich, Huber t A. Gasteiger , Arnold Lamm and Harumi Yokokawa. Handbook of Fuel Cells - Fundamentals, Technology and Applications. 2010 John Wiley & Sons, Ltd. ISBN: 978-0-470-97400-1.

[16] Larminie, J., & Dicks, A. L. (2003). Fuel Cell Systems Explained (2nd ed.). Chichester, UK: Wiley.

[17] Søren Juhl Andreasen, Jakob Rabjerg Vang, Søren Knudsen Kær. High temperature PEM fuel cell performance characterisation with CO and CO2 using electrochemical impedance spectroscopy. International Journal of Hydrogen Energy 2011;36: 9815-9830.

[18] Fuel Cell Today (2011). The Fuel Cell Today Industry Review 2011. Technical report, Fuel Cell Today. xiii, 5, 6, 11.

[19] T.A. Zawodzinski, J. Davey, J. Valerio, S. Gottesfeld, Electrochim. Acta 40 (1995) 297.

[20] G Sasikumar, J.W Ihm, H Ryu. Dependence of optimum Nafion content in catalyst layer on platinum loading. Journal of Power Sources 132(2004) 11-17.

[21] Lee J.H. and Lalk T.R. (1998a) "Modelling fuel cell stack systems", Journal of Power Sources, 73(2), 229-241.

[22] Giorgi L., Antolini E., Pozio A., and Passalacqua E. (1998) "Influence of the PTFE content in the diffusion layer of low-Pt loading electrodes for polymer electrolyte fuel cells", Electrochimica Acta, 43(24), 3675-3680.

[23] Ralph T.R., Hards G.A., Keating J.E., Campbell S.A., Wilkinson D.P., Davis H., StPierre J., and Johnson M.C. (1997) "Low cost electrodes for proton exchange membrane fuel cells", Journal of the Electrochemical Society, 144(11), 3845-3857.

[24] Mench, M. M. (2008). Fuel Cell Engines (1st ed.). Hoboken, New Jersey: Wiley.

[25] Xuan Cheng, Zheng Shi, Nancy Glass, Lu Zhang, Jiujun Zhang, Datong Song, Zhong-Sheng Liu, Haijiang Wang, Jun Shen. A review of PEM hydrogen fuel cell contamination: Impacts, mechanisms, and mitigation. Journal of Power Sources 165 (2007) 739-756.

[26] J.S. Wainright, J-T. Wang, D. Weng, R. F. Savinell and M. H. Litt. J. Electrochem. Soc. 142. L121 (1995).

[27] Wang, J., R. Savinell, J. Wainright, M. Litt, and H. Yu (1996). A H2/O2 fuel cell using acid doped polybenzimidazole as polymer electrolyte. Electrochimica Acta 41(2), 193-197.

[28] Y. Zhai, H. Zhang, G. Liu, J. Hu, B. Yi, J. Electrochem. Soc. 154 (2007) B72.

[29] D. Weng, J. S. Waimight, U. Landau and R. F. Savinell, Ext. Abstract, 188th Electrochemical Society Meeting. Chicago, IL, Oct 8-13, (1995).

[30] T.A. kawodziiski, Jr., T. E. Springer, J. Davey, R. Jestel. C. Lonez. J. Valerio and S. Gottesfeld. J. Electrochem.. Soc. 140, 1981 (l993).

[31] T.F. Fuller and J. Newman, J. Electrochem. Sot. 139, 1332 (1992).

[32] Serenus 166/390 Air C fuel cell module. http://serenergy.com/wp-content/uploads/2012/11/166_390-Air-C-data-sheet_v2.5-0210.pdf

[33] Das SK, Reis A, Berry K. Experimental evaluation of CO poisoning on the performance of a high temperature proton exchange membrane fuel cell. J Power Sources 2009;193(2): 691-8.

[34] Bellows RJ, Marucchi-Soos EP, Terence Buckley D. 1996. Analysis of reaction kinetics for carbon monoxide and carbon dioxide on polycrystalline platinum

relative to fuel cell operation. Industrial Engineering and Chemical Research 35(4):1235-1242.

[35] D.S. Watkins, 1993. Research, development and demonstration of solid polymer fuel cell systems. In Fuel Cell Systems, Blomen L, Mugerwa M (ed.). Plenum Press: New York, 493-530.

[36] Salvador M. Aceves, Gene D. Berry, Joel Martinez-Frias, Francisco Espinosa-Loza. Vehicular storage of hydrogen in insulated pressure vessels. International Journal of Hydrogen Energy 31(2006) 2274-2283.

[37] Joan M. Ogden, Margaret M. Steinbugler, Thomas G. Kreutz. A comparison of hydrogen, methanol and gasoline as fuels for fuel cell vehicles: implications for vehicle design and infrastructure development. Journal of Power Sources 79(1999) 143-168.

[38] Bård Lindström, Lars J. Pettersson. Hydrogen generation by steam reforming of methanol over copper-based catalysts for fuel cell applications. International Journal of Hydrogen Energy 26(2001) 923-933.

[39] Divisek J, Oetjen H-F, Peinecke V, Schmidt VM, Stimming U. 1998. Components for PEM fuel cell systems using hydrogen and CO containing fuels. Electrochimica Acta, 43(24):3811-3815.

[40] Yuka Oono, Atsuo Sounai, Michio Hori. Influence of the phosphoric acid-doping level in a polybenzimidazole membrane on the cell performance of high-temperature proton exchange membrane fuel cells. Journal of Power Sources 189(2009) 943-949.

[41] Jinfeng Wu, Xiao Zi Yuan, Jonathan J. Martin, Haijiang Wang, Jiujun Zhang, Jun Shen, Shaohong Wu, Walter Merida. A review of PEM fuel cell durability: Degradation mechanisms and mitigation strategies. Journal of Power Sources 184(2008) 104-119.

[42] Jinfeng Wu, Xiao-Zi Yuan, Jonathan J. Martin, Haijiang Wang, Daijun Yang, Jinli Qiao, Jianxin Ma. Proton exchange membrane fuel cell degradation under close to open-circuit conditions Part I: In situ diagnosis. Journal of Power Sources 195(2010) 1171-1176.

[43] Samuel Simon Araya. High Temperature PEM Fuel Cells: Degradation and Durability. PhD dissertation, Aalborg University, 2012; ISBN: 978-87-92846-14-3.

[44] Stolten, D. (2010). Hydrogen and Fuel Cells: Fundamentals, Technologies and Applications (1st ed.). Weinheim, Germany: Wiley-VCH.

[45] Alexandros Arsalis. Development of Next Generation micro-CHP System: Based on High Temperature Proton Exchange Membrane Fuel Cell Technology. PhD dissertation, Aalborg University, 2011; ISBN: 978-87-92846-03-7.

[46] http://serenergy.com/wp-content/uploads/2013/05/S-165L_datasheet_v1.0_0313.pdf

[47] X. Gao, M. Chen, G. J. Snyder, S. J. Andreasen and S. K. Kær. Thermal management optimization of a thermoelectric-integrated methanol evaporator using a compact CFD modeling approach. Journal of Electronic Materials. In press, DOI: 10.1007/s11664-013-2514-2.

[48] X. Gao, M. Chen, S. J. Andreasen, S. K. Kær. Potential usage of thermoelectric devices in a high-temperature polymer electrolyte membrane (PEM) fuel cell system: Two case studies. Journal of Electronic Materials 2012; 41(6): 1838-1844.

[49] Methanex Corporation, Technical Information & Safe Handling Guide for Methanol (Version 3.0, September 2006).

[50] Francis J. DiSalvo. Thermoelectric Cooling and Power Generation. Science 285, 703-706 (1999).

[51] Lon E. Bell. Cooling, Heating, Generating Power, and Recovering Waste Heat with Thermoelectric Systems. Science 321, 1457 (2008); DOI: 10.1126/science.1158899.

[52] A.F. Ioffe. Semiconductor thermoelements and thermoelectric cooling. London: Infoseach Limited; 1957.

[53] H. Julian Goldsmid. Introduction to Thermoelectricity. New York: Springer; 2010.

[54] Thermoelectrics Handbook Macro to Nano (ed. Rowe, D. M.), CRC Taylor & Francis, Boca Raton, 2006.

[55] Lazard M, Fraisse G, Goupil C, Scherrer H. Thermal analysis of a thermoelectric: a way to non conventional design. In: Proceedings of the 6th European Conference on thermoelectrics, vol. 1; 2008. p. 2-15.

[56] G. Jeffrey Snyder and Eric S. Toberer. Complex thermoelectric materials. Nature Materials 2008;7(2):105-114.

[57] J. Zhang, Thermoelectric Technology, 1st ed. Tianjin: China Tianjin Institute of Power Sources, 2008.

[58] G. Jeffrey Snyder. Application of the compatibility factor to the design of segmented and cascaded thermoelectric generators. APPLIED PHYSICS LETTERS, VOL 84, No. 13.

[59] G. Jeffrey Snyder and Tristan S. Ursell. Thermoelectric Efficiency and Compatibility. PHYSICAL REVIEW LETTERS, VOLUME 91, NUMBER 14.

[60] http://www.thermoelectrics.caltech.edu/

[61] Cronin B. Vining. The Limited Role for Thermoelectrics in the Climate Crisis. Solutions Summit, 20080501, NYC.

[62] D.M. Rowe, ed., CRC Handbook on Thermoelectrics (CRC Press, Boca Raton, FL, 1995).

[63] Seijiro Sano, Hiroyuki Mizukami, Hiromasa Kaibe. Development of High-Efficiency Thermoelectric Power Generation System. KOMATSU Technical Report, 2003 VOL. 49 NO.152.

[64] http://tegnology.dk/p/materials

[65] Cronin B. Vining. ZT ~ 3.5: Fifteen Years of Progress and Things to Come. The European Conference on Thermoelectrics, ECT2007, Odessa, Ukraine, Sept. 10-12, 2007.

[66] A. J. Minnich, M. S. Dresselhaus, Z. F. Ren and G. Chen. Bulk nanostructured thermoelectric materials: current research and future prospects. Energy Environ. Sci., 2009, 2, 466-479.

[67] Jihui Yang and Thierry Caillat. Thermoelectric Materials for Space and Automotive Power Generation. MRS Bulletin 31(03),2006: 224-229.

[68] C.B. Vining, "The thermoelectric limit ZT~1: Fact or Artifact," Eleventh International Conference on Thermoelectrics (ICT92), K. R. Rao, Ed. Arlington, TX USA: Univ. of Texas at Arlington, Arlington, TX, 1992, pp. 223-231.

[69] N. Espinosa, M. Lazard, L. Aixala, and H. Scherrer. Modeling a Thermoelectric Generator Applied to Diesel Automotive Heat Recovery. Journal of Electronic Materials. 23 June 2010.

[70] J. LaGrandeur, D. Crane, S. Hung, B. Mazar, and A. Eder. Automotive waste heat conversion to electric power using skutterudite, TAGS, PbTe and BiTe. Int. Conf. Thermoelectrics, Aug. 2006, Paper B10-2, pp. 1-6.

[71] D. Crane and L. E. Bell. Progress towards maximizing the performance of a thermoelectric power generator. Proc. Int. Conf. Thermoelectrics, pp. 1 2006.

[72] Rama Venkatasubramanian, Edward Siivola, Thomas Colpitts & Brooks O'Quinn. Thin-film thermoelectric devices with high room-temperature figures of merit. NATURE, VOL 413, 11 OCTOBER 2001.

[73] Gao Min and D M Rowe. Ring-structured thermoelectric module. Semicond. Sci. Technol. 22 (2007) 880-883.

[74] L.E. Bell and D.T. Crane, Int. Conf. Thermoelect. (Freiburg, Germany, 2009).

[75] Andreas Schmitz, Christian Stiewe, and Eckhard Müller. Preparation of Ring-Shaped Thermoelectric Legs from PbTe Powders for Tubular Thermoelectric Modules. Journal of Electronic Materials, Vol. 42, No. 7, 2013; DOI: 10.1007/s11664-012-2402-1.

[76] J. Weber, K. Potje-Kamlotha, F. Haasea, P. Detemple, F. Völklein, T. Doll. Coin-size coiled-up polymer foil thermoelectric power generator for wearable electronics. Sensors and Actuators A 132 (2006) 325-330.

[77] Wulf Glatz, Simon Muntwyler, Christofer Hierold. Optimization and fabrication of thick flexible polymer based micro thermoelectric generator. Sensors and Actuators A 132 (2006) 337-345.

[78] Christophe Goupil, Wolfgang Seifert, Knud Zabrocki, Eckhard Müller and G. Jeffrey Snyder. Thermodynamics of Thermoelectric Phenomena and Applications. Entropy 2011, 13, 1481-1517; doi:10.3390/e13081481.

[79] Ursell, T. S. and Snyder, G. J. Compatibility of Segmented Thermoelectric Generators.Twenty-first International Conference on Thermoelectrics ICT'02 412 (IEEE, Long Beach, California, USA, 2002).

[80] http://www.kryothermusa.com/indexd2f9.html?tid=79

[81] http://www.rmtltd.ru/company/news/details/?id=71

[82] S. Lee, Establishing a new performance paradigm with ultra-thin thermoelectric modules. (Nextreme Thermal Solutions) www.nextreme.com/media/pdf/articles/Thermoelectric_Cooling.pdf.

[83] Kunihito Koumoto, et al. Thermoelectric Ceramics for Energy Harvesting. J. Am. Ceram. Soc., 96 (1) 1-23 (2013). DOI: 10.1111/jace.12076.

[84] Jingfeng Li, et al. High-performance nanostructured thermoelectric materials. NPG Asia Mater. 2(4) 152-158 (2010). DOI: 10.1038/asiamat.2010.138.

[85] L.D. Hicks and M. S. Dresselhaus, Phys. Rev. B 47, 12727 (1993).

[86] L.D. Hicks and M. S. Dresselhaus, Phys. Rev. B 47, 16631 (1993).

[87] Raseong Kim, Supriyo Datta, and Mark S. Lundstrom. Influence of dimensionality on thermoelectric device performance. Journal of Applied Physics 105, 034506 (2009); Doi: 10.1063/1.3074347.

[88] Yanzhong Pei, Heng Wang, and G. J. Snyder. Band Engineering of Thermoelectric Materials. Adv. Mater. 2012, 24, 6125-6135. DOI: 10.1002/adma.201202919.

[89] J. P. Heremans et al., Enhancement of Thermoelectric Efficiency in PbTe by Distortion of the Electronic Density of States. Science 321, 554 (2008).

[90] Jong-Soo Rhyee et al. Peierls distortion as a route to high thermoelectric performance in $In_4Se_{3-\delta}$ crystals. Nature 459, 965-968, 2009. doi:10.1038/nature08088.

[91] V. Jovanovich and S. Ghmaty, "Design, Fabrication and Testing of Energy Harvesting Thermoelectric Generator," Proc. of SPIE, vol. 6173, pp. 1-8, 2006.

[92] G. Chen, M. S. Dresselhaus, J. P. Fleurial, and T. Caillat, "Recent Developments in Thermoelectric Materials," International Materials Review, vol. 48, pp. 45-66, 2003.

[93] J.P. Heremans, G. Chen, et al., Thermoelectricity: Thermoelectric And Thermomagnetic Properties in Lowdimensional And Nanoscale Materials: Springer-Verlag, 2007.

[94] J. Sharp, H. J. Goldsmid, et al., Principles of Thermoelectrics: Basics and New Materials Development: Springer Verlag, 2001.

[95] Joseph R. Sootsman, Duck Young Chung, and Mercouri G. Kanatzidis. New and Old Concepts in Thermoelectric Materials. Angew. Chem. Int. Ed. 2009, 48, 8616-8639.

[96] Terry M. Tritt. Recent Advances in Thermoelectric Nanocomposite Materials. http://meetings.aps.org/link/ BAPS.2010.MAR.P29.4.

[97] M.S. Dresselhaus, G. Chen, et al., "New Directions for Low-Dimensional Thermoelectric Materials," Advanced Materials, vol. 19, pp. 1043-1053, 2007.

[98] Min Chen, Design, modeling and utilization of thermoelectrical materials and devices in energy systems. Ph. D dissertation, Aalborg University, 2009.

[99] G. Min and D. M. Rowe, "Optimisation of thermoelectric module geometry for 'waste heat' electric power generation," Journal of Power Sources, vol. 38, pp. 253-259, 1992.

[100] N.M. Zhukova, et al, Sov. Phys. Semicond. 23 (1989) 1183.

[101] D.L. Medlin and G. J. Snyder. Atomic-Scale Interfacial Structure in Rock Salt and Tetradymite Chalcogenide Thermoelectric Materials. JOM, 65(3), 390-400, 2013; DOI: 10.1007/s11837-012-0530-y.

[102] A.K. Pramanick, P.K. Das. Constructal design of a thermoelectric device. International Journal of Heat and Mass Transfer 49 (2006) 1420-1429.

[103] Sisman A, Yavuz H. The effect of Joule losses on the total efficiency of a thermoelectric power-cycle. Energy, 1995;20(6):573-576.

[104] Chen J, Yan Z. The influence of the Thomson effect on the maximum power-output and maximum efficiency of a thermoelectric generator. J Appl Phys 1996;79(11):8823-8828.

[105] David Tai-ko Shaw. The static temperature distribution of a thermoelement with temperature varying parameters. Advanced Energy Conversion, 6 (1966) 57-65.

[106] Meijiau Huang, Ruey-Hor Yen, An-Bang Wang. The influence of the Thomson effect on the performance of a thermoelectric cooler. International Journal of Heat and Mass Transfer, 48 (2005) 413-418.

[107] Meijiau Huang, Po-Kuei Chou, Ming-Chyuan Lin. Thermal and thermal stress analysis of a thin-film thermoelectric cooler under the influence of the Thomson effect. Sensors and Actuators A 126 (2006) 122-128.

[108] E.F. Thacher. Heat loss and thermoelectric generator design. Energy Conversion and Management, 25 (1985) 519-525.

[109] Min Gao. Improving the conversion efficiency of thermoelectric generators through "pulse mode" operation. AIP Conference Proceedings 1449, 447 (2012); doi: 10.1063/1.4731592.

[110] Naji M, Alata M, Al-Nimr MA. Transient behavior of a thermoelectric device. Proc IMechE Part A: J Power & Energy 2003;217(6A):615-21.

[111] X.C. Xuan.On the optimal design of multistage thermoelectric coolers. Semicond. Sci. Technol. 17 (2002) 625-629.

[112] Lingen Chen, Jun Li, Fengrui Sun, Chih Wu.Performance optimization of a two-stage semiconductor thermoelectric-generator. Applied Energy 82 (2005) 300-312.

[113] Stilbans LS, Fedorovich NA. Cooling of thermoelectric cells under nonstationary conditions. Sov Phys Tech Phys 1958;3:460-3.

[114] Hoyos GE, Rao KR, Jerger D. Numerical analysis of transient behavior of thermoelectric coolers. Energy Conversion 1977;17:45-54.

[115] Snyder GJ, Fleurial J-P, Caillat T, Yang RG, Chen G. Supercooling of Peltier cooler using a current pulse. J Appl Phys 2002;92:1564-9.

[116] Richard J. Buist and Pad G. Lau. Thermoelectric Power Generator Design and Selection from TE Cooling Module Specifications. Thermoelectrics, 1997. Proceedings ICT '97. XVI International Conference on; DOI:10.1109/ICT.1997.667589.

[117] Bimrew Tamrat Admasu, Xiaobing Luo, Jiawei Yao. Effects of temperature non-uniformity over the heat spreader on the outputs of thermoelectric power generation system. Energy Conversion and Management, 76 (2013) 533-540.

[118] D. Martin, U.S. patent US20040042957 Al (4 March 2004).

[119] Jihui Yang and Francis R. Stabler. Automotive Applications of Thermoelectric Materials. Journal of Electronic Materials, Vol. 38, No. 7, 2009; DOI: 10.1007/s11664-009-0680-z.

[120] Min Gao, D.M. Rowe. Measurement of Electrical and Thermal Contact Resistance of Thermoelectric Device. Chinese Journal of Infrared Technology, 15(2), 1993, 15-18.

[121] X.C. Xuan. Optimum design of a thermoelectric device. Semicond. Sci. Technol. 17 (2002) 114-119.

[122] S. Wisniewski, B. Staniszewski, R. Szymanik. Thermodynamics of nonequilibrium processes, PWN-Polish Scientific Publishers, 1976.

[123] S.L. Soo, Direct Energy Conversion, Prentice-Hall Inc, 1968.

[124] K.F. Hsu, S. Loo, F. Guo, W. Chen, J.S. Dyck, C. Uher, T. Hogan, E.K. Polychroniadis, M.G. Kanatzidis, Cubic $AgPbmSbTe^{2+m}$: bulk thermoelectric materials with high figure of merit, Science 303 (2004) 818-821.

[125] V. Damodara Das, N. Soundararajan, Size and temperature effects on the Seebeck coefficient of thin bismuth films, Phys. Rev. B 35 (1987) 5990-5996.

[126] D.M. Rowe, V.L. Kuznetsov, L.A. Kuznetsova, G. Min, Electric and thermal transport properties of intermediate-valence YbAl3, J. Phys. D 35 (2002) 2183-2186.

[127] Yasmine Ammar, Sharon Joyce, Rosemary Norman, Yaodong Wang, Anthony P. Roskilly. Low grade thermal energy sources and uses from the process industry in the UK. Applied Energy 89 (2012) 3-20.

[128] Terry J. Hendricks and Jason A. Lustbader. Advanced Thermoelectric Power System Investigations for Light-Duty and Heavy Duty Applications: Part II. The 21st International Conference on Thermoelectrics, IEEE (2002), p. 381.

[129] John Huston, Chris Wyatt, Chris Nichols, Michael J. Binder, and Franklin H. Holcomb. Application of Thermoelectric Devices to Fuel Cell Power Generation Demonstration and Evaluation, 2004. http://oai.dtic.mil/oai/oai?verb=getRecord&metadataPrefix=html&identifier=ADA432046

[130] Chen M, Andreasen SJ, Rosendahl L, Kær SK, Condra T. System modeling and validation of a thermoelectric fluidic power source: PEMFC-TEG. Journal of Electronic Materials 2010; 39(9):1593-00.

[131] X. Chen, Y. Pan, and J. Chen. Performance and Evaluation of a Fuel Cell-Thermoelectric Generator Hybrid System. Fuel Cells 10, 2010, No. 6, 1164-1170; DOI: 0.1002/fuce.200900208.

[132] L.A. Rosendahl, Paw V. Mortensen, and Ali A. Enkeshafi. Hybrid Solid Oxide Fuel Cell and Thermoelectric Generator for Maximum Power Output in Micro-CHP Systems. Journal of Electronic Materials, Vol. 40, No. 5, 2011; DOI: 10.1007/s11664-011-1552-x.

[133] Jenn-Kun Kuo, Jenn-Jiang Hwang, Chin-Hong Lin. Performance Analysis of a Stationary Fuel Cell Thermoelectric Cogeneration System. Fuel Cells 12, 2012, No. 6, 1104-1114; DOI: 10.1002/fuce.201200111.

[134] Tao Wei, Yun-Hui Huang, Qin Zhang, et al. Thermoelectric Solid-Oxide Fuel Cells with Extra Power Conversion from Waste Heat. Chem. Mater. 2012, 24, 1401−1403; dx.doi.org/10.1021/cm300159w.

[135] Birkholz, U., et al. Conversion of Waste Exhaust Heat in Automobile using FeSi2 Thermoelements. Proc. 7th International Conference on Thermoelectric Energy Conversion. 1988, Arlington, USA, pp. 124-128.

[136] Shinohara, K., et al. Application of Thermoelectric Generator for Automobile. Journal of the Japan Society of Powder and Powder Metallurgy, Vol. 46, No. 5, (1999), pp. 524-528.

[137] Ikoma, K., et al. Thermoelectric Generator for Gasoline Engine Vehicles Using Bi2Te3 Modules. J. Japan Inst. Metals. Special Issue on Thermoelectric Energy Conversion Materials, Vol. 63, No. 11, (1999), pp. 1475-1478.

[138] http://www.nedo.go.jp/english/

[139] Jorge Vázquez, Miguel A. Sanz-Bobi, Rafael Palacios, Antonio Arenas. State of the Art of Thermoelectric Generators Based on Heat Recovered from the Exhaust Gases of Automobiles. Proc., 7th European Workshop on Thermoelectrics, Pamplona, Spain, Paper No. 17, 2002.

[140] K.M. Saqr, M. K. Mansour and M. N. Musa. Thermal design of automobile exhaust based thermoelectric generators: Objectives and challenges. International Journal of Automotive Technology, Volume 9, Number 2, 155-160.

[141] J. Lagrandeur, 2009 Hydrogen Program and Vehicle Technologies Program Annual Merit Review (2009).

[142] H. Shock, 2009 Hydrogen Program and Vehicle Technologies Program Annual Merit Review (2009).

[143] D.T. Crane and J.W. Lagrandeur. Progress Report on BSST-Led US Department of Energy Automotive Waste Heat Recovery Program. Journal of ELECTRONIC MATERIALS, published online: 13 November 2009.

[144]http://www1.eere.energy.gov/vehiclesandfuels/pdfs/thermoelectrics_app_2011/monday/meisner.pdf

[145] Gregory P. Meisner. Program Final Report - Develop Thermoelectric Technology for Automotive Waste Heat Recovery. 2012.

[146] Chuen-Sen Lin. Capture of Heat Energy from Diesel Engine Exhaust, Final Report. DOE Award Number: DE-FC26-01NT41248, Task: 1.03.5. November 2008.

[147] Hendricks TJ, Lustbader JA. Advanced thermoelectric power system investigations for light-duty and heavy duty applications: part I. In: Proceedings of the twenty-first international conference on thermoelectrics, Long Beach, CA; 2002. p. 381-6.

[148] Hendricks TJ. Thermal system interactions in optimizing advanced thermoelectric energy recovery systems. J Energy Resour Technol - Trans ASME 2007;129(3):223-31.

[149] Terry J. Hendricks, Naveen K. Karri, Tim P. Hogan, Charles J. Cauchy. New Perspectives in Thermoelectric Energy Recovery System Design Optimization. Journal of Electronic Materials, Vol. 42, No. 7, 2013; DOI: 10.1007/s11664-012-2406-x.

[150] Madhav A. Karri, Eric F. Thacher, Brian T. Helenbrook, Marc S. Compeau. Thermoelectrical Energy Recovery from the Exhaust of a Light Truck. Proceedings of 2003 Diesel Engine Emissions Reduction Conference Newport, Rhode Island, August 24-28, 2003.

[151] Thacher EF, Helenbrook BT, Karri MA, Richter CJ. Testing an automobile exhaust thermoelectric generator in a light truck. Proc IMechE, Part D: J Automobile Eng 2007; 221(D1):95-107.

[152] M.A. Karri, E.F. Thacher, B.T. Helenbrook. Exhaust energy conversion by thermoelectric generator: Two case studies. Energy Conversion and Management 52 (2011) 1596-1611.

[153] Björn Andersson. A comparison of different connection techniques for thermoelectric generators in vehicle waste heat recovery. Degree Project in Industrial Electrical Engineering and Automation, EIE920, 2012.

[154] Navneesh Phillip, Othman Maganga, Keith J. Burnham, et al. Investigation of Maximum Power Point Tracking for Thermoelectric Generators. Journal of Electronic Materials, Vol. 42, No. 7, 2013; Doi: 10.1007/s11664-012-2460-4.

[155] Panagiotis G. Chatzidakis, Georgios C. Christidis and Emmanuel C. Tatakis. Comparative Study of MPPT Algorithms for Thermoelectric Generators. 2013 15th European Conference on Power Electronics and Applications (EPE), 2013; Doi: 10.1109/EPE.2013.6634607.

[156] Olle Högblom and Ronnie Andersson. CFD modeling of thermoelectric generators in automotive EGR-coolers.AIP Conference Proceedings 1449, 497 (2012); Doi: 10.1063/1.4731602.

[157] Kuniaki Mizuno, Kazunori Sawada, Takashi Nemoto, and Tsutomu Iida. Development of a Thermal Buffering Device to Cope with Temperature Fluctuations for a Thermoelectric Power Generator. Journal of Electronic Materials, Vol. 41, No. 6, 2012; Doi: 10.1007/s11664-012-1911-2.

[158] Jing-Hui Meng, Xin-Xin Zhang, Xiao-Dong Wang. Dynamic response characteristics of thermoelectric generator predicted by a three-dimensional heat-electricity coupled model. Journal of Power Sources, 245(2014), 262-269.

[159] Jeffrey W. Fergus, Kirk Yerkes, and Kevin Yost. Numerical Modeling of Multimaterial Thermoelectric Devices Under Static and Cyclic Thermal Loading. Journal of Electronic Materials; Doi: 10.1007/s11664-013-2858-7.

[160] Yuchao Wang, Chuanshan Dai, Shixue Wang. Theoretical analysis of a thermoelectric generator using exhaust gas of vehicles as heat source. Applied Energy, 112(2013), 1171-1180.

[161] Sumeet Kumar, Stephen D. Heister, Xianfan Xu, James R. Salvador, and Gregory P. Meisner. Thermoelectric Generators for Automotive Waste Heat Recovery Systems Part I: Numerical Modeling and Baseline Model Analysis. Journal of Electronic Materials, Vol. 42, No. 4, 2013; Doi: 10.1007/s11664-013-2471-9.

[162] M.F. Silva, J.F. Ribeiro, J.P. Carmo, L.M. Gonçalves, and J.H. Correia. Thin Films for Thermoelectric Applications. NanoScience and Technology 2013, pp 485-528.

[163] T. Ota, C. Tokunaga, K. Fujita. Development of Thermoelectric Power Generation system for Industrial Furnaces. 24th International Conference on Thermoelectrics, 2005. ICT 2005, 335-338; Doi: 10.1109/ICT.2005.1519952.

[164] N.R. Kristiansen and H.K. Nielsen. Potential for Usage of Thermoelectric Generators on Ships. Journal of Electronic Materials, Vol. 39, No. 9, 2010; Doi: 10.1007/s11664-010-1189-1.

[165] J.P. Ploteau, P. Glouannec, H. Noel. Conception of thermoelectric flux meters for infrared radiation measurements in industrial furnaces. Applied Thermal Engineering, 27(2007): 674-681.

[166] Vladimir Leonov, Tom Torfs, Paolo Fiorini, Chris Van Hoof. Thermoelectric Converters of Human Warmth for Self-Powered Wireless Sensor Nodes. IEEE Sensors Journal, Vol. 7, No. 5, 2007.

[167] Mizue Mizoshiri, Masashi Mikami, Kimihiro Ozaki. Thermal--Photovoltaic Hybrid Solar Generator Using Thin-Film Thermoelectric Modules. Japanese Journal of Applied Physics, Volume 51, Issue 6, pp. 06FL07-06FL07-5 (2012).

[168] R. Chein, G. Huang. Thermoelectric cooler application in electronic cooling. Appl Therm Eng 2004;24: 2207-17.

[169] M. Davis, R. Weymouth, P. Clarke. Thermoelectric CPU Cooling using High Efficiency Liquid Flow Heat Exchangers. 2005, Hydrocool Pty Ltd, Fremantle, Australia.

[170] Min Gao, D.M. Rowe, F. Volklein. Integrated thin film thermoelectric cooler. Electron Lett 1998;34:222-3.

[171] Vian JG, Astrain D, Dominguez M. Numerical modeling and a design of a thermoelectric dehumidifier. Applied Thermal Engineering 2002; 22(4): 407-422.

[172] M. Jradi, N. Ghaddar, K. Ghali. Experimental and theoretical study of an integrated thermoelectric-photovoltaic system for air dehumidification and fresh water production. INTERNATIONAL JOURNAL OF ENERGY RESEARCH 2012; 36:963-974.

[173] http://www.gentherm.com/page/climate-seats

[174] M. Rahmoun, A. El Hassani, D. Leclerq, E. Bendada. Peltier Effect Applied to the Design and Realization of a New Mass Flow Sensor. Active andPassive Elec. Comp., 1999, Vol. 22, pp. 165-174; http://dx.doi.org/10.1155/2000/78576.

[175] Shigenao Maruyama, Atsuki Komiya, Hiroki Takeda, Setsuya Aiba. Development of Precise-temperature-controlled Cooling Apparatus for Medical Application by Using Peltier Effect. 2008 International Conference on BioMedical Engineering and Informatics. DOI 10.1109/BMEI.2008.239.

[176] Dener F. Cheddie, Norman D. H. Munroe, A two-phase model of an intermediate temperature PEM fuel cell. International Journal of Hydrogen Energy, 32 (2007)832- 841.

[177] Dener F. Cheddie, Norman D. H. Munroe, Parametric model of an intermediate temperature PEMFC. Journal of Power Sources 156(2006)414-423.

[178] Dener F. Cheddie, Norman D. H. Munroe, Semi-analytical proton exchange membrane fuel cell modeling. Journal of Power Sources, 183 (2008) 164-173.

[179] Dener F. Cheddie, Norman D. H. Munroe, Three dimentional modeling of high temperature PEM fuel cells. Journal of Power Sources 160 (2006) 215-223.

[180] Dener F. Cheddie, Norman D. H. Munroe. Mathematical model of a PEMFC using a PBI membrane. Energy Conversion and Management 47 (2006)1490-1504.

[181] Dener F. Cheddie, Norman D. H. Munroe, modeling of High Temperature PEM fuel cells using FEMLAB. Excerpt from the proceedings of the COMSOL Multiphysics User's Conference 2005 Boston.

[182] Dener F. Cheddie, Norman D. H. Munroe, Analytical corelations for intermediate tempertature PEM fuel cells. Journal of Power Sources 160 (2006) 299-304.

[183] T. Sousa, M. Mamlouk , Kehth Scott. An isothermal model of a laboratory intermediate temperature fuel cell using PBI doped phosphoric acid membranes. Chemical Engineering Science 65 (2010) 2513-2530.

[184] Keith Scott, M. mamlouk. A cell voltage equation for an intermediate temperature proton exchange membrane fuel cell. International journal of hydrogen energy, 34 (2009) 9195-9202.

[185] Jie Peng, Seung Jae Lee. Numerical simulation of proton exchange membrane fuel cells at high operating temperature. Journal of Power sources 162 (2206) 1182-1191.

[186] Justo Lobato, Pablo Cañizares, Manuel A. Rodrigo et al. PBI-based polymer electrolyte membranes fuel cells Temperature effects on cell performance and catalyst stability. Electrochimica Acta, 52 (2007)3910-3920.

[187] Justo Lobato, Pablo Cañizares, Manuel A. Rodrigo et, al. Three-dimensional model of a 50 cm2 high temperature PEM fuel cell. Study of the flow channel geometry influence. International Journal of Hydrogen Energy xxx (2010) I-II.

[188] Anders R. Korsgaard, Rasmus Refshauge, Mads P. Nielsen, Mads Bang, Søren K. Kær. Experimental characterization and modeling of commercial polybenzimidazole-based MEA performance. Journal of Power Sources 162 (2006)239-245.

[189] Anders R. Korsgaard, Rasmus Refshauge, Mads P. Nielsen, Mads Bang, Søren K. Kær. Modeling of CO influence in PBI electroyte PEM fuel cells. The 4th international conference of fuel cell science, engineering and technology.

[190] Anders R. Korsgaard, Mads P. Nielsen, Søren K. Kær. Part one: A novel model of HTPEM-based micro-combined heat and power fuel cell system. International journal of hydrogen energy 33 (2008) 1909- 1920.

[191] Anders R. Korsgaard, Mads P. Nielsen, Søren K. Kær. Part two: Control of a novel HTPEM- based micro combined heat and power fuel cell system. International Journal of Hydrogen Energy. 33 (2008) 1921-1931.

[192] Søren Juhl Andreasen, Søren Knudsen Kær. Dynamic Model of the High Temperature Proton Exchange Membrane fuel cell stack temperature. Journal of Fuel cell science and technology, 6 (2009).

[193] Federico Zenith. Control of fuel cells. Doctoral thesis, Norwegian University of Science and Technology, 2007; ISBN 978-82-471-1447-6.

[194] Federico Zenith, Frode Seland, Ole Edvard Kongstein, Børre Børresen, Reidar Tunold, Sigurd Skogestad. Control-Oriented modelling and experimental study of the transient response of a high-temperature polymer fuel cell. Journal of Power Sources 162 (2006) 215-227.

[195] Federico Zenith, Sigurd Skogestad. Control of fuel cell power output. Journal of Process Control 17 (2007) 333- 347.

[196] Federico Zenith, Sigurd Skogestad. Control of the mass and energy dynamic of polybenzimidazole-membrane fuel cells. Journal of Process Control 19 (2009) 425- 432.

[197] Federico Zenith, Sigurd Skogestad. Dynamic modeling and control of polybenzimidazole fuel cells. Proceedings of ECOS 2005, Tondheim, Norway. June 20-22, 2005.

[198] Simon Lineykin and Shmuel Ben-Yaakov. Modeling and Analysis of Thermoelectric Modules. Ieee Transactions on Industry Applications, VOL. 43, NO. 2, 2007.

[199] Jincan Chen, Chih Wu. Analysis on the performance of a thermoelectric generator. Journal of Energy Resources Technology 2000; 122(2):61-63.

[200] D.M. Rowe, Gao Min. Evaluation of thermoelectric modules for power generation. Journal of Power Sources 73 (1998), 193-198.

[201] Crane D, Jackson G. Optimization of cross flow heat exchangers for thermoelectric waste heat recovery. Energy Convers Manage 2004; 45(9-10):1565-82.

[202] Yu J, Zhao H. A numerical model for thermoelectric generator with the parallel-plate heat exchanger. Journal of Power Sources 2007; 172(1):428-34.

[203] Smith KD. An investigation into the viability of heat sources for thermoelectric power generation systems. Master thesis, Rochester (NY): Rochester Institute of technology, 2009.

[204] Elena E. Antonova and David C. Looman. Finite Elements for Thermoelectric Device Analysis in ANSYS. International Conference on Thermoelectrics (2005), p.200.

[205] Martin Jaegle. Simulating Thermoelectric Effects with Finite Element Analysis using COMSOL. Proceedings ECT2007 (2007), p. 222.

[206] Min Chen, G. Jeffrey Snyder. Analytical and numerical parameter extraction for compact modeling of thermoelectric coolers. International Journal of Heat and Mass Transfer 60 (2013) 689-699. doi:10.1016/j.ijheatmasstransfer.2013.01.020.

[207] J. Esartea, G. Min, D.M. Rowe. Modelling heat exchangers for thermoelectric generators. Journal of Power Sources 93 (2001) 72-76.

[208] Suzuki RO, Tanaka D. Mathematical simulation of thermoelectric power generation with the multi-panels. Journal of Power Sources 2003;122(2): 201-9.

[209] Suzuki RO, Tanaka D. Mathematic simulation on thermoelectric power generation with cylindrical multitubes. Journal of Power Sources 2003;124(1):293-8.

[210] Reiyu Chein, Guanming Huang. Thermoelectric cooler application in electronic cooling. Applied Thermal Engineering 24 (2004) 2207-2217.

[211] A. Rezania, L.A. Rosendahl. Thermal effect of a thermoelectric generator on parallel microchannel heat sink. Energy 37 (2012) 220-227.

[212] Nellis G, Klein S. Heat transfer. New York: Cambridge University Press; 2009.

[213] Kays WM, London AL. Compact heat exchangers. 3rd ed. New York: McGraw Hill; 1984.

[214] http://www.engineeringagenda.com/heat-exchangers/

[215] Jainender Dewatwal. Design of Compact Plate Fin Heat Exchanger. Bachelor thesis, National Institute of Technology Rourkela, 2009.

[216] Taylor BN, Kuyatt CE. Guidelines for evaluating and expressing the uncertainty of NIST measurement results. National Institute of Standards and Technology Technical Note 1297; 1994.

[217] N. Rajalakshmi, G. Velayutham, K. S. Dhathathreyan. Sensitivity Analysis of a 2.5 kW Proton Exchange Membrane Fuel Cell Stack by Statistical Method. Journal of Fuel Cell Science and Technology, FEBRUARY 2009, Vol. 6, 011003.1-011003.6.

[218] A. Arsalis, Mads P. Nielsen, Søren K. Kær. Modeling and parametric study of a 1 kWe HT-PEMFC-based residential micro-CHP system. International Journal of Hydrogen Energy 36 (2011) 5010-5020.

[219] Anders Christian Olesen and Julian Ralf Jensen. Solid Oxide Fuel Cell Micro Combined Heat and Power system - choosing the right reformer. Master thesis, Aalborg University, 2009.

Paper 1

Potential Usage of Thermoelectric Devices in a High-Temperature Polymer Electrolyte Membrane (PEM) Fuel Cell System: Two Case Studies

Gao, Xin; Chen, Min; Andreasen, Søren Juhl; Kær, Søren Knudsen

Journal of Electronic Materials, 41(6), 2012, p. 1838-1844.

Journal of ELECTRONIC MATERIALS, Vol. 41, No. 6, 2012
DOI: 10.1007/s11664-012-2098-2

Potential Usage of Thermoelectric Devices in a High-Temperature Polymer Electrolyte Membrane (PEM) Fuel Cell System: Two Case Studies

XIN GAO,[1,2] MIN CHEN,[1] SØREN JUHL ANDREASEN,[1] and SØREN KNUDSEN KÆR[1,3]

1.—Department of Energy Technology, Aalborg University, Aalborg DK-9220, Denmark. 2.—e-mail: xga@et.aau.dk. 3.—e-mail: skk@et.aau.dk

Methanol-fueled, high-temperature polymer electrolyte membrane fuel cell (HTPEMFC) power systems are promising as the next generation of vehicle engines, efficient and environmentally friendly. Currently, their performance still needs to be improved, and they still rely on a large Li-ion battery for system startup. In this article, to handle these two issues, the potential of thermoelectric (TE) devices applied in a HTPEMFC power system has been preliminarily evaluated. First, right after the fuel cell stack or the methanol reformer, thermoelectric generators (TEGs) are embedded inside a gas–liquid heat exchanger to form a heat recovery subsystem jointly for electricity production. It is calculated that the recovered power can increase the system efficiency and mitigate the dependence on Li-ion battery during system startup. To improve the TEG subsystem performance, a finite-difference model is then employed and two main parameters are identified. Second, TE coolers are integrated into the methanol steam reformer to regulate heat fluxes herein and improve the system dynamic performance. Similar modification is also done on the evaporator to improve its dynamic performance as well as to reduce the heat loss during system startup. The results demonstrate that the TE-assisted heat flux regulation and heat-loss reduction can also effectively help solve the abovementioned two issues. The preliminary analysis in this article shows that a TE device application inside HTPEMFC power systems is of great value and worthy of further study.

Key words: Thermoelectric devices, fuel cell, heat recovery, heat regulation, heat loss

Nomenclature

A_{stk}	Total reaction area in a stack (m^2)
c_h	Specific heat capacity (J/kg-K)
F	Faraday constant (C/mole)
I	Electric current (A)
M	Molar mass (kg/kmole)
$\dot{m}$	Mass flow rate (kg/s)
n_x	Total number of segments along the flow
n_y	Total number of segments crossing the flow
P	Power output (W)
Q	Heat flux (W)
R	Resistance
T	Temperature (K or °C)
UA	Heat exchanger conductance (W/K)
w	Power output of each segment (W)
Δh	Enthalpy difference (J/kg)
Δp	Pressure drop (Pa)
Z	Figure of merit of TE module (1/K)
zT	Figure of merit of TE material (−)
G	Core mass velocity (Kg/s-m^2)
f_{hx}	Friction factor
L_{hx}	Heat exchanger length (m)
D_h	Hydraulic diameter (m)
NTU	Number of transfer units

Greek Symbols

α	Seebeck coefficient (V/K)
ε_{ctf}	The effectiveness

(Received July 20, 2011; accepted April 4, 2012; published online May 9, 2012)

η Efficiency
ρ Exhaust gas density (kg/m^3)
σ Minimum free flow area/frontal area

Subscripts/Superscripts

ex	Cathode exhaust
am	Ambient
peak	Peak value
ave	Average value
TE	TEG module
HX	Heat exchanger
h	Hot gas
c	Coolant
i	Segment index
in	Inlet
out	Outlet
e	Electric resistance
tot	Total value
t	Thermal resistance
TEA	Whole TEG assembly

INTRODUCTION

In recent years, the desire to alleviate the environmental pollution, find more efficient energy conversion devices, and reduce the dependence on fossil recourses has driven more and more attention onto fuel cells. Among kinds of fuel cell systems, high-temperature polymer electrolyte membrane fuel cell (HTPEMFC) power systems with onboard methanol reformers are particularly practical and ideal for automotive applications.[1,2] But as conventional technologies, a large amount of exhaust heat is wasted without any utilization by these systems. Their dependence on a Li-ion battery during system startup also needs to be alleviated. Moreover, the system dynamic performance is still challenging because some heat fluxes inside are almost uncontrollable under the working condition fluctuations. To accommodate these challenges, novel system configurations even new technologies are needed.

Thermoelectric devices can be used as thermal electric generators (TEGs) and thermal electric coolers (TECs), respectively. TEGs are strongly advantageous compared with conventional technologies in waste heat recovery for electricity.[3] Generally, TEGs could be deployed in any place as long as a temperature difference exists. By now, there have been a few projects using TEGs for waste heat recovery in fuel cell systems.[4,5] TECs have been widely used as miniature heat pumps because of their outstanding scalability. But it is believed there is still room for looking into fully analyzing and utilizing their entire potential, such as quick response and bidirectional heating/cooling capabilities.[6]

In this article, to improve the system efficiency, dynamic performance including the startup process, TEGs and TECs are introduced into a HTPEMFC power system. The heat sources in the system possible for TEGs to recover are preliminarily assessed. For further optimizing the TEG subsystem, a finite-difference model is validated and employed later in this article. Two factors affecting the subsystem performance most significantly are identified. Finally, the feasibility of using TECs to improve the system dynamic performance, to reduce the heat loss, and in turn to make the system less dependent on initial Li-ion battery capacity is preliminarily evaluated.

TEG APPLICATION

One typical configuration of a HTPEMFC power system is shown in Fig. 1.[7] It is a configuration for normal working conditions, different from system startup. The system electrical power output is approximately 1 kW. Its fuel cell stack is cooled by the cathode air flow. Usually the stoichiometry λ_c of

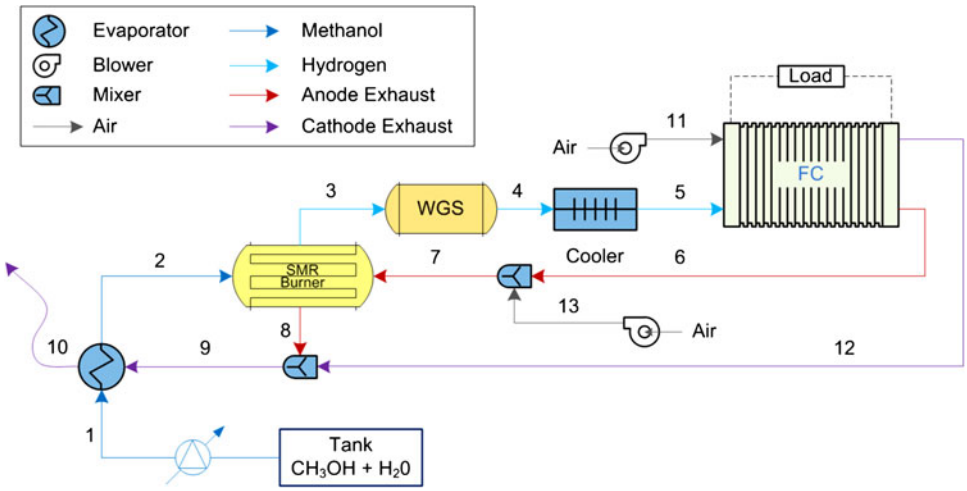

Fig. 1. A HTPEMFC power system configuration under normal working conditions.[7]

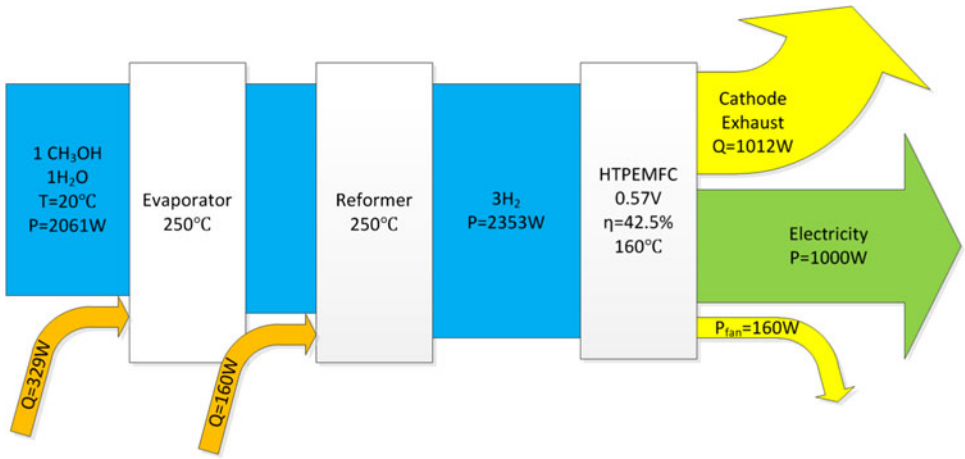

Fig. 2. Energy flow Sankey diagram.

the cathode air is ~20. Under the normal working conditions, consisting of current density $i = 0.6\,\mathrm{A/cm^2}$, the energy flow of the system is illustrated in Fig. 2.

Considering the energy flow, the largest heat flux is the cathode exhaust, the stream 12 in Fig. 1. Based on energy balance, the stream temperature can be calculated from

$$Q_{\mathrm{ex}} = \dot{m}_{\mathrm{ex}} \cdot \Delta h_{\mathrm{ex}}, \tag{1}$$

m_{ex}can be obtained by the Faraday's law

$$\dot{m}_{\mathrm{ex}} = M_{\mathrm{ex}} \cdot \lambda_{\mathrm{c}} \cdot A_{\mathrm{stk}}/(0.21 \cdot 4 \cdot F). \tag{2}$$

Then, the cathode exhaust temperature is $T_{\mathrm{ex}} = 145^{\circ}\mathrm{C}$. Assuming the ambient temperature is $T_{\mathrm{am}} = 25^{\circ}\mathrm{C}$, the maximum TEG recovered power from the exhaust can be deduced from[8]

$$\eta_{\mathrm{peak}} = Z \cdot (T_{\mathrm{ex}} - T_{\mathrm{am}})/(4 + Z \cdot T_{\mathrm{ex}} + \mathrm{Z}\cdot(T_{\mathrm{ex}} + T_{\mathrm{am}})/2). \tag{3}$$

A constant figure-of-merit value $zT_{\mathrm{ave}} = 1.1$ is used in this calculation to assess roughly the TEG power output. It is the average value of Bi_2Te_3 and $(Bi,Sb)_2Te_3$ bulk materials, which are widely applied in TEG modules working in this temperature range. Considering the relatively mild temperature difference between T_{ex} and T_{am} plus the material science progress, TEG material properties herein are temporarily assumed temperature independent.[9,10] Then calculated by$P_{\mathrm{peak}} = \eta_{\mathrm{peak}} \cdot \mathrm{Q}_{\mathrm{ex}}$, the TEG power output is about 58 W. To obtain this power, TEG heat recovery system needs to be carefully designed and optimized.

The chosen architecture of the TEG heat recovery system is illustrated in Fig. 3. Basically, it is similar to a counter-flow plate heat exchanger. Cathode exhaust passes through the heat exchanger housing in the middle. Two aluminum blocks with flow field inside are at the top and the bottom. Inside the flow field is the liquid coolant circulating to establish the temperature difference. TEG modules are assembled between the housing and the blocks.

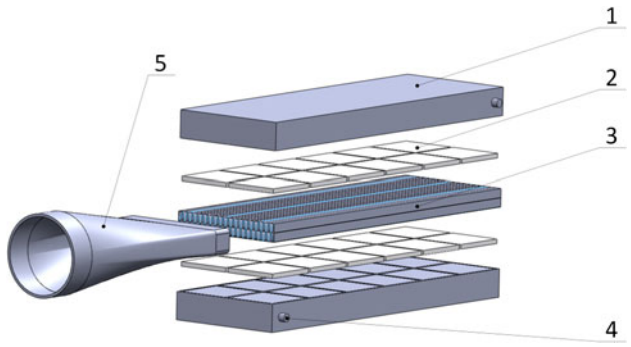

Fig. 3. The configuration of TEG heat recovery system: 1, aluminum block; 2, TEG assembly; 3, compact heat exchanger housing; 4, coolant inlet/outlet; and 5, diffuser.

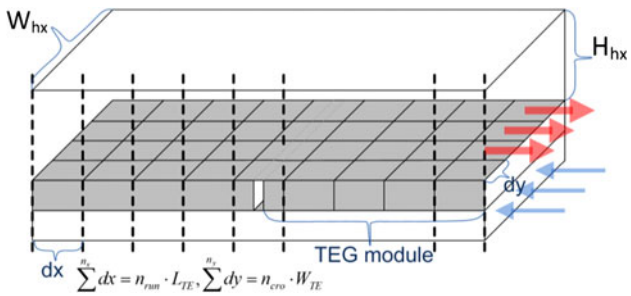

Fig. 4. Finite-difference scheme of the TEG heat recovery system.

To optimize this system, a finite-difference model is used, as illustrated in Fig. 4. The main equations are listed in Table I.

This model has the following advantages:

1. More precise description of the fluid properties and the heat transfer on each discretized segment along the flow direction.
2. Obtain the TEG power output more precisely by the discretized module model and the temperature-dependent material properties.

Table I. Main equations[11]

Description	Equations
TEG properties	$\sum^{n_{x,\mathrm{TE}}}\sum^{n_{y,\mathrm{TE}}}\alpha_i=\alpha_{\mathrm{TE}},\ \sum^{n_{x,\mathrm{TE}}}\sum^{n_{y,\mathrm{TE}}}R_{e,i}=R_{\mathrm{TE},e},\ \sum^{n_{x,\mathrm{TE}}}\sum^{n_{y,\mathrm{TE}}}R_{t,i}=R_{\mathrm{TE},t}$
TEG power output	$I_i=0.5(\alpha_i)(\bar{T}_{h,\mathrm{TE}}(i)-\bar{T}_{c,\mathrm{TE}}(i))/R_{e,i}.$
	$w_{\mathrm{TE,peak}}(i)=\alpha_i I_i\left(T_{h,\mathrm{TE}}(i)-T_{c,\mathrm{TE}}(i)\right)-I_i^2R_{e,i},\ P_{\mathrm{TEA}}=\sum^{n_x}\sum^{n_y}w_{\mathrm{TE,peak}}(i)$
Heat transfer	$\dot{m}_h c_{h,i}(T_h(i)-T_h(i+1))=UA_{\mathrm{HX}}(i)(T_h(i)-T_{h,\mathrm{TE}}(i))$
	$\dot{m}_h c_{h,i}(T_h(i)-T_h(i+1))=\varepsilon_{\mathrm{ctf}}(i)\dot{m}_h c_{h,i}(T_h(i)-T_c(i))$
	$\varepsilon_{\mathrm{ctf}}(i)=1-\exp(-\mathrm{NTU}(i)),\ \mathrm{NTU}(i)=UA_{\mathrm{tot}}(i)/(\dot{m}_h c_{h,i}),$
	$1/UA_{\mathrm{tot}}(i)=1/UA_{\mathrm{HX}}(i)+1/UA_{\mathrm{TE}}(i)$
Pressure drop	$\Delta p=(G^2/(2\rho_{\mathrm{in}}))[4f_{\mathrm{hx}}\cdot L_{\mathrm{flow}}\rho_{\mathrm{in}}/(D_{\mathrm{h}}\bar{\rho})+(1+\sigma^2)((\rho_{\mathrm{in}}/\rho_{\mathrm{out}})-1)]$

HX, heat exchanger; *NTU,* number of transfer units; *TE*, TEG module; *TEA*, whole TEG assembly.

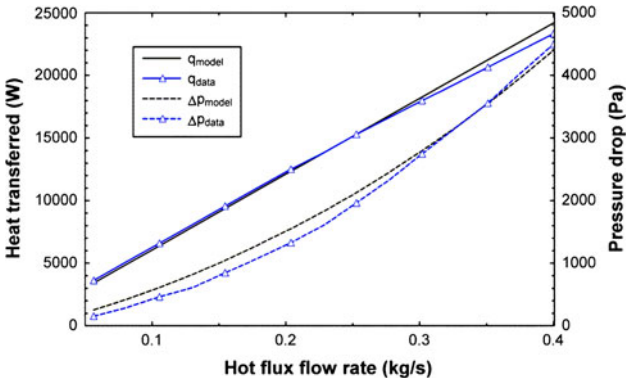

Fig. 5. Model validation by heat transferred and pressure drop.

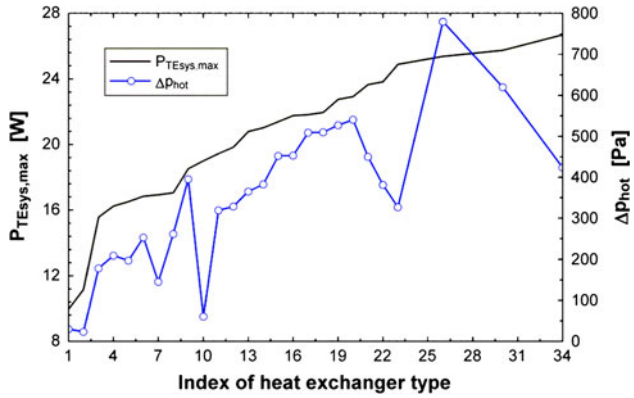

Fig. 6. System power output and pressure drop using different heat exchangers.

3. Heat-transfer and TEG performance are coupled in calculations.
4. Facilitate the heat exchanger structure optimization with an integrated heat exchanger structure database.[12]
5. Be able to cooptimize the system with larger power output and lower pressure drop.
6. TEG modules and heat exchangers used are both commercial available.
7. Easier and faster to get solved through using the discretized epsilon-NTU method.[13–15]

This model has data in Ref.13 The results are shown in Fig. 5. Using this model, the maximum electricity output from the previously mentioned cathode exhaust turns out to be 23 W, only approximately half of P_{peak}. One main reason is that TEG performance is highly correlated with temperature. A sensitivity study is performed on the model, and it is found that the cathode exhaust temperature contributes 73.98% of the power output sensitivity. When the temperature goes down, the TEG power output drops down sharply, and vice versa. Another main factor is the heat exchanger structure. When properly adjusted, it can enhance the heat transfer and reduce system pressure drop simultaneously. The pressure drop is roughly proportional to the system parasitic loss. Screening the heat exchanger structure database, three types are identified with outstanding performance, as shown in Fig. 6. They are Plain plate-fin, surface 10.27′ (index 10), Strip-fin plate-fin, surface 1/6-12.18(D) (23), and Wavy-fin plate-fin, surface 17.8-3/8 W (34). Further system optimization will be mainly focused on these three types.

In addition to the cathode exhaust heat recovery, the TEG heat recovery system can be used in assisting the HTPEMFC system startup. During the startup, approximately 300 W electricity from a Li-ion battery is consumed to vaporize the methanol and warm up the HTPEMFC stack.[7] The vaporized methanol then combusts with air catalytically in the burner side of the reformer (SMR-burner in Fig. 1). After that, the hot flue gas mixed with some fresh air is pumped to heat up the fuel cell stack to its working temperature. The fresh air is to protect the fuel cell stack from overheated by the flue gas. Instead of the fresh air, TEG heat recovery system can be introduced to cool down the flue gas as well

as to produce electricity. Based on fluid parameters from Ref. 7, electric power recovered in this study is approximately 100 W. On the contrary, if installed after the stack, the recovered electricity is only about 34 W. Obviously, installing the TEG system after the reformer is preferable and can approximately reduce the Li-ion battery capacity by one-third. Although this preliminary estimation needs further verification, it reveals the great potential contribution of TEG to the fuel cell system.

Inside the system in Fig. 1, some other places are also available for TEG heat recovery. For convenience of further study, all possible positions are roughly evaluated and listed in Table II. Some corresponding information is also included, such as the original temperature difference and suitable TEG materials.

As a total, the efficiency of the fuel cell system will be ideally increased by 9.6% through the TEG heat recovery. In practice, the power capacity of a fuel cell system is usually approximately 60 kW.[16] In these systems, the TEG-recovered electricity can be more easily harnessed to drive the auxiliaries, charge batteries, assist the system startup/shutdown processes, act as a back-up power supply, etc.[17] With TEG efficiency improved in the future, a HTPEMFC engine without relying on a large Li-ion battery can be envisaged.

Reconsidering this HTPEMFC power system, efficiency can be improved by TEG heat recovery. But its dynamic performance still remains unsatisfactory. The idea is to use TECs to regulate heat fluxes in and between its components. Through the heat regulation, hopefully, system dynamic performance, system reliability, and durability can be improved.

TEC APPLICATION

Two issues affect the system dynamic performance significantly. One is the unsatisfactory dynamic performance of the steam reformer (in Fig. 7) and the exchanger-based methanol evaporator (in Fig. 8a). The other is the heat loss in the methanol evaporator during system startup. Both are mainly from the limited controllability of heat fluxes inside the two components.

When the electric load increases in Fig. 1, the fuel cell stack demands more hydrogen from the reformer. Hydrogen production from methanol steam reforming is endothermic, as in formula 4,

$$CH_3OH + H_2O \rightarrow CO_2 + 3H_2 \,(\Delta H = +49\,\text{kJ/mol}) \quad (4)$$

So the reformer needs more heat. But the heat generated by the hydrogen catalytic combustion is contrarily depressed inside the burner side. The reason is that more hydrogen now has been consumed by the stack and less is left for the burner. In turn, the heat supply shortage and temperature decline appear. When the electric load decreases, the condition is vice versa. The consequence is the poor dynamic performance of the reformer. Behind this problem is the limited controllability of interlayer heat fluxes inside the reformer. Solutions include modifications on system configuration and/or components, such as the hybrid of fuel cell and Li-ion battery, the integration of the reformer and the evaporator, etc. Among them, the component modification done using TECs seems promising.

Redesign the reformer in Fig. 7, TECs will be embedded into the walls between the burner and the reformer layers. Then, they will work as heat pumps to regulate the interlayer heat fluxes and their working modes are illustrated in Fig. 8. When the spontaneous heat flux (SF) is insufficient for the reformer, heat pumped (HP) by TECs toward the reformer side will slow down the temperature decline, as shown in Fig. 8a. On the contrary, when the reformer is getting overheated, HP will be set to be opposite to SF and keep the reformer from

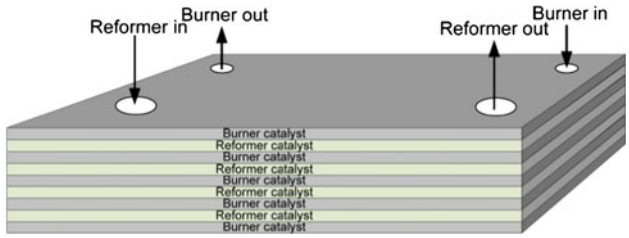

Fig. 7. Exchanger-based methanol steam reformer.[7]

Table II. Possible TEG installation positions

Position	T_H (°C)/T_C (°C)	Heat Flux (W)	Representative Materials[13,14]	P_{peak}
Cathode exhaust	145/25	1012	Bi_2Te_3 and $(Bi,Sb)_2Te_3$	58 W
Evaporator	250/70	329	Mg_2SiSn and Zn_4Sb_3	24 W
Reformer	400[a]/250	160	Mg_2SiSn and Zn_4Sb_3	7 W[a]
Cooler	205/25	39	Bi_2Te_3 and $(Bi,Sb)_2Te_3$	3.1 W
Burner exhaust	137.5/25	34.5	Bi_2Te_3 and $(Bi,Sb)_2Te_3$	2 W

[a]The temperature of hydrogen catalytic combustion is in the range 100°C to 2210°C. Here, a typical temperature is used.

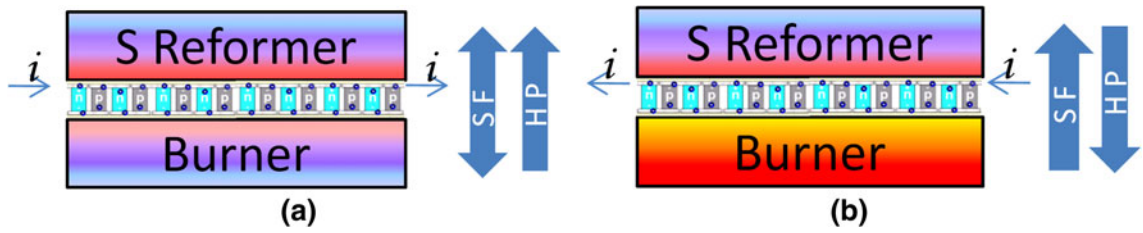

Fig. 8. Working modes of TECs in the steam reformer.

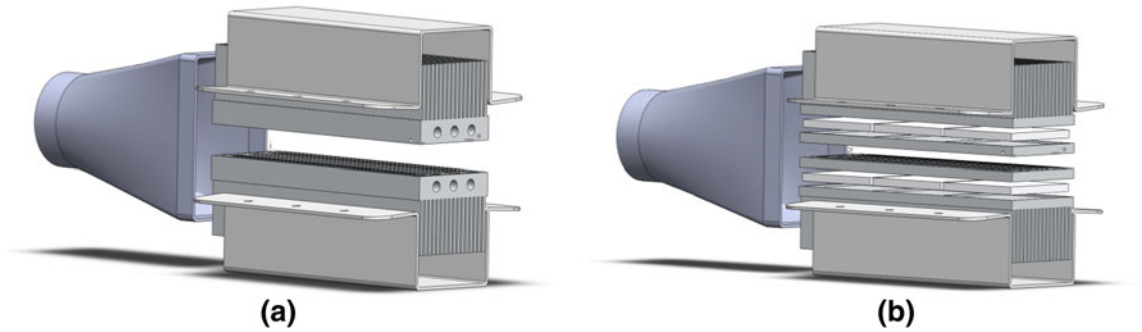

Fig. 9. (a) Original and (b) modified methanol evaporator.

temperature overshoot, as shown in Fig. 8b. As a result, the TE-modified reformer can work more smoothly around its standard working temperature.

The preceding heat supply and temperature fluctuations also take place in the original methanol evaporator in Fig. 9a. The modification is similar, as illustrated in Fig. 9b. TECs working in these two cases are different from heat pumps keeping temperature difference but rather act as heat regulators.

To act as heat regulators, two characteristics make the TECs superior. One is their quick response capability. TECs can change temperature very fast. An ordinary single-stage TEC module can realize a cooling target in a few seconds; novel thin-film TEC modules are even on the order of milliseconds![18] Considering the methanol reforming speed,[19] this characteristic is of critical importance. The other is the bidirectional heating/cooling capability. Changing the current direction, TECs pump heat to the opposite direction. As Yang and Stabler mentioned,[6] these two characteristics still have not been fully utilized. Applying these characteristics in the current fuel cell system to regulate heat flux can probably make full use of them.

Considering the regulating capability, a single conventional TEC module can achieve a temperature difference up to 70°C, or can transfer heat at a rate of 125 W.[20] As mentioned, 300 W heat at most is requested by the evaporator.[7] It means several TEC modules working together can easily meet the regulating demand, not to mention the more capable TEC modules in the future. These conventional modules are also capable enough in the reformer. Another feature makes TECs superior as heat regulators: According to Eq. 5, the coefficient of performance (COP) of TEC modules increases with smaller temperature difference ΔT.

$$\mathrm{COP} = \left(\alpha_{\mathrm{pn}} I T_{\mathrm{c}} - I^2 R/2 - K\Delta T\right)/\left(\alpha_{\mathrm{pn}} I \Delta T + I^2 R\right) \tag{5}$$

Working as heat regulators, ΔT is normally around 0°C. It means the COP value is much higher when TECs act to regulate heat flux other than keep temperature difference. Furthermore, under a lower ΔT, the reverse heat flow inside TEC modules is less significant. This also benefits the COP. Other characteristics, such as high reliability, long lifetime, no movable parts, and outstanding scalability just make TECs excellent in heat regulation.

TECs in the evaporator have another working mode. They can also be set to keep a temperature difference during the fuel cell system startup. In the original evaporator in Fig. 9a, electric heating rods are charged to vaporize the methanol in the flow field during system startup. They are settled in the holes. As mentioned, the peak power needed is approximately 300 W. When vaporizing the methanol, electric heat is simultaneously being dissipated by the fins. This heat dissipation is serious during the system startup. To suppress the heat dissipation, the scenario is to have TEC modules and membrane electric heaters assembled between the fins and the flow field, as illustrated in Fig. 9b. Now flow field is still in the middle. The outer images are the membrane electric heaters. Outmost are the TEC modules and then the fins. Now during system

startup, TECs will be charged as a heat resistor to keep the fin temperature low. In this way, the heat dissipation and the electricity consumption are both less during the system startup.

DISCUSSION AND CONCLUSIONS

Modifying the HTPEMFC system with TEGs and TECs has mutual benefits. The performances of the fuel cell system can be significantly improved and the characteristics of the TE devices can be better utilized.

TEG heat recovery can increase the system efficiency by about 1/10 and help the system out of Li-ion battery dependence. Under normal working condition, the major heat source TEGs can recover is the fuel cell cathode exhaust. During system startup, the major heat source is the flue gas from the methanol reformer; TEG heat recovery can significantly reduce the capacity of the Li-ion battery. To recover heat more efficiently, two main parameters of the TEG subsystem are identified using a finite-difference model. They are the cathode exhaust temperature and the heat exchanger structure. Based on the preliminary analysis, three heat exchanger structures with superior performance are identified for further subsystem optimization.

The benefits of using TECs are twofold: I) improving the system dynamic performance through the TE-assisted heat regulation and II) mitigating the system dependence on Li-ion battery through the TE-assisted suppression of the heat dissipation. Working as heat regulators, TECs seem capable and their characteristics can probably be fully utilized.

Through the preliminary analyses in this article, it can be concluded that the applications of TE devices inside HTPEMFC power systems could be of benefit and are worthy of further study.

ACKNOWLEDGEMENTS

The authors gratefully acknowledge financial support from Aalborg University and China Scholarship Council.

REFERENCES

1. S.J. Andreasen, L. Ashworth, I.N.M. Remón, and S.K. Kær, *Int. J. Hydrogen Energy* 33, 7137 (2008).
2. Y. Wang, K. Chen, J. Mishler, S.C. Cho, and X.C. Adroher, *Appl. Energy* 88, 981 (2011).
3. D.M. Rowe, *Renew. Energy* 5, 1470 (1994).
4. D. Geng and C. Xie, *Chin. J. Power Sour.* 3, 34 (2010).
5. X. Chen, Y. Pan, and J. Chen, *Fuel Cells* 10, 1164 (2010).
6. J. Yang and F.R. Stabler, *J. Electron. Mater.* 38, 7 (2009).
7. S.J. Andreasen (Ph.D. dissertation, Aalborg University, 2009).
8. J. Zhang, Thermoelectric Technology, 1st ed. (Tianjin: China Tianjin Institute of Power Sources, 2008), pp. 23.
9. M. Lazard, G. Fraisse, C. Goupil, and H. Scherrer, (Paper presented at the Proceedings of the 6th European Conference on Thermoelectrics, Paris, France, 2–4 July 2008), p. 2.
10. G.J. Snyder and E.S. Toberer, *Nat. Mater.* 7, 105 (2008).
11. X. Gao, S.J. Andreasen, M. Chen, and S.K. Kær, *Int. J. Hydrogen Energy*. doi:10.1016/j.ijhydene.2012.03.009.
12. F-Chart Software, *EES Manual,* v8.590 Edition (Madison, WI: F-Chart Software, LLC, 2010), www.fchart.com.
13. N. Espinosa, M. Lazard, L. Aixala, and H. Scherrer, *J. Electron. Mater.* 39, 1446 (2010).
14. K.D. Smith (Master's thesis, Rochester Institute of Technology, 2009).
15. G. Nellis and S. Klein, *Heat Transfer*, 2nd ed. (New York: Cambridge University Press, 2009), pp. 841–851.
16. C.E. Thomas and J. Hydrog, *Energy* 34, 6005 (2009).
17. M. Chen, S.J. Andreasen, L.A. Rosendahl, S.K. Kær, and T. Condra, *J. Electron. Mater.* 39, 9 (2010).
18. S. Lee, *Establishing a New Performance Paradigm with Ultra-Thin Thermoelectric Modules* (Research Triangle Park, NC: Nextreme Thermal Solutions, 2010), www.nextreme.com/media/pdf/articles/Thermoelectric_Cooling.pdf.
19. K. Takeda, A. Baba, Y. Hishinuma, and T. Chikahisa, *JSAE Rev.* 23, 183 (2002).
20. D. Martin, U.S. patent US20040042957 Al (4 March 2004).

Paper 2

Numerical Model of a Thermoelectric Generator with Compact Plate-Fin Heat Exchanger for High Temperature PEM Fuel Cell Exhaust Heat Recovery

Gao, Xin; Andreasen, Søren Juhl; Chen, Min; Kær, Søren Knudsen

International Journal of Hydrogen Energy, 37(10), 2012, p. 8490-8498.

INTERNATIONAL JOURNAL OF HYDROGEN ENERGY 37 (2012) 8490–8498

Available online at www.sciencedirect.com

SciVerse ScienceDirect

journal homepage: www.elsevier.com/locate/he

Numerical model of a thermoelectric generator with compact plate-fin heat exchanger for high temperature PEM fuel cell exhaust heat recovery

Xin Gao, Søren Juhl Andreasen, Min Chen, Søren Knudsen Kær*

Department of Energy Technology, Aalborg University, Pontoppidanstræde 101, Aalborg DK-9220, Denmark

ARTICLE INFO

Article history:
Received 25 December 2011
Received in revised form
22 February 2012
Accepted 4 March 2012
Available online 28 March 2012

Keywords:
Thermoelectric generator
Heat recovery
Fuel cell
Discretized model
Heat exchanger database

ABSTRACT

This paper presents a numerical model of an exhaust heat recovery system for a high temperature polymer electrolyte membrane fuel cell (HTPEMFC) stack. The system is designed as thermoelectric generators (TEGs) sandwiched in the walls of a compact plate-fin heat exchanger. Its model is based on a finite-element approach. On each discretized segment, fluid properties, heat transfer process and TEG performance are locally calculated for higher model precision. To benefit both the system design and fabrication, the way to model TEG modules is herein reconsidered; a database of commercialized compact plate-fin heat exchangers is adopted. Then the model is validated against experimental data and the main variables are identified by means of a sensitivity analysis. Finally, the system configuration is optimized for recovering heat from the exhaust gas. The results exhibit the crucial importance of the model accuracy and the optimization on system configuration. Future studies will concentrate on heat exchanger structures.

1. Introduction

With the diminishing reserve of fossil fuels and the rising concern on global green-house gas emissions, more attention is being drawn by fuel cells [1]. Among other fuel cell technologies, high temperature polymer electrolyte membrane fuel cell (HTPEMFC) power systems are considered to be promising in practice [2]. Due to the high operating temperatures of HTPEMFCs (160°C–180 °C), the waste heat is of high quality and thermoelectric generators (TEGs) are introduced herein to recover this exhaust heat for electricity. As electric power generators, TEGs are advantageous in low grade heat recovery [3]. As opposed to traditional energy conversion devices, they have very simple structures and no moving parts. In addition, they are environmentally friendly, silent, reliable, exhibit excellent scalability and pure DC power output. Currently, TEGs are restricted to low heat-to-power conversion ratios. They are primarily competitive in niche applications, such as exhaust heat recovery, remote power supply and back-up power units [4,5]. If their efficiency can be improved in the future, for example from the present device figure of merit (ZT) $\approx$ 1 to ZT $\geq$ 2, many applications will materialize [6,7]. More widespread use of thermoelectrics requires not only novel materials with improved performance characteristics [8–10], but also TEG systems properly constructed [11–13].

Research on TEG systems can be categorized into optimization of the TEG modules themselves, and assembly of TEG modules with heat transfer structures. There are numerous publications considering the inner structure of TEG modules [14–17]. However, as mentioned by Hendricks and Lustbader [18], the whole TEG system should be studied as an integrated

* *Corresponding author*. Tel.: +45 21370579, fax: +45 98151411.
E-mail addresses: xga@et.aau.dk (X. Gao), skk@et.aau.dk (S.K. Kær).
0360-3199/$ – see front matter
doi:10.1016/j.ijhydene.2012.03.009

solution, because TE material properties and heat exchanging performance are tightly intertwined. Modeling and simulation plays the main role in the studies referenced in the next section.

Much effort has been made to study a single-/multi-element TEG module with its external heat reservoirs [19–21]. However, in practice, a concrete TEG system is always a combination of TEG modules with proper heat exchanging structures in very large scale installations to duly account for the magnitude of the exhaust heat sources. Suzuki and Tanaka compared the performance of 15 flat thermoelectric panels [22] and 6 different geometrical arrangements of cylindrical thermoelectric tubes [23]. Crane and Jackson [24] proposed a numerical model of a practical TEG waste heat recovery system with an advanced cross-flow heat exchanger and later the model was validated in experiments. Based on the aforementioned research work, Yu and Zhao [25], Smith [26] and Espinosa et al. [27] used different numerical models in a TEG system investigation for different waste heat sources. Recovering exhaust heat from fuel cells is a relatively novel application of TEGs. Chen et al. [28] proposed a module-level three dimensional TEG model in ANSYS FLUENT for the convenience of the co-design and co-optimization of a PEMFC-TEG system. The PEMFC-TEG system was also preliminarily demonstrated in the lab. A solid oxide fuel cell-TEG (SOFC-TEG) hybrid system was optimized on the main variables and the operating conditions in [29] using a zero-dimensional system model. Overall, the previous work has significant attributes in analyzing TEGs in practical applications. Some features can be further enhanced, including the following:

1) Fluid properties, flow condition, heat transfer [20] and TEG performance are locally resolved on each segment in a discretized TEG heat recovery system model for higher model accuracy.
2) The recovery system model is engineering-oriented. Factors affecting the system performance are able to be co-optimized in the model.
3) Mature heat exchanger structures and commercially available TEG modules are used in the model to benefit the system optimization and fabrication.

In the present paper, a TEG exhaust heat recovery system is modeled and optimized for the cathode exhaust gas of a HTPEMFC stack. Basically, it is a system similar to compact plate-fin heat exchangers but with TEG modules mounted on the walls. Cathode exhaust gas and coolant water are the working media. A numerical model for the system is proposed and validated. The model is intended to optimize the system design and operation with higher accuracy and flexibility as well as to assist the system fabrication. Sensitivity analyses are then carried out to identify the parameter priority for later configuration optimization. Finally, the system configuration is optimized.

2. Model description

The chosen architecture of the TEG exhaust heat recovery system is illustrated in Fig. 1. The compact heat exchanger housing is placed in the middle for the exhaust gas. Two aluminum blocks are settled at the top and the bottom.

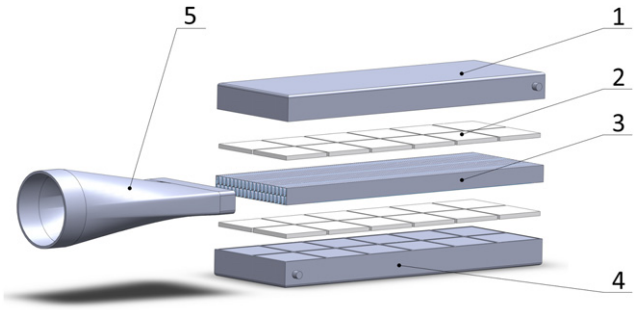

Fig. 1 – The architecture of the TEG exhaust heat recovery system. (1,4 – Aluminum block; 2 – TEG module assembly; 3 – Compact heat exchanger housing; 5 – Diffuser).

Coolant water circulates through the flow fields inside the aluminum blocks to establish the temperature difference. TEG modules are assembled between the housing and the blocks.

Apart from part 5, the other four parts in Fig. 1 form the main body of the system. The size of the main body is determined by the number of TEG modules along and perpendicular to the flow direction, namely n_{run} and n_{cro}. These four parts are discretized into segments using a control volume methodology. As illustrated in Fig. 2, the segments are shaped via evenly dividing the whole system along and perpendicular to the flow direction by designated numbers, n_x and n_y. Each segment includes a part of TEG modules and the heat reservoirs on both sides.

Part 5 in Fig. 1 is the diffuser, the function of which is to distribute the exhaust gas homogeneously among the flow passages inside the heat exchanger housing. The exhaust gas is from a 1 kW HTPEMFC stack operating under normal conditions. The gas flow rate is $\dot{m}_{gas} = 12.61$ g/s. Its temperature is $t_{gas} = 148.2$ °C. Its humidity ratio is $\omega_{gas} = 0.02076$. Considering that the stoichiometry is as high as 20 and the oxygen depletion is small, it is of satisfactory accuracy to model the exhaust gas as ideal moist air. The thermodynamic data are from Hyland and Wexler [30]. The remaining assumptions of the numerical model are as follows:

1) There is no heat loss from the system to the surroundings.
2) The electrical/thermal contact resistances between the TEG modules and the electric load/heat reservoirs are neglected. There are no heat bypasses through the gaps between the TEG modules.

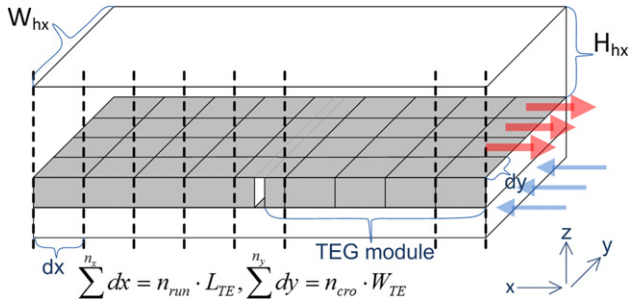

Fig. 2 – Control-volume scheme of the system.

3) Thermoelectric materials distribute homogeneously inside each module.
4) No phase change occurs inside the heat exchanger. Axial heat conduction is neglected. System performance is identical in the direction perpendicular to the exhaust gas flux.
5) When calculating the pressure drop, contraction and expansion pressure losses are neglected.
6) Heat conduction and convection in the aluminum blocks as well as between the TEG modules and the aluminum blocks are not taken into account. The coolant water flow is set to be high enough so a uniform temperature of 20 °C can represent the cold side.

Based on the above assumptions, the governing equations for each segment can be given based on the energy balance.

2.1. TEG modules

The way to model TEG modules is reconsidered compared to other publications in the field to better serve the system level study. Modules are treated as black boxes in the model. Inside each module, thermoelectric materials are supposed homogeneously distributed. Unlike most of the above literature, module parameters are from the experiments in [26], not directly substituted by material properties. Module performance calculated from empirical parameters is more reproducible in real-life applications. After the module is discretized in the x and y directions but not along the z axis, TEG performance is assumed uniform in each segment but vary with temperature between segments. For system design and fabrication, the advantage of modeling TEG modules in this way would be twofold: a) mitigating the model complexity and b) keeping the model precision from being affected by simplifying the details inside the TEG modules. The module parameters used in the current system are listed in Table 1. The Thomson effect is neglected because the temperature difference is relatively moderate in this case [31].

For each TEG segment, the corresponding energy balance is described by the following equations:

$$\dot{q}_{h,TE}(i) = (\overline{T}_{h,TE}(i) - \overline{T}_{c,TE}(i))/R_{t,i} + \alpha_i \overline{T}_{h,TE}(i) I_i - 0.5 I_i^2 R_{e,i}, \quad (1)$$

$$\dot{q}_{c,TE}(i) = (\overline{T}_{h,TE}(i) - \overline{T}_{c,TE}(i))/R_{t,i} + \alpha_i \overline{T}_{c,TE}(i) I_i + 0.5 I_i^2 R_{e,i}, \quad (2)$$

$$w(i) = \dot{q}_{h,TE}(i) - \dot{q}_{c,TE}(i). \quad (3)$$

All segments can either electrically work in series or in standalone mode. In standalone mode, the external ohmic resistance equals the internal when one segment reaches its peak power output and the corresponding electric current is:

$$I_i = 0.5(\alpha_i)(\overline{T}_{h,TE}(i) - \overline{T}_{c,TE}(i))/R_{e,i}. \quad (4)$$

The total power output of the whole TEG assembly can be summed up as:

$$P_{TEA} = \sum^{nx} \sum^{ny} w(i). \quad (5)$$

Table 1 – TEG module parameters [26].

Properties	Values
Type	Melcor HT8
$W_{TE} \cdot L_{TE}$ (m^2)	0.04001·0.04001
α_{TE} (V/K)	$-0.0000438 \cdot T_{av} + 0.05$
$R_{TE,e}$ (Ω)	$0.00638 \cdot T_{av} + 2.00$
$R_{TE,t}$ (K/W)	$0.000284 \cdot T_{av} + 1.54$

T_{av}–(°C), the average temperature between the two sides of each module.

2.2. Compact plate-fin heat exchanger

Choosing the best heat exchanger for heat recovery is a common problem. In the current model, a lookup table is integrated to alleviate this problem. The table contains 59 types of commercialized compact plate-fin heat exchangers. All the heat exchanger geometry and relevant parameters in the table are taken from [32]. Attempts towards numerical prediction of heat exchanger performance easily fail in matching experimental data. However the correlations and parameter data herein were generated from experimental work by Kays and London. These correlations and data have found extensive application in industry, particularly in less-critical designs. Compared to homemade heat exchanging structures, modeling in this way can better fulfill the system optimization and fabrication requests.

The governing equations to describe the heat transfer between the TEG assembly and the hot/cold fluids in each segment, respectively, are:

$$\dot{q}_{h,TE}(i) = \dot{q}_{gas}(i) = \dot{m}_{gas}(h_{gas,i} - h_{gas,i+1}), \quad (6)$$

$$\dot{q}_{gas}(i) = \varepsilon_{ctf}(i)\dot{m}_{gas}\left(h_{gas,i} - h_{gas,i}^{cw}\right), \quad (7)$$

$$\dot{q}_{h,TE}(i) = UA_{hx}(i)(\overline{T}_{gas}(i) - \overline{T}_{h,TE}(i)), \quad \overline{T}_{gas}(i) = (T_{gas}(i) + T_{gas}(i+1))/2. \quad (8)$$

The coefficients in the above functions are given as follows:

$$1/UA_{tot}(i) = 1/UA_{hx}(i) + 1/UA_{TE}(i), \quad (9)$$

$$\varepsilon_{ctf}(i) = 1 - \exp(-NTU(i)), \quad NTU(i) = 2UA_{tot}(i)\overline{T}_{gas}(i)/\dot{m}_{gas}(h_{gas,i} + h_{gas,i+1}). \quad (10)$$

h_{gas} is the enthalpy of the exhaust gas and h_{gas}^{cw} is the exhaust gas enthalpy at the temperature of the coolant water. They are calculated on each segment from functions found in [30]. $UA_{hx}(i)$ is the heat exchanger conductance in each segment, which describes both the air-exchanger heat convection and the heat conduction in the exchanger body. It is determined by the exchanger material and structure, the local fluid properties as well as the flow condition of the exhaust gas. In details, the key functions are [32]:

$$A_{hx}(i) = \tau(i) H_{hx} W_{hx} dx/n_y \quad (11)$$

$$Co(i) = j_{hx} u_{gas}(h_{gas,i} + h_{gas,i+1})/2Pr_i^{(2/3)}\overline{T}_{gas}(i) \quad (12)$$

$$u_{gas} = \dot{m}_{gas}/A_{ff} \quad (13)$$

$$RE_i = u_{gas} D_h/\nu_{gas,i} \quad (14)$$

For any kind of heat exchanger, there is an operational region of Reynolds number. This information is also available in the lookup table.

In addition, the pressure drop through the heat exchanger housing can be evaluated from the following function,

$$\Delta p_{hx} = \left(u_{gas}^2/\left(2\rho_{gas,in}\right)\right)\left[4f_{hx}L_{hx}\rho_{gas,in}/\left(D_h\bar{\rho}_{gas}\right) + (1+\sigma^2)\left(\left(\rho_{gas,in}/\rho_{gas,out}\right)-1\right)\right] \quad (15)$$

The Colburn factor j_{hx} and the Friction factor f_{hx} of plate-fin surfaces are also from the experimental source [32].

2.3. Solution methodology

The solution methodology of the numerical model is implemented by using a discretized ε-NTU approach [33]. Input parameters include the thermo-physical properties and electrical connection style of TEG modules, configuration parameters of TEG modules and plate-fin heat exchangers as well as the inlet exhaust gas parameters into the plate-fin heat exchanger. Then the fluid properties, thermoelectric performance and heat transfer process are updated on each segment along the flow direction. Finally, results are exported.

The discretized ε-NTU harnessed here is to make sure the model is better suited for both simulation-type and design-type problems [34]. Algebraically, it is identical with the log-mean temperature difference method (LMTD) [34].

3. Simulation results and discussion

In the following numerical simulation, the heat exchanger type used is called 'Strip-fin plate-fin, surface 1/4(s)-11.1' [35]. It is characterized by a low pressure drop for high heat exchanging capability [27]. More details of its specifications can be found in [32]. The only exception is in Section 3.5, where the performance of different heat exchangers is compared.

3.1. Model validation

A check is carried out to balance the computational requirements and the result accuracy. There are 10 Melcor HT8 modules along and perpendicular to the flow direction, under which case the system is oversized. All TEG segments during the simulation run are in standalone mode. In other words, each segment is assumed to be connected to a matched load to maximize its power output. According to the 4th assumption above, only the number of segments along the flow direction can potentially affect the simulation results. Therefore the segment number per TEG module is varied from 1 to 20 to observe its influence. The representative results of the TEG hot side temperature and the system power output are shown below.

In Fig. 3, it is clear that the effect of the number of segments on the TEG hot side temperature distribution is not significant. If this temperature distribution was studied independently, there would be no need to pay attention on the number of segments. On the other hand, it impacts the system power output evidently. Fig. 4 illustrates the system power output and its relative error versus the segment number. For a deviation less than 0.5%, cutting each module into 6 segments in the flow direction is the minimum requirement. It means it is not necessary to discretize each module by the width of each thermoelement or the distance between adjacent thermoelements as in literature. In the following simulations, this number is adjusted accordingly.

Simulations are then conducted to validate the system model with experimental data. Firstly, the discretized TEG model is compared with experimental results from [26]. Throughout the validation, three temperatures are respectively set to the module hot side, while the cold side is kept constant at 50 °C, to follow the experiment settings. Sorted by the temperature difference, the module power outputs are plotted in Fig. 5. The results show a perfect correspondence between the discretized TEG model and the experiments.

Secondly, the performance of the heat exchanger part is verified against the experimental results from [27]. The heat exchanger type harnessed in the experiments was also the one, 'Strip-fin plate-fin, surface 1/4(s)-11.1'. For comparison, the heat transferred and the pressure drop are used for comparison. Results are shown in Fig. 6.

According to Fig. 6, it can be concluded that the simulation results are in good agreement with the experimental results. They also show similar trends. The difference relatively observable only lies in the low flow rate region. The reason is that some vital details are missing in the reference, such as the exact temperature difference, the hot gas composition, among others. As a whole, the deviation still falls inside a 10% range. So it is concluded that the accuracy of the heat exchanger model is acceptable.

The numerical model of the TEG exhaust heat recovery system model is thus considered developed and validated. Before conducting optimization on the system configuration, a sensitivity analysis is essential to identify which parameters have more significant impact on the system performance.

3.2. Sensitivity analysis

A multiple parameter sensitivity analysis is carried out in this section to determine the main variables of this system that

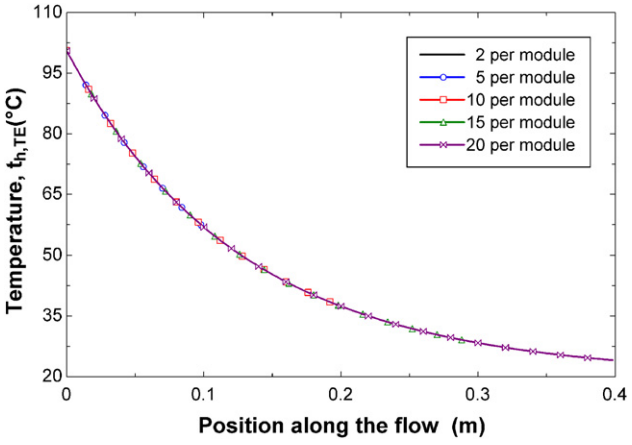

Fig. 3 – TEG hot side temperature distribution vs. the segment number.

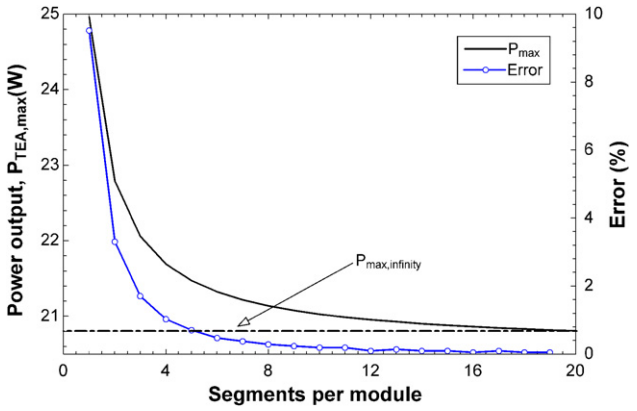

Fig. 4 – System power output with segments from 1 to 20 per module.

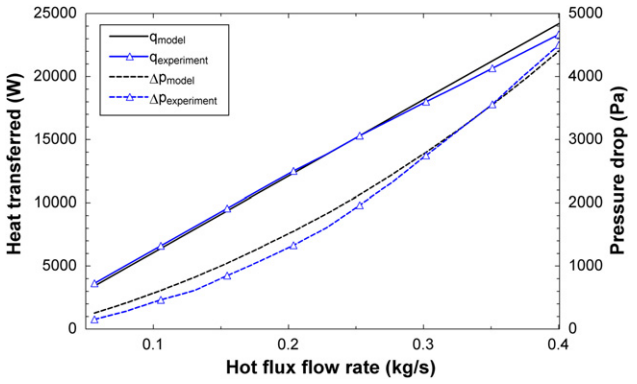

Fig. 6 – Heat exchanger model validation by heat transferred and pressure drop.

affect the performance. An uncertainty propagation tool is used to study the effects on system model output when the independent parameters vary in given ranges [35]. This method was initially designed for experiments to assess the deviations in measurement of the calculated variables. As described in [36], this calculation assumes the independent variables are uncorrelated and random, i.e. neglecting covariance between them; the uncertainty in the system performance can be expressed as

$$U_\eta = \sqrt{\sum_i (\partial\eta/\partial X_i)^2 U_{X_i}^2}, \text{ where } \eta = f(X_1, X_2, \ldots, X_n). \quad (16)$$

Here factors that affect the system power output $P_{TEA,max}$ and the heat exchanger pressure drop Δp_{hx} are analyzed using the uncertainty propagation. These factors can be distinguished into three categories: system structural parameters, TEG properties and operating conditions. System structural parameters further have two subcategories, namely system dimensions and heat exchanger type. Results are listed in Tables 2 and 3. Every input variable is set with a relative uncertainty of 5.00%.

The results show that the system power output and the pressure drop are affected by an uncertainty of 17.08% and 13.46%, respectively. The influences are rather significant, which means that some of the input parameters should be carefully treated in the simulation for higher model accuracy as well as in practice for better system performance.

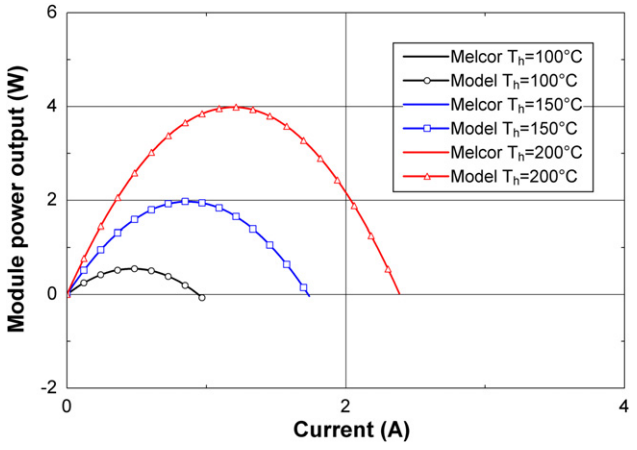

Fig. 5 – Validation of the discretized TEG model.

By observation it can be seen that the larger sources of the power output uncertainty are five parameters. These are the exhaust gas temperature, mass flow rate, specific heat, heat resistance of each TEG module and the module's Seebeck coefficient. As verified by many literatures, the exhaust gas temperature has extremely significant influence on the TEG power output. The exhaust gas temperature, together with the mass flow rate and the specific heat, determines the capacity of the heat source, which is available for TEGs to convert into electricity. Similarly, the module heat resistance and the Seebeck coefficient dominate the conversion efficiency of the whole TEG assembly. If any of the above parameters becomes larger, the system power output will increase and vice versa.

On the other hand some input parameters have negligible effect on the system power output. These include the exhaust gas pressure and most system structural parameters, such as the number of modules crossing the flow direction, number of modules along the flow direction and so on. The power output insensitivity to these structural parameters actually indicates that the current system is oversized. This insensitivity is also the side effect of all TEG segments working in standalone mode in the current system. The structural parameters will be more thoroughly analyzed in the following sections. Another parameter with little effect is the exhaust gas pressure. This can have a positive effect on the system electrical efficiency because little pressure boost is required for the recovery system. This can also simplify the connection between the recovery system and the fuel cell stack, because the feed gas pressure also has a minor effect on the fuel cell performance. As a whole, the system parasitic losses are decreased.

Parasitic losses and system pressure drops are roughly proportional in the current system. From Table 3, it can be concluded that almost all the uncertainty of the pressure drop comes out of the system structural parameters and the exhaust gas magnitude. Among them, the exhaust gas flow rate and number of TEG modules perpendicular to the flow have the most significant effect. The influence of the exhaust gas pressure, the height of the heat exchanger and number of TEG modules along the flow direction is also rather significant. These influences have been clearly described by the above Eq.

Table 2 – Sensitivity study on system power output.

Input parameters and description		Value	Uncertainty contribution (%)
$A_{fin\backslash A}$	Fin area/total area	0.756	−0.00
α_{hx}	Heat transfer area/total volume (m^2/m^3)	915.6	1.35
H_{hx}	Height of heat exchanger (m)	0.00635	0.71
fin_{thk}	Thickness of fins (not applicable to pin-fin) (m)	0.000152	0.00
$Co_{hx,av}$	The exchanger average heat conductivity (W/m^2-K)	80.58	1.30
n_{cro}	Number of modules cross the flow direction	10	0.01
n_{run}	Number of modules along the flow direction	10	0.01
α_{TE}	Seebeck coefficient of each TEG module (V/K)	0.05	19.67
$R_{TE,e}$	Electric resistance of each TEG module (Ω)	2	−4.92
$R_{TE,t}$	Heat resistance of each TEG module (K/W)	1.54	10.71
$\dot{m}_{gas}$	The exhaust gas mass flow rate (kg/s)	0.01261	7.96
Cp_{gas}	Average exhaust gas specific heat (J/kg-°C)	1047	7.96
ω_{gas}	Humidity Ratio	0.02076	−0.00
p_{gas}	Gas pressure (Pa)	1	0.00
t_{gas}	Gas temperature (°C)	148.2	44.51
t_{cw}	Coolant water temperature (°C)	20	−0.89
Output	Variable description	Value	Uncertainty (%)
$P_{TEA,max}$	Maximum power output of the system	24.10 (W)	± 4.12 (W) (±17.08%)

(15). On the contrary, the effect of the exhaust gas temperature and its specific heat is relatively moderate. It can be noticed that, even in the current oversized system, the system structural parameters still have dramatic impact on the system pressure drop. To lower the pressure drop, as well as maximize the system net power output, the system dimensions and the heat exchanger types need a more detailed analysis.

3.3. *Influence of* n_{cro}

The number of TEG modules perpendicular to the flow direction is varied to investigate the impact of the heat exchanger width on the system power output and the pressure drop. All TEG segments in this study worked in standalone mode. The number of TEG modules along the flow direction was designated to 30. Under this condition the system was always oversized along the flow direction for every n_{cro}. In the simulation, n_{cro} increased from the minimum value of 2. Under the above settings, the system power output will reach its upper limit in all cases.

The simulation results are shown in Fig. 7. The width tends to decrease the electric power generated and the pressure drop simultaneously. The pressure drop falls sharply down in the beginning. But after n_{cro} reaches 8, the effect is rather moderate. On the other hand the system power output drops gradually all the way down with n_{cro} increasing, although a little bit faster in the first half range. The increasing width increases the cross section area of the flow passage. The flow speed then drops. In turn, it can be calculated by Eq. (15) that the pressure drop will decrease. But with decreasing flow speed, Reynolds number is also becoming smaller. As a result, poorer convective heat transfer in the heat exchanger will reduce the temperature difference on TEG modules and reduce the power output.

Table 3 – Sensitivity study on the system pressure drop.

Input parameters and description		Value	Uncertainty contribution (%)
$A_{fin\backslash A}$	Fin area/total area	0.756	0.00
α_{hx}	Heat transfer area/total volume (m^2/m^3)	915.6	−0.00
H_{hx}	Height of heat exchanger (m)	0.00635	−15.64
fin_{thk}	Thickness of fins (not applicable to pin-fin) (m)	0.000152	−0.00
$Co_{hx,av}$	The exchanger average heat conductivity (W/m^2-K)	80.58	−0.00
n_{cro}	Number of modules cross the flow direction	10	−28.11
n_{run}	Number of modules along the flow direction	10	13.13
α_{TE}	Seebeck coefficient of each TEG module (V/K)	0.05	0.00
$R_{TE,e}$	Electric resistance of each TEG module (Ω)	2	0.00
$R_{TE,t}$	Heat resistance of each TEG module (K/W)	1.54	0.01
$\dot{m}_{gas}$	The exhaust gas mass flow rate (kg/s)	0.01261	28.06
Cp_{gas}	Average exhaust gas specific heat (J/kg-°C)	1047	0.03
ω_{gas}	Humidity Ratio	0.02076	−0.00
p_{gas}	Gas pressure (Pa)	1	−13.80
t_{gas}	Gas temperature (°C)	148.2	1.20
t_{cw}	Coolant water temperature (°C)	20	0.02
Output	Variable description	Value	Uncertainty (%)
Δp_{hx}	Pressure drop of the system	383.10 (Pa)	± 51.58 (Pa) (±13.46%)

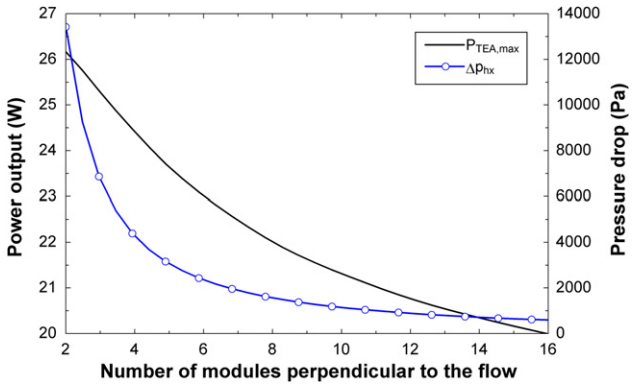

Fig. 7 – Power output and pressure drop vs. number of TEG modules cross the gas flow.

As mentioned above, the pressure drop accounts for most of the system parasitic losses, through determining the power demand of the blower in the system. If only the following function from [37] is used to assess the power demand, an n_{cro} value higher than 8 will be the preferred choice. But actually, the blower in the whole fuel cell and TEG integrated system mainly serves the fuel cell stack. Therefore a further systematic study is essential here to more properly predict the effect of the recovery system pressure drop on the net power output of the whole system. In this paper, the value of n_{cro} is set to 6 in the following analysis.

$$P_{comp} = \dot{m}_{gas} R_{gas} T_{in} \ln(p_{out}/p_{in}) / M_{gas} \eta_{comp} \quad (17)$$

3.4. *Influence of* n_{run}

A simulation was also carried out to study the effect on the system performance from the length of the flow channels, which is determined by the number of TEG modules along the exhaust gas flow direction, n_{run}. The other settings were: n_{cro} was fixed to 6; all TEG segments were either in series or in standalone mode. The results are compared in Fig. 8.

It can be seen that the two system power output curves are overlapped and increase very fast in the beginning. Then the power output curve, when all TEG segments are operating in standalone mode, tends to approach the theoretical upper limit. There is no optimum value of n_{run}. But the power output of all segments in series starts to drop down slowly after reaching the maximum point, where $n_{run} = 7$. This effect is similar as what has been reported in [38]. It was believed that the peak point is the trade-off between the electromotive force and the internal resistance, when all TEG modules are in series. In real-life applications, both of the above connection methods of the TEG segments are either lacking feasibility or reliability. A mixed connection method and an intermediate power output are considered more feasible.

On the other hand the system pressure drop under both connection conditions is roughly proportional to n_{run} in the whole range. It can also be noticed that the two curves are completely overlapping. This phenomenon corresponds with the above sensitivity analysis, which proved that the system pressure drop is independent from the performance of the TEG modules.

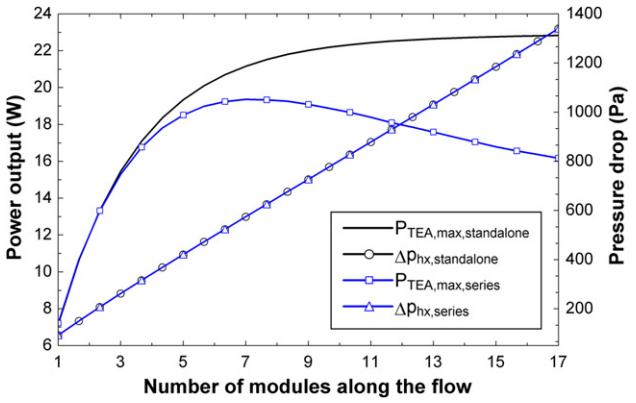

Fig. 8 – Power output and pressure drop vs. n_{run}.

3.5. *Influence of heat exchanger design*

In this section, different types of heat exchangers are compared by the influence on the system power output and the pressure drop. Based on the analyses above, 6 TEG modules were aligned across the exhaust gas flow in the simulation; 7 modules were along the flow direction. All TEG segments were electrically connected in standalone mode. Judged by their feasible Reynolds number interval, the results from 33 types of plate-fin heat exchangers among all 59 types are shown in Fig. 9. The results are sorted by the power output. Heat exchangers with pressure drop larger than 900 Pa are not included.

It can be seen that with the ascending power output, the pressure drop fluctuates significantly between different heat exchangers. Obviously, heat exchangers with higher power output and lower pressure drop are superior. From Fig. 9, four types are identified of interest for further study, namely 'Plain plate-fin, surface 15.08' (17), 'Pin-fin plate-fin, surface PF-10(F)' (25), 'Strip-fin plate-fin, surface 1/6–12.18(D)' (28) as well as 'Pin-fin plate-fin, surface PF-4(F)' (33). The type 'Strip-fin plate-fin, surface 1/4(s)-11.1' currently used in the exhaust heat recovery system is the type (19) in Fig. 9.

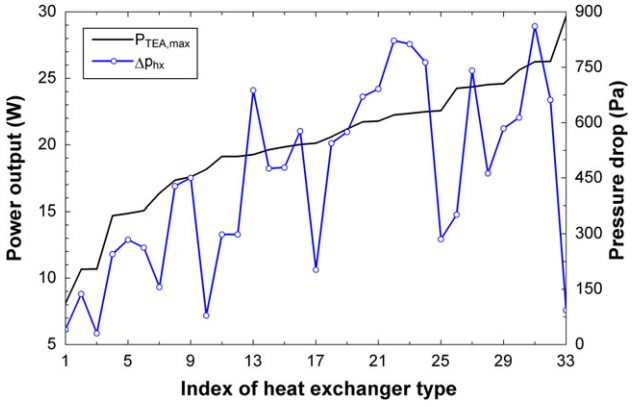

Fig. 9 – Power output and pressure drop using different heat exchangers.

4. Conclusions

A numerical model of a TEG heat recovery system for the exhaust gas from a HTPEMFC stack was developed. It is based on a finite-element approach with more precisely described gas properties and heat transfer. For both design-type and simulation-type problems, the versatility of the model is enhanced by the integrated database of 59 types of plate-fin heat exchangers and the discretized ε-NTU solution method. In summary, the model can help optimize the system design and operation with higher accuracy and flexibility. In turn, this can benefit the system fabrication.

A sensitivity analysis was then carried out on the system model. It is found that exhaust gas parameters and heat exchanger structure have a significant effect on the system power output and the pressure drop. Gas properties should be precisely described. The configuration of the system should be carefully optimized to maximize its performance.

Based on the model, the optimized system configuration of the heat recovery system is finally depicted. There are 6 TEG modules crossing the exhaust gas flow and 7 modules along the flow. In the system, the TEG module type is assumed to be the Melcor HT8 type. They are all electrically connected in series. The heat exchanger, type 'Strip-fin plate-fin, surface 1/4(s)-11.1', is implemented, which was also chosen by other researchers [27].

Screening the whole database of different heat exchangers, it turns out that the heat exchanger structure currently used in the system is probably not the best choice; Four other types are identified with superior performance and worthy of further analysis.

Future work is needed; Experiments are still needed to verify the model accuracy. The heat transfer phenomena in the coolant water side and water vapor phase change in the exhaust gas could be included to improve the model robustness. In the sensitivity analysis, uncertainty intervals of the input parameters need further consideration to better reflect realistic conditions. In comparing different heat exchangers, the system dimensions will be optimized for them respectively. More types of heat exchangers can also be included in the database.

Acknowledgments

The authors gratefully acknowledge financial support from Aalborg University and China Scholarship Council. The authors would like to thank Alexandros Arsalis for reviewing.

REFERENCES

[1] Wang Y, Chen KS, Mishler J, Cho SC, Adroher XC. A review of polymer electrolyte membrane fuel cells: technology, applications, and needs on fundamental research. Applied Energy 2011;88(4):981–1007.

[2] Andreasen SJ, Ashwortha L, Remóna INM, Kær SK. Directly connected series coupled HTPEM fuel cell stacks to a Li-ion battery DC-bus for a fuel cell electrical vehicle. International Journal of Hydrogen Energy 2008;33(23): 7137–45.

[3] Rowe DM. Thermoelectric generators as alternative sources of low power. Renewable Energy 1994;5(2):1470–8.

[4] Crane DT, LaGrandeur JW. Progress report on BSST-Led US department of energy automotive waste heat recovery program. Journal of Electronic Materials 2010;39(9):2142–248.

[5] Auckland DW, Shuttleworth R, Luff AC, Axcell BP, Rahman M. Design of a semiconductor thermoelectric generator for remote subsea wellheads. Electric Power Applications, IEE Proceedings 1999;142(2):65–70.

[6] Yang J, Stabler FR. Automotive applications of thermoelectric materials. Journal of Electronic Materials 2009;38(7):1245–51.

[7] Chen M, Sasaki Y, Suzuki RO. Computational modeling of thermoelectric generators in marine power plants. Materials Transactions 2011;52(8):1549–52.

[8] Snyder GJ, Toberer ES. Complex thermoelectric materials. Nature Materials 2008;7(2):105–14.

[9] Minnich AJ, Dresselhaus MS, Ren ZF, Chen G. Bulk nanostructured thermoelectric materials: current research and future prospects. Energy & Environmental Science 2009; 2(5):466–79.

[10] Venkatasubramanian R, Siivola E, Colpitts T, O'Quinn B. Thin-film thermoelectric devices with high room-temperature figures of merit. Nature 2001;413(6856):597–602.

[11] Gao M, Rowe DM. Ring-structured thermoelectric module. Semiconductor Science and Technology 2007; 22(8):880–3.

[12] Bell LE. Cooling, heating, generating power, and recovering waste heat with thermoelectric systems. Science 2008; 321(5895):1457–61.

[13] Chen M, Lund H, Rosendahl L, Condra T. Energy efficiency analysis and impact evaluation of the application of thermoelectric power cycle to today's CHP systems. Applied Energy 2010;87(4):1231–8.

[14] Ioffe AF. Semiconductor thermoelements and thermoelectric cooling. London: Infoseach Limited; 1957.

[15] Rowe DM, Gao M. Evaluation of thermoelectric modules for power generation. Journal of Power Sources 1998;73(2):193–8.

[16] Crane D, Bell LE. Progress towards maximizing the performance of a thermoelectric power generator. In: Proceedings of International Conference on thermoelectrics, vol. 1; 2006. p. 11–6.

[17] Chen M, Rosendahl LA, Condra T. A three-dimensional numerical model of thermoelectric generators in fluid power systems. International Journal of Heat and Mass Transfer 2011;54(1–3):345–55.

[18] Hendricks TJ, Lustbader JA. Advanced thermoelectric power system investigations for light-duty and heavy duty applications: part II. In: Proceedings of the 21st International Conference on thermoelectrics, vol. 1; 2002. p. 381–94.

[19] Chen J, Wu C. Analysis on the performance of a thermoelectric generator. Journal of Energy Resources Technology 2000;122(2):61–3.

[20] Esartea J, Gao M, Rowe DM. Modelling heat exchangers for thermoelectric generators. Journal of Power Sources 2001; 93(1–2):72–6.

[21] Pramanick AK, Das PK. Constructal design of a thermoelectric device. International Journal of Heat and Mass Transfer 2006;49(7–8):1420–9.

[22] Suzuki RO, Tanaka D. Mathematical simulation of thermoelectric power generation with the multi-panels. Journal of Power Sources 2003;122(2):201–9.

[23] Suzuki RO, Tanaka D. Mathematic simulation on thermoelectric power generation with cylindrical multi-tubes. Journal of Power Sources 2003;124(1):293–8.

[24] Crane DT, Jackson GS. Optimization of cross flow heat exchangers for thermoelectric waste heat recovery. Energy Conversion and Management 2004;45(9–10):1565–82.

[25] Yu J, Zhao H. A numerical model for thermoelectric generator with the parallel-plate heat exchanger. Journal of Power Sources 2007;172(1):428–34.
[26] Smith KD. An investigation into the viability of heat sources for thermoelectric power generation systems, [Master thesis]. Rochester (NY): Rochester Institute of technology; 2009.
[27] Espinosa N, Lazard M, Aixala L, Scherrer H. Modeling a thermoelectric generator applied to diesel automotive heat recovery. Journal of Electronic Materials 2010;39(9):1446–55.
[28] Chen M, Andreasen SJ, Rosendahl L, Kær SK, Condra T. System modeling and validation of a thermoelectric fluidic power source: PEMFC-TEG. Journal of Electronic Materials 2010;39(9):1593–600.
[29] Chen X, Pan Y, Chen J. Performance and evaluation of a fuel cell – thermoelectric generator hybrid system. Fuel Cells 2010;10(6):1164–70.
[30] Hyland RW, Wexler A. Formulations for the thermodynamic properties of the saturated phases of H_2O from 173.15 K to 473.15 K. ASHRAE Transactions 1983;89(2A):500–19.
[31] Lazard M, Fraisse G, Goupil C, Scherrer H. Thermal analysis of a thermoelectric: a way to non conventional design. In: Proceedings of the 6th European Conference on thermoelectrics, vol. 1; 2008. p. 2–15.
[32] Kays WM, London AL. Compact heat exchangers. 3rd ed. New York: McGraw Hill; 1984.
[33] Iu I, Weber NA, Bansal P, Fisher DE. Applying the effectiveness-NTU method to elemental heat exchanger models. ASHRAE Transactions 2007;113(1):504–13.
[34] Nellis G, Klein S. Heat transfer. New York: Cambridge University Press; 2009.
[35] F-Chart Software. EES manual, www.fchart.com; 2010. v8.590 Edition.
[36] Taylor BN, Kuyatt CE. Guidelines for evaluating and expressing the uncertainty of NIST measurement results. National Institute of Standards and Technology; 1994 [Technical Note 1297].
[37] Kolb G. Fuel processing: for fuel cells. Weinheim, Germany: Wiley-VCH; 2008.
[38] Mori M, Yamagami T, Oda N, Hattori M, Sorazawa M, Haraguchi T. Current possibilities of thermoelectric technology relative to fuel economy. Society of Automotive Engineering; 2009. 2009-2101–0170.

Nomenclature

A_{ff}: minimum free flow area, m^2
A_{hx}: total heat transfer area, m^2
c: gas specific heat, J/kg-K
D_h: hydraulic diameter, m
f_{hx}: Friction factor
h: exhaust gas enthalpy, kJ/kg
H: component height, m
I: electric current, A
j_{hx}: Colburn factor
L: component length, m
n_x: total number of segments along the flow
n_y: total number of segments crossing the flow
P: power output or consumption, W
Δp: pressure drop, Pa
q: heat transferred, W
T, t: temperature, K, °C
u_{gas}: core mass velocity, Kg/s-m^2
w: power output of each segment, W
W: component width, m

Greek symbols

ε_{ctf}: the effectiveness
ν: kinematic viscosity, m^2/s
ρ: exhaust gas density, kg/m^3
σ: minimum free flow area/frontal area
τ: heat transfer area/exchanger volume, 1/m

Subscripts/Superscripts

c,TE: cold side of the TEG module
cw: coolant water
e: electrical resistance
gas: exhaust gas
h,TE: hot side of the TEG module
hx: heat exchanger
i: segment index
max: maximum value
t: thermal resistance
TEA: whole TEG assembly

Abbreviation

Co: exchanger heat conductivity, W/m^2-K
NTU: number of transfer units
Pr: Prandtl number
RE: Reynolds number
UA: heat exchanger conductance, W/K
ZT: nondimensional figure-of-merit of module

Paper 3

Optimization of a Thermoelectric Generator Subsystem for High Temperature PEM Fuel Cell Exhaust Heat Recovery

Gao, Xin; Andreasen, Søren Juhl; Kær, Søren Knudsen; Rosendahl, Lasse Aistrup

International Journal of Hydrogen Energy, 2014; Doi: 10.1016/j.ijhydene.2014.01.193.

INTERNATIONAL JOURNAL OF HYDROGEN ENERGY XXX (2014) 1–9

Available online at www.sciencedirect.com

ScienceDirect

journal homepage: www.elsevier.com/locate/he

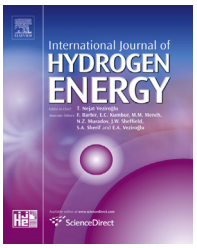

Optimization of a thermoelectric generator subsystem for high temperature PEM fuel cell exhaust heat recovery

Xin Gao, Søren Juhl Andreasen, Søren Knudsen Kær*, Lasse Aistrup Rosendahl*

Department of Energy Technology, Aalborg University, Pontoppidanstræde 101, Aalborg DK-9220, Denmark

ARTICLE INFO

Article history:
Received 17 September 2013
Received in revised form
26 January 2014
Accepted 27 January 2014
Available online xxx

Keywords:
TEG subsystem
Fuel cell
Heat recovery
Heat exchanger
Electrical connection
Optimization

ABSTRACT

In previous work, a thermoelectric (TE) exhaust heat recovery subsystem for a high temperature polymer electrolyte membrane (HT-PEM) fuel cell stack was developed and modeled. Numerical simulations were conducted and have identified an optimized subsystem configuration and 4 types of compact heat exchangers with superior performance for further analysis.

In this work, the on-design performances of the 4 heat exchangers are more thoroughly assessed on their corresponding optimized subsystem configurations. Afterward, their off-design performances are compared on the whole working range of the fuel cell stack. All through this study, different electrical connection styles of all the thermoelectric generator (TEG) modules in the subsystem and their influences are also discussed. In the end, the subsystem configuration is further optimized and a higher subsystem power output is achieved. All TEG modules are now connected into branches. The procedures of designing and optimizing this TE exhaust heat recovery subsystem are drawn out. The contribution of TE exhaust heat recovery to the HT-PEM fuel cell power system is preliminarily concluded. Its feasibility is also discussed.

1. Introduction

Fuel cells are considered as a cornerstone of the approaching hydrogen economy [1,2]. Among other fuel cell technologies, high temperature polymer electrolyte membrane (HT-PEM) fuel cells, operating around 160 °C, offers promising market potential [3–5]. Thanks to the increased operating temperature, they have better fuel impurity tolerance and easier cooling (greater temperature differences versus ambient air), in turn much simpler system configuration and possibility of high system efficiencies [6,7]. Yet another benefit of the relatively high operating temperature, the HT-PEM fuel cell exhaust heat is of higher quality and easier to utilize as process heat or recycle. To recover the exhaust heat for electricity and further boost the system efficiency, a thermoelectric (TE) exhaust heat recovery subsystem has already been introduced to the cathode exhaust of the fuel cell stack in a previous work [8].

In the previous work [8], the subsystem architecture was decided, model was made, and configuration was

* *Corresponding authors*. Tel.: +45 21370579; fax: +45 98151411.
E-mail addresses: xga@et.aau.dk (X. Gao), skk@et.aau.dk (S.K. Kær).

0360-3199/$ – see front matter
http://dx.doi.org/10.1016/j.ijhydene.2014.01.193

Table 1 – -Main equations [8,10].

Description	Equations
TEG properties	$\sum^{n_{x,TE}}\sum^{n_{y,TE}}\alpha_i=\alpha_{TE},\ \sum^{n_{x,TE}}\sum^{n_{y,TE}}R_{e,i}=R_{TE,e},\ \sum^{n_{x,TE}}\sum^{n_{y,TE}}R_{t,i}=R_{TE,t}$
TEG power output	$I_i=0.5(\alpha_i)-(\overline{T}_{h,TE}(i)\overline{T}_{c,TE}(i))/R_{e,i}$ $w(i)=\alpha_i I_i(\overline{T}_{h,TE}(i)-\overline{T}_{c,TE}(i))-I_i^2R_{e,i},\ P_{TEA}=\sum^{nx}n_x\sum^{ny}n_y w(i)$
Heat transfer	$\dot{q}_{h,TE}(i)=\dot{q}_{gas}(i)=\dot{m}_{gas}(h_{gas,i}-h_{gas,i+1})$ $\dot{q}_{gas}(i)=\varepsilon_{ctf}(i)\dot{m}_{gas}(h_{gas,i}-h^{cw}_{gas,i})$ $\dot{q}_{h,TE}(i)=UA_{hx}(i)(\overline{T}_{gas}(i)-\overline{T}_{h,TE}(i)),\ \overline{T}_{gas}(i)=(T_{gas}(i)+T_{gas}(i+1))/2$
Pressure drop	$\Delta p_{hx}=(u^2_{gas}/(2\rho_{gas,in}))[4f_{hx}L_{hx}\rho_{gas,in}/(D_h\overline{\rho}_{gas})+(1+\sigma^2)((\rho_{gas,in}/\rho_{gas,out})-1)]$

preliminarily optimized. As illustrated in Fig. 1, the subsystem is constructed in a way similar to a compact plate-fin gas–liquid heat exchanger. Part No. 3 is the compact heat exchanger housing for the fuel cell stack exhaust gas, which works as the heat source. Part No. 1&4 are two aluminum blocks with a liquid coolant circulating inside, as the heat sink. The coolant is actually a methanol–water mixture, which is stored in a tank primarily as fuel and will be gradually reformed into hydrogen for the fuel cell stack [9]. Thermoelectric generator (TEG) modules, namely part No. 2, are interposed between the aforementioned two parts. As a whole, these parts form the sandwich structure subsystem. The subsystem was then modeled using a finite-element approach with higher precision and better versatility for both design-type and simulation-type problems. Main equations are presented in Table 1. On the model, a sensitivity analysis was carried out and has identified the subsystem main variables. In the end, the subsystem configuration was optimized. There were 6 TEG modules crossing the exhaust gas flow by 7 modules along the flow. They together scale the subsystem size. All the modules were electrically in series. On this optimized configuration, 4 types of heat exchangers with superior performance were also identified.

In this work, instead of keeping the subsystem size invariant in all cases, it is adjusted correspondingly to each of the 4 chosen heat exchangers to more properly assess their performances. Besides the above on-design performance optimization under the same fixed fuel cell stack operating point as in the previous work, research is also carried out on the whole working range of the stack. It is the off-design performance optimization. Another factor that evidently affects the subsystem performance, the electrical connection styles of TEG modules, is also more thoroughly investigated in this work. Finally, the further optimized subsystem is depicted; a more efficient and practical electrical connection scenario of all the TEG modules is proposed; the procedures of designing and optimizing the TEG subsystem are generalized. At the end of this work, the contribution and perspectives of the TE exhaust heat recovery to the HT-PEM fuel cell power system are also discussed.

2. On-design performance optimization

In this paper, all simulation settings not explicitly given are corresponding with the previous work [8] and 'the subsystem power output' refers in particular to its maximum value. The 4 types of heat exchangers studied here were identified by their outstandingly low pressure drop still with high heat transfer performance. Table 2 lists their brief information. More details can be found in Ref. [11].

In this section, the on-design performances of 4 different subsystems denoted by their equipped heat exchangers are analyzed. The word "on-design" refers to the nominal working point of the HT-PEM fuel cell stack. The stack current density is fixed to ≈0.67 A/cm^2; the stack cathode stoichiometry is assumed to be around 19 [12,13]. To this nominal working condition, 4 subsystems are optimized respectively for determining the final optimal subsystem configuration. Results are as follows.

2.1. *Heat transfer process optimization*

To enhance the heat transfer process, the size of the subsystem needs to be optimized, which is scaled by the number of TEG modules crossing the exhaust gas flow and the number of modules along the flow, n_{cro} and n_{run}. Two steps are needed here: 1) finding out the candidate n_{cro}, and 2) choosing the optimum n_{cro} and n_{run}.

Before finding out the candidate n_{cro}, an adequate n_{run} for all the 4 heat exchangers needs to be identified. It requires, under any n_{cro} and any heat exchanger type, all possible exhaust heat will be always recovered by the subsystem. The minimum applicable n_{cro} of 2 is used to pinpoint the adequate n_{run}. For each heat exchanger, there is a smallest n_{run} when the subsystem power output varies less than 0.5% between n_{run} and $n_{run}-1$. Then the largest n_{run} among the four is the adequate n_{run}, which equals 26 in this study. Afterward, this n_{run} is kept invariant to identify the candidate n_{cro} for each of the 4 heat exchangers. Results are presented in the following figures.

Table 2 – The 4 types of heat exchangers [8].

Index	Name	Page no. in Ref. [11]
1	'Plain plate-fin, surface 15.08'	229
2	'Pin-fin plate-fin, surface PF-10(F)'	262
3	'Strip-fin plate-fin, surface 1/6-12.18(D)'	250
4	'Pin-fin plate-fin, surface PF-4(F)'	260

Please cite this article in press as: Gao X, et al., Optimization of a thermoelectric generator subsystem for high temperature PEM fuel cell exhaust heat recovery, International Journal of Hydrogen Energy (2014), http://dx.doi.org/10.1016/j.ijhydene.2014.01.193

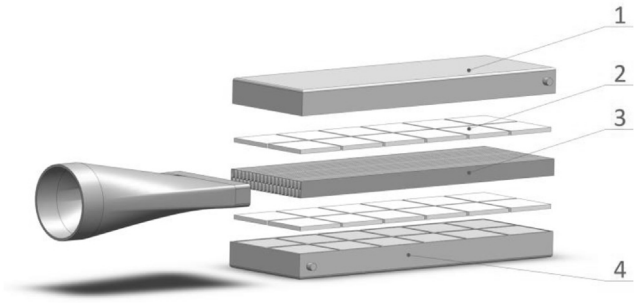

Fig. 1 – The architecture of the subsystem main body (1,4 – Aluminum blocks; 2 – TEG module assembly; 3 – Compact heat exchanger housing).

Fig. 2 shows the subsystem power output and its pressure drop changing with n_{cro} on each of the 4 heat exchangers. On the whole in all 4 cases, the subsystem power output drops monotonically with n_{cro} increasing and the trend becomes moderate in the second half range. The exception is the rise happening at the beginning in case 4. This is explained by the possible whistle problems and should be avoided in practice [11]. Considering the subsystem pressure drop in each case, there is a steep decrease in the first half range and then the effect of increasing n_{cro} fades out. It is clear the candidate n_{cro} is a tradeoff between the subsystem power output and its pressure drop [8]. In this study, the subsystem pressure drop is not allowed to go above 900 Pa. Constrained by this, the candidate n_{cro} for each heat exchanger can only be selected among 4, 6 and 8. The final choice is the result of the interplay between n_{cro} and n_{run}.

From Fig. 2, it can also be observed that the subsystem on the 4th heat exchanger has the highest power output and lowest pressure drop. It is also less sensitive to n_{cro}, as illustrated by Fig. 3. It is clearly shown that changing n_{cro} barely influences the power output compared to the other 3 types. This also means possible higher off-design performance of the 4th type. In a word, heat exchanger type 4 is probably the best choice. This will be more thoroughly examined in the following sections.

With the candidate n_{cro} prepared, the next step here is to identify the optimum n_{cro} and n_{run} for each heat exchanger. Calculations are still carried out for the subsystem power output and pressure drop on different heat exchangers, except now not only versus n_{cro} but also versus n_{run}. Results are plotted in Fig. 4. The 900 Pa criterion is the grey dash-dot line in each figure. It can be seen there is a peak power output for each subsystem setup but the pressure drop is nearly proportional to n_{run} on the whole range. Trends are quite similar to [14,15]. Under each setup, there is an intersection between the pressure drop curve and the 900 Pa line. It can be concluded that the final optimal subsystem configuration for each heat exchanger is the setup under which the subsystem reaches its highest peak power output point provided that the peak point comes before the intersection point. They are listed in Table 3. As shown, the subsystem installed with the 4th heat exchanger has the highest power output, the lowest press drop and the least number of TEG modules. It is most likely to be the final optimal subsystem configuration. Following study is carried out on it.

Throughout deciding Table 3, all TEG segments (fragments of the TEG modules from the finite-element discretization [8,10]) in the subsystem were electrically in series. Under this condition, the TEG subsystem has the lowest power output

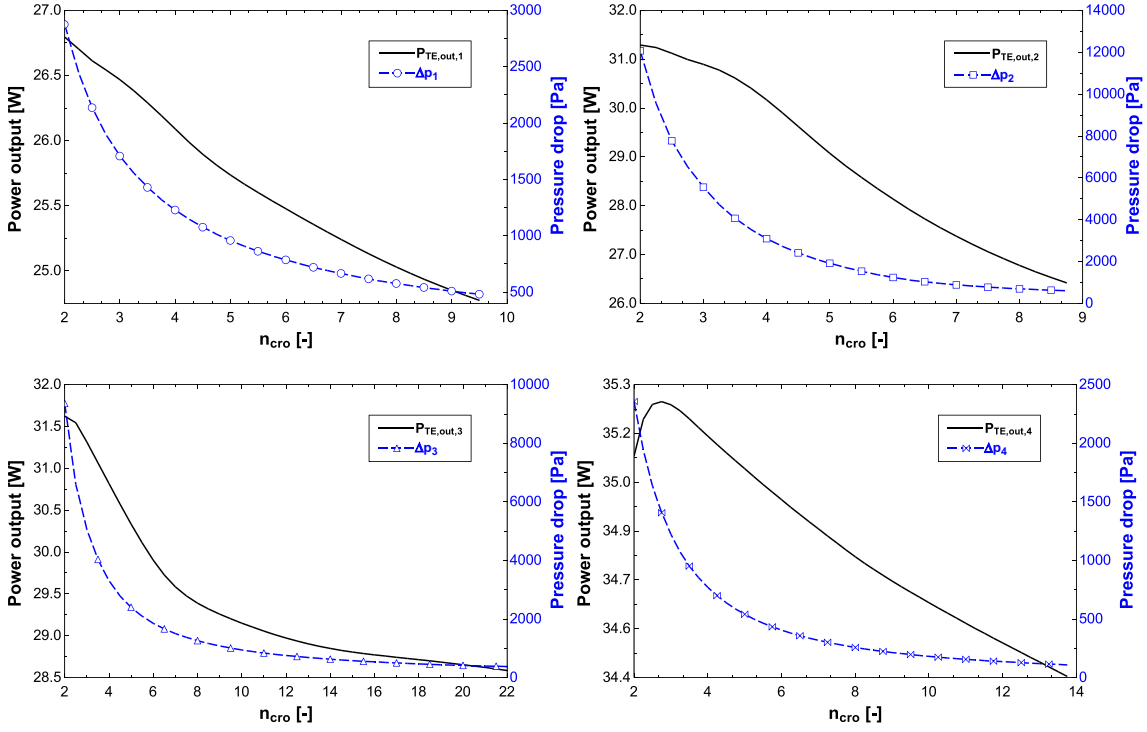

Fig. 2 – Subsystem power output and pressure drop vs. n_{cro} on different heat exchangers.

Please cite this article in press as: Gao X, et al., Optimization of a thermoelectric generator subsystem for high temperature PEM fuel cell exhaust heat recovery, International Journal of Hydrogen Energy (2014), http://dx.doi.org/10.1016/j.ijhydene.2014.01.193

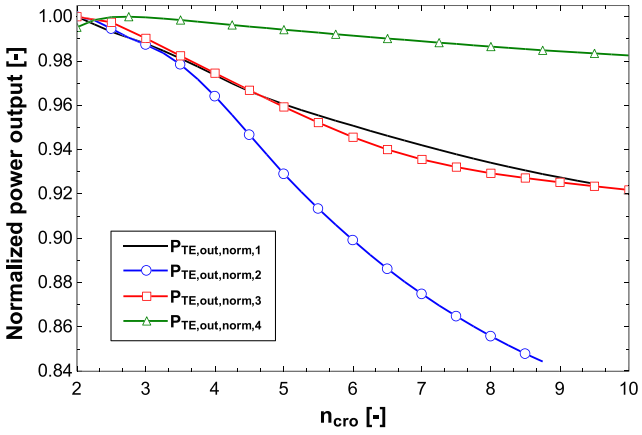

Fig. 3 – Normalized subsystem power output by the peak value of each heat exchanger.

and the worst reliability [16]. On the contrary, during determining the candidate n_{cro}, all TEG segments were kept working in standalone mode, i.e., each TEG segment is assumed connected with an external resistance equivalent to its internal. Under this condition, every TEG segment together with the subsystem has its maximum power output. It is a reasonable simplification in these calculations since it can avoid this electrical connection effect from interfering with deciding the candidate n_{cro}. However, the standalone mode is obviously lack of feasibility in practice. With the progress of power conditioning techniques [17–19], it is apparently more practical to divide all the TEG modules into branches. This electrical connection style affects the system design and performance.

2.2. *Electrical power output enhancement*

The demand of power conditioning for TEGs is based on two simple facts: 1) their maximum power point drifts significantly with their working temperature, as concluded by the sensitivity analysis in Refs. [8]; 2) series connection of all the TEG modules has the worst performance and reliability [16], as mentioned above. To alleviate these two issues, all the TEG modules of the subsystem will be electrically divided into branches. Since it is assumed that the subsystem performance in the direction perpendicular to the exhaust gas flow is identical [8], the TEG assembly will only evenly fall into branches along the flow in the following study. Inside each branch, all modules are electrically in series. Each branch is connected with a dedicated power conditioning circuit, i.e., branches work standalone, electrically independent from each other. The total number of branches n_b affects the subsystem performances. Analysis is carried out as follows.

Fig. 5 illustrates the effects of n_b with n_{run} on the subsystem power output on the 4th heat exchanger. Under every n_b, the subsystem power output overlaps and ascends fast initially, reaches the peaks and then starts to drop gradually. With larger n_b, the dropping trend becomes dimmer, i.e., the power output is less sensitive to n_{run}. The two curves of the standalone mode and the serial mode give the upper and lower bounds of the power output. It is notable from Fig. 5 that n_b stimulates the subsystem power output significantly. However, when there are more branches this effect becomes less significant. This phenomenon is illustrated quantitatively in

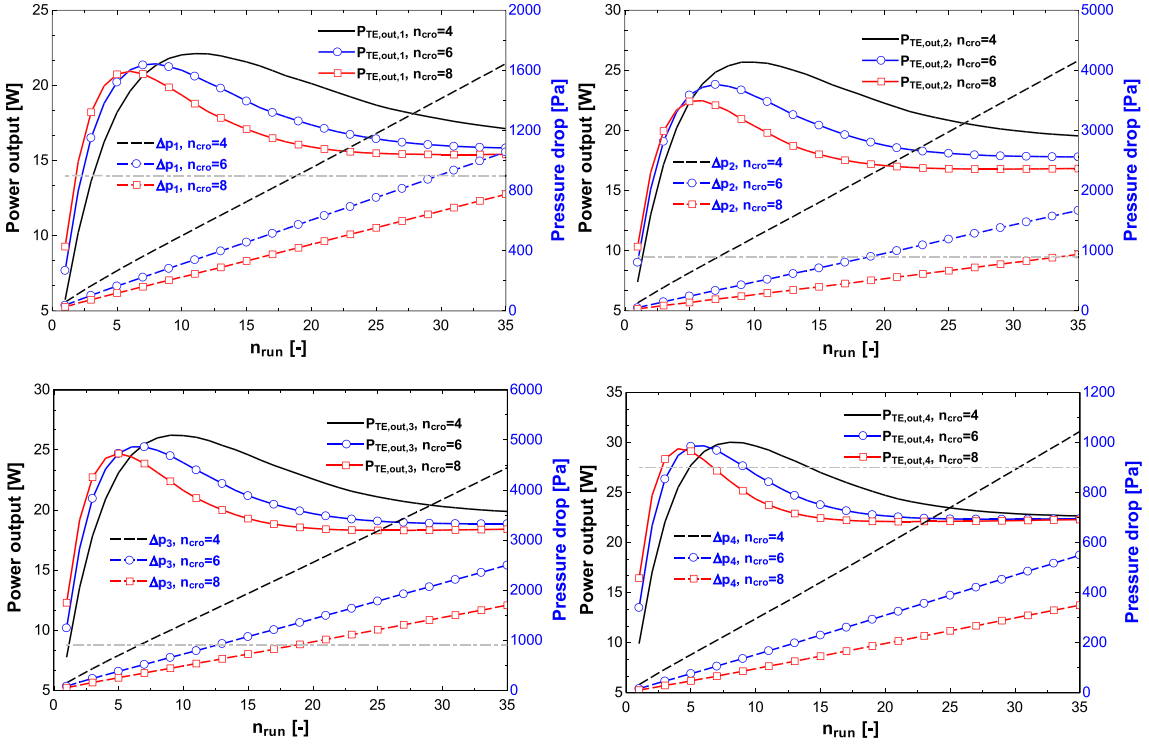

Fig. 4 – Subsystem power output and pressure drop vs. both n_{cro} and n_{run}.

Please cite this article in press as: Gao X, et al., Optimization of a thermoelectric generator subsystem for high temperature PEM fuel cell exhaust heat recovery, International Journal of Hydrogen Energy (2014), http://dx.doi.org/10.1016/j.ijhydene.2014.01.193

Table 3 – The final optimal subsystem configurations.

Index[a]	n_{cro}	n_{run}	Power output [W]	Pressure drop [Pa]
1	4	11	22.12	545.95
2	6	7	23.83	337.43
3	6	7	25.27	520.72
4	4	8	30.01	238.17

[a] Corresponding to Table 2.

Table 4 by the normalized power output. As n_b changing from 1 to 2, the power output increases by 8.4%. Then the increment drops to 2.8% and 1.4%.

It can also be noticed that n_b encourages a larger n_{run} from Table 4 and Fig. 5. Balanced between the subsystem power output and pressure drop, the 3-branch combination is chosen as the final optimal configuration of the subsystem for the on-design working condition. Compared to the in-series configuration, this configuration can boost the subsystem power output by 12.9%. The improvement is then up to 40.6% over the optimized configuration in the previous work [8]! Still, the subsystem pressure drop is now 7.8% less.

3. Off-design performance optimization

In this section, the performances of the four configurations in Table 3 and the final on-design optimal configuration are assessed under off-design working conditions. "Off-design" means the fuel cell stack working mode changes in the whole operational range, off the abovementioned "on-design" nominal spot. According to [12,13,20], the operational current density range of the stack in this study is from 0 A/cm^2 to1 A/cm^2. To avoid fast degradation of the stack [21], the exhaust gas temperature is chosen as the control parameter and kept at 155 °C invariant in this study.

3.1. Assessment of the subsystem configurations

Fig. 6 shows the off-design performances of the four configurations in Table 3. Limited by the Reynolds-number operating interval of each heat exchanger [11], subsystem performance data are only available as presented in the figures. Outside of these intervals, compact heat exchangers will lose their advantages because their performances are no better than ordinary smooth-passage heat exchangers [11]. It can be seen that curves in Fig. 6 have similar trends as in Ref. [8]. Among them, the 4th configuration has the highest subsystem power output and lowest pressure drop on the whole range. It has higher performance and a wider operating interval. In other words, the 4th heat exchanger is still the ideal choice for the off-design operations. In the above study, all TE segments work in standalone mode.

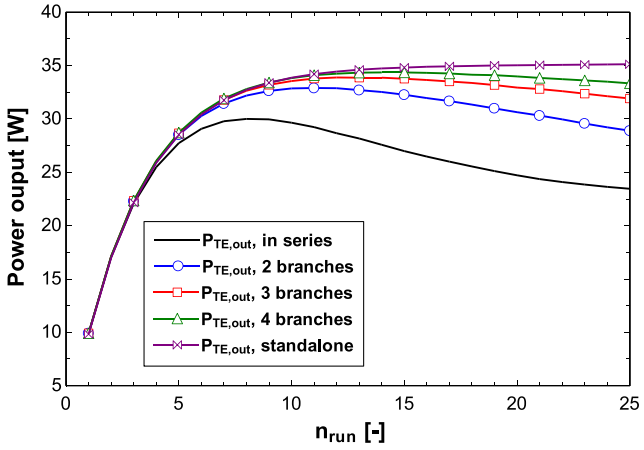

Fig. 5 – Effects of n_b with n_{run} on the 4th heat exchanger.

3.2. The final optimal configuration

The effect of power conditioning on the final on-design optimal configuration, the 4th combination in Table 3, under off-design operating conditions is illustrated below.

It is clearly illustrated in Fig. 7 the benefits of power conditioning for off-design operations. In the worst case, the final subsystem in the serial mode ($n_b = 1$) can only produce approximately 60% power as in the standalone mode. Under the same working condition, electrically dividing all the modules into three branches ($n_b = 3$) can improve the power output to about 80%. It is then nearly 90% when $n_b = 4$, which is about 30% higher than the serial mode! Since the fuel cell system mostly working in the second half operational range, balanced between the performance and system complexity $n_b = 3$ is still the preferable final choice. In this half range, dividing into three branches can guarantee no less than 96% power output. On the contrary, in the whole range the subsystem power output under the serial mode is typically less than 85%.

Furthermore, it can also be noticed in Fig. 7 that the normalized power output curve of the serial mode is slightly different from the others. It has milder power output drop at the low current density end. This is questionable since the curves are from the same subsystem configuration except only with n_b changed from 1 to 4. They should have similar trends. Checking the exhaust gas temperature distribution under two current densities $i = 0.25$ A/cm^2 and 0.67 A/cm^2 as shown in Fig. 8, it can be noticed that the downstream modules almost have no temperature difference on them under 0.25 A/cm^2. Large non-uniform temperature distribution between modules happens in the current subsystem. Electrically in series with the large non-uniformity, the downstream modules become under-temperature. It is the condition these TE modules working at much lower temperature differences regarding their output electric current. Since TEGs and thermoelectric coolers (TECs) are inherently twinborn working modes of a single TE module, these under-temperature modules probably have already shifted to the TEC mode. Then they act similarly as the TEC modules in the directly

Please cite this article in press as: Gao X, et al., Optimization of a thermoelectric generator subsystem for high temperature PEM fuel cell exhaust heat recovery, International Journal of Hydrogen Energy (2014), http://dx.doi.org/10.1016/j.ijhydene.2014.01.193

Table 4 – Effects of n_b with n_{run} to the subsystem power output.

Connection Style[a]	n_b[a]	n_{run}[a]	$P_{TE,out}$ [W]	Normalized $P_{TE,out}$[b]	Pressure drop [Pa]
In series (1 branch)	4	8	30.01	0.87	238.17
2 branches	4	11	32.91	0.95	324.30
3 branches	4	12	33.88	0.98	353.24
4 branches	4	14	34.36	0.99	411.50

[a] The optimal subsystem configuration.
[b] Normalized by the standalone style.

coupled TEG–TEC systems in Refs. [22,23]. Instead of generating electricity, these modules are actually wasting it. Besides this TEC power dissipation, the internal ohmic resistances of these under-temperature modules can be counted as line loss and jointly reduce the system net power output. Without considering this shift possibility, the current subsystem model seems having overestimated the power output at the low current density end. Thanks to introducing power conditioning, this deviation is mitigated temporally.

The above possible TEG–TEC shift was rarely considered in TEG system-level modeling in literature. It seems TEC working mode should also be included in modeling a TEG system, especially when under-temperature phenomenon happens. This TEG-TEC shift also raises another necessity of power conditioning for TEG systems.

From all the above analyses, the final optimal configuration of the subsystem on its whole working range can be finally concluded. As shown in the following Fig. 9, there are 2 blocks, each with 2 rows of 12 TEG modules in the subsystem. As a total, there are 48 modules. They together decide the size of the subsystem including the heat exchanger housing. The type of the installed heat exchanger is 'Pin-fin plate-fin, surface PF-4(F)'. Its detailed geometry is given in Fig. 10. TEG module type is Melcor HT8 [8]. All the modules are electrically divided in 3 branches along the exhaust gas flow, as illustrated in different colors in the figure.

4. Contribution of TE heat recovery to the fuel cell system

On the final optimized TEG subsystem, the contribution of the TE heat recovery to the current 1 kW fuel cell power system is assessed.

Assume that there is no power loss during power conditioning, Fig. 11 shows the benefits of TE heat recovery to the fuel cell system. It raises the system power output, i.e., the system voltage or electric current is higher. From the normalized system power output, it can be seen the gain is around 3.5%. It should be mentioned that the figure of merit (ZT) of the TEG modules being used is fairly low. It is only around 0.50 [8,24]. Commonly, it can reach up to 0.8 to 1.1 in practice by tuning the carrier concentration of the module's materials or changing them [25]. However, it is widely agreed in the research community that for TEGs to be economically viable in most applications, ZT must have values of 2 or higher [26]. Refer to the achievements in the lab as shown in Refs. [27], this seems soon achievable.

Substitute ZT = 2 into the above calculation, the contribution of the TE heat recovery can be expected as Fig. 12. Now around 10% gain in the power output of the 1 kW fuel cell system is realized. This is extra 90.20 W power under its nominal operating condition, which is approximately 3 times as the condition ZT = 0.50. It is already able to be easily used to drive the auxiliaries, charge batteries, assist the system startup/shutdown processes, etc. For further system level study, the equations of the normalized power output (NPo) to the fuel cell stack operating current density (i) are given below. The unit of i is A/cm^2.

$$\mathrm{NPo} = \begin{cases} 1.010 + 0.045\cdot i - 0.011\cdot i^2, & \mathrm{ZT} = 0.50 \\ 1.032 + 0.104\cdot i - 0.020\cdot i^2, & \mathrm{ZT} = 2.0 \end{cases} \quad (1)$$

5. Conclusions

The configuration of the TEG exhaust heat recovery subsystem is further optimized. There are 4 x 12 TEG modules in the

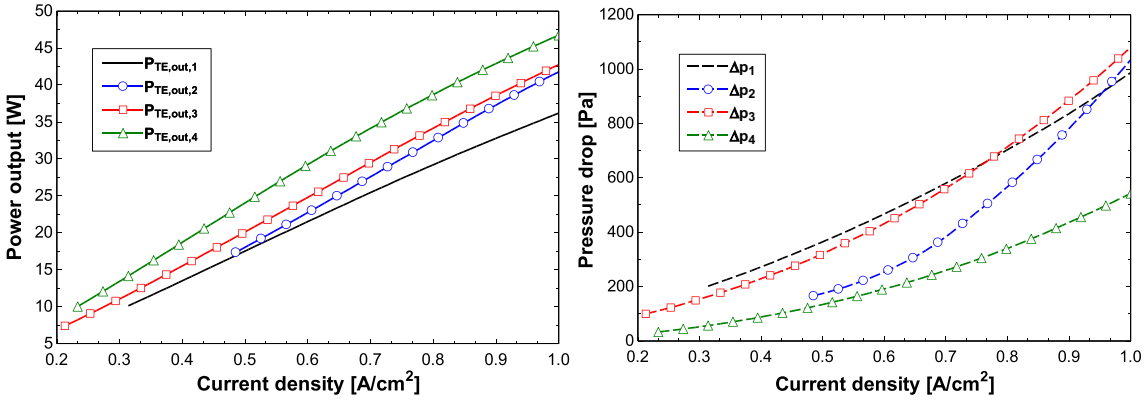

Fig. 6 – The off-design performances of the 4 configurations in Table 3.

Please cite this article in press as: Gao X, et al., Optimization of a thermoelectric generator subsystem for high temperature PEM fuel cell exhaust heat recovery, International Journal of Hydrogen Energy (2014), http://dx.doi.org/10.1016/j.ijhydene.2014.01.193

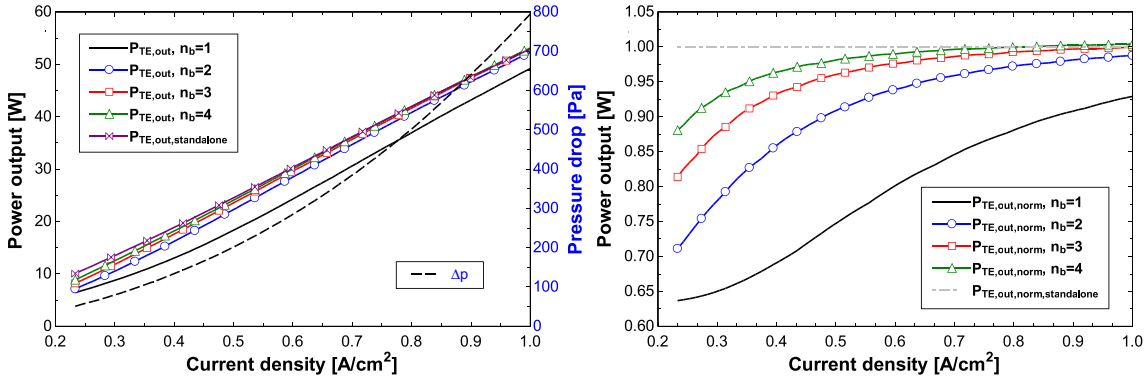

Fig. 7 – The off-design performances of the final optimal configuration.

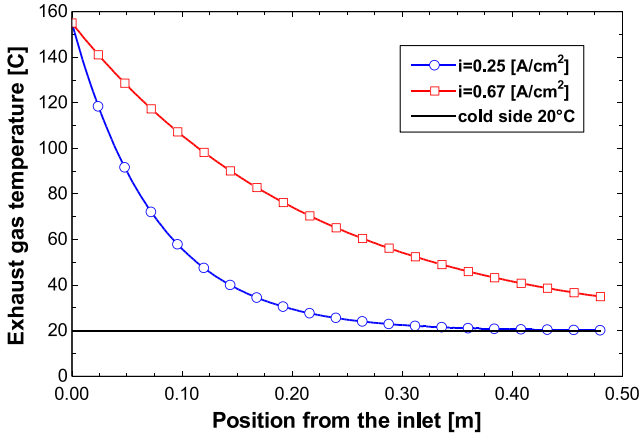

Fig. 8 – Exhaust gas temperature distribution under two different current densities.

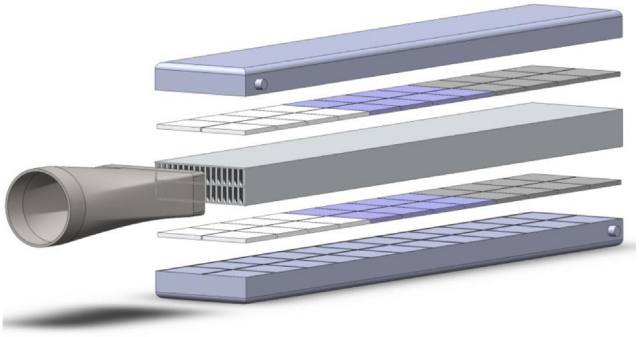

Fig. 9 – The final optimal architecture of the TEG subsystem.

subsystem. Module type is Melcor HT8. All the TEG modules are electrically divided into 3 branches along the exhaust gas flow. The heat exchanger 'Pin-fin plate-fin, surface PF-4(F)' is installed. This subsystem configuration is the optimal choice for both on-design and off-design operating conditions. The procedures of optimizing the TE exhaust heat recovery subsystem are also clearly presented.

The electrical connection style of the TEG assembly is analyzed. It affects the subsystem in various aspects: the optimal size, the reliability and the performance, both on-design and especially off-design. In the end, balanced between the subsystem performance and complexity, 3-branch scenario is chosen. This increases the subsystem power output by 12.9%.

Please cite this article in press as: Gao X, et al., Optimization of a thermoelectric generator subsystem for high temperature PEM fuel cell exhaust heat recovery, International Journal of Hydrogen Energy (2014), http://dx.doi.org/10.1016/j.ijhydene.2014.01.193

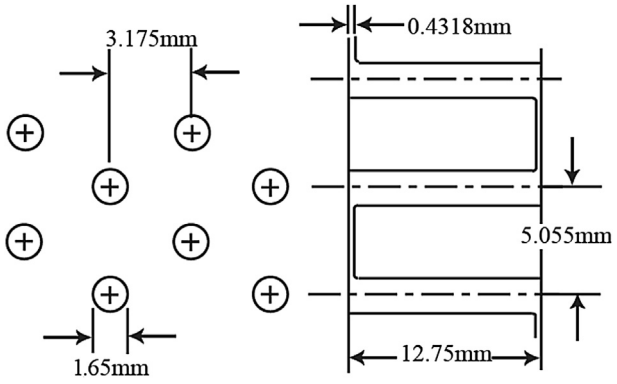

Fig. 10 – Detailed geometry of 'Pin-fin plate-fin, surface PF-4(F)'.

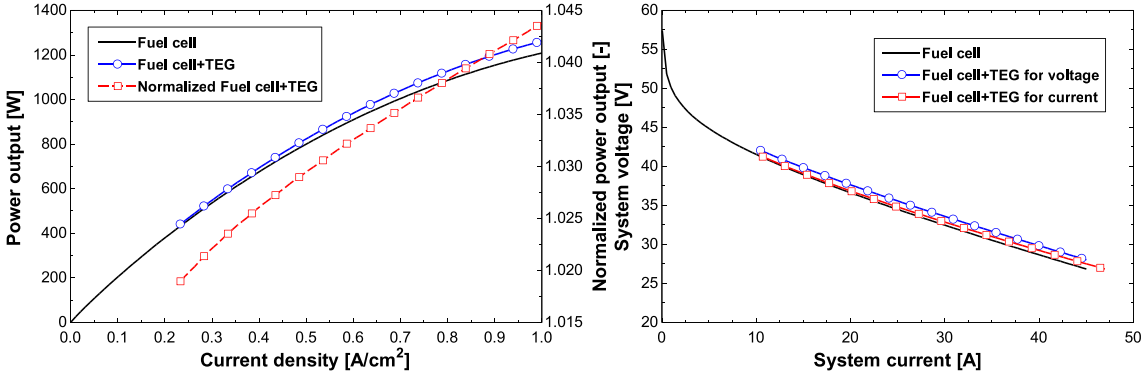

Fig. 11 – Contribution of TE heat recovery to the fuel cell system, ZT = 0.50.

It seems the possible TEG–TEC working mode shift in the current subsystem should also be included in simulating its performance. The current TEG system-level model widely used in literature probably overestimates the subsystem performance when large temperature unevenness happens among modules.

The current TEG modules of the subsystem only have a ZT = 0.50. Under this condition, the subsystem can boost the fuel cell system power output by around 3.5%. With achievements in material science, this number can be expected up to 10% in the near future.

By now, the TEG subsystem for HT-PEM fuel cell exhaust heat recovery has been optimized through simulations. Practical concerns and the feasibility of deploying this TEG subsystem to increase the fuel cell system efficiency still need further experimental assessments. Larger scale system-level modeling and simulation study would also be beneficial.

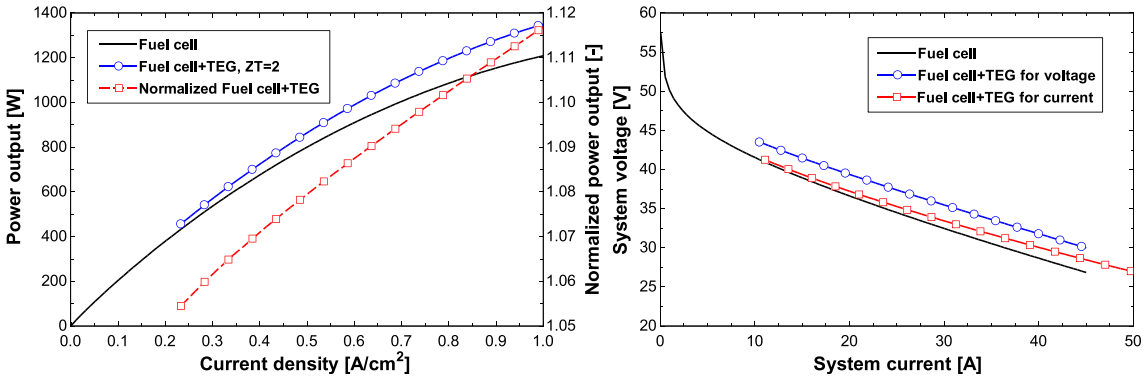

Fig. 12 – Expected contribution of TE heat recovery to the fuel cell system, ZT = 2.

Please cite this article in press as: Gao X, et al., Optimization of a thermoelectric generator subsystem for high temperature PEM fuel cell exhaust heat recovery, International Journal of Hydrogen Energy (2014), http://dx.doi.org/10.1016/j.ijhydene.2014.01.193

Acknowledgments

The authors gratefully acknowledge financial support from Aalborg University and China Scholarship Council.

REFERENCES

[1] Cheddie Denver, Munroe Norman. Review and comparison of approaches to proton exchange membrane fuel cell modeling. J Power Sources 2005;147:72–84.
[2] Crabtree George W, Dresselhaus Mildred S, Buchanan Michelle V. The hydrogen economy. Phys Today 2004;57(12):39. http://dx.doi.org/10.1063/1.1878333.
[3] Quartarone Eliana, Mustarelli Piercarlo. Polymer fuel cells based on polybenzimidazole/H_3PO_4. Energy Environ Sci 2012;5:6436–44.
[4] Andreasen Søren Juhl, Ashworth Leanne, Menjon Remon Ian Natanael, Rasmussen Peder Lund, Nielsen Mads Pagh. Modeling and implementation of a 1 kW, air cooled HTPEM fuel cell in a hybrid electrical vehicle. ECS Trans 2008;12(1):639–50.
[5] Arsalis Alexandros, Nielsen Mads P, Kær Søren K. Application of an improved operational strategy on a PBI fuel cell-based residential system for Danish single-family households. Appl Therm Eng 2013;50(1):704–13.
[6] Advantages of HTPEM fuel cells over LTPEM fuel cells. http://www.serenergy.com/htpem_technology.htm.
[7] Andreasen Søren Juhl, Vang Jakob Rabjerg, Kær Søren Knudsen. High temperature PEM fuel cell performance characterisation with CO and CO_2 using electrochemical impedance spectroscopy. Int J Hydrogen Energy 2011;36:9815–30.
[8] Gao Xin, Andreasen Søren Juhl, Chen Min, Kær Søren Knudsen. Numerical model of a thermoelectric generator with compact plate-fin heat exchanger for high temperature PEM fuel cell exhaust heat recovery. Int J Hydrogen Energy 2012;37:8490–8.
[9] Gao Xin, Chen Min, Snyder G Jeffrey, Andreasen Søren Juhl, Kær Søren Knudsen. Thermal management optimization of a thermoelectric-integrated methanol evaporator using a compact CFD modeling approach. J Electron Mater 2013;42(7):2035–42.
[10] Gao Xin, Chen Min, Andreasen Søren Juhl, Kær Søren Knudsen. Potential usage of thermoelectric devices in a high-temperature polymer electrolyte membrane (PEM) fuel cell system: two case studies. J Electron Mater 2012;41(6):1838–44.
[11] Kays WM, London AL. Compact heat exchangers. 3rd ed. New York: McGraw Hill; 1984.
[12] Andreasen Søren Juhl, Ashworth Leanne, Menjón Remón Ian Natanael, Kær Søren Knudsen. Directly connected series coupled HTPEM fuel cell stacks to a Li-ion battery DC-bus for a fuel cell electrical vehicle. Int J Hydrogen Energy 2008;33(23):7137–45.
[13] Serenus 166/390 AirC Datasheet. http://www.serenergy.com/Downloads.htm [accessed: 22.10.12].
[14] Suzuki RO, Tanaka D. Mathematical simulation of thermoelectric power generation with the multi-panels. J Power Sources 2003;122(2):201–9.
[15] Suzuki RO, Tanaka D. Mathematic simulation on thermoelectric power generation with cylindrical multitubes. J Power Sources 2003;124(1):293–8.
[16] Mori M, Yamagami T, Oda N, Hattori M, Sorazawa M, Haraguchi T. Current possibilities of thermoelectric technology relative to fuel economy. Society of Automotive Engineering; 2009. 2009-2101-0170.
[17] Yu Chuang, Chau KT. Thermoelectric automotive waste heat energy recovery using maximum power point tracking. Energy Convers Manag 2009;50:1506–12.
[18] Jong-Pil Im, Se-Won Wang, Seung-Tak Ryu, Gyu-Hyeong Cho. A 40 mV transformer-reuse self-startup boost converter with MPPTcontrol for thermoelectric energy harvesting. IEEE Journal of Solid-State Circuits 2012;47(12):3055–67.
[19] Chatzidakis Panagiotis G, Christidis Georgios C, Tatakis Emmanuel C. Comparative study of MPPT algorithms for thermoelectric generators. In: 2013 15th European conference on power electronics and applications (EPE; 2013. http://dx.doi.org/10.1109/EPE.2013.6634607.
[20] Korsgaard Anders R, Refshauge Rasmus, Nielsen Mads P, Bang Mads, Kær Søren K. Experimental characterization and modeling of commercial polybenzimidazole-based MEA performance. J Power Sources 2006;162:239–45.
[21] Arsalis Alexandros, Nielsen Mads P, Kær Søren K. Modeling and off-design performance of a 1 kWe HT-PEMFC (high temperature-proton exchange membrane fuel cell)-based residential micro-CHP (combined-heat-and-power) system for Danish single-family households. Energy 2011;36:993–1002.
[22] Khattab NM, El Shenawy ET. Optimal operation of thermoelectric cooler driven by solar thermoelectric generator. Energy Convers Manag 2006;47:407–26.
[23] Meng Fankai, Chen Lingen, Sun Fengrui. Performance analysis for two-stage TEC system driven by two-stage TEG obeying Newton's heat transfer law. Math Comput Model 2010;52:586–95.
[24] Smith KD. An investigation into the viability of heat sources for thermoelectric power generation systems. Master thesis. Rochester (NY): Rochester Institute of technology; 2009.
[25] Snyder G Jeffrey, Toberer Eric S. Complex thermoelectric materials. Nat Mater 2008;7:105–14.
[26] Yang J, Stabler FR. Automotive applications of thermoelectric materials. J Electron Mater 2009;38(7):1245–51.
[27] Jovanovich V, Ghmaty S. Design, fabrication and testing of energy harvesting thermoelectric generator. In: Proc of SPIE, vol. 6173; 2006. pp. 1–8.

Please cite this article in press as: Gao X, et al., Optimization of a thermoelectric generator subsystem for high temperature PEM fuel cell exhaust heat recovery, International Journal of Hydrogen Energy (2014), http://dx.doi.org/10.1016/j.ijhydene.2014.01.193

Paper 4

Heat Exchanger Selection and Optimization of a Thermoelectric Generator Subsystem for HT-PEM Fuel Cell Exhaust Heat Recovery

Gao, Xin; Andreasen, Søren Juhl; Kær, Søren Knudsen; Rosendahl, Lasse Aistrup; Kolaei, Alireza Rezania

Under review by International Conference on Thermoelectrics, July 2014.

Heat exchanger selection and optimization of a thermoelectric generator subsystem for HT-PEM fuel cell exhaust heat recovery

Xin Gao[1,2], Søren Juhl Andreasen[1], Søren Knudsen Kær[1], Lasse Aistrup Rosendahl[1], Alireza Rezania Kolaei[1]

1- Department of Energy Technology, Aalborg University, Pontoppidanstraede 101, Aalborg, DK-9220, Denmark

2- xga@et.aau.dk

Abstract: A thermoelectric generator (TEG) subsystem is introduced to recover the exhaust heat from a high temperature polymer electrolyte membrane (HT-PEM) fuel cell stack. In optimizing the subsystem performance, three key factors have been identified: heat exchanger surface type, its housing dimensions and TEG power conditioning. Previous studies also reveal that their effects are interlocked. However, the three factors were occasionally considered in sequence in previous studies. This work reappraises the published heat exchanger selection and subsystem optimization approach. The three factors are now combined and assessed simultaneously and globally. For each surface type, its housing dimensions are optimized accordingly. Besides, TEG power conditioning is also adjusted in detail. Moreover, the previous 900Pa pressure-drop criterion is removed herein with the purpose to have a more comprehensive heat exchanger selection and a more thorough understanding of the interplay between the subsystem and the stack. In the current study, the selection is extended to a prepared whole heat exchanger collection including the precluded surfaces previously. Finally, the selection and optimization approach is refined and documented. The on- and off- design performance of the subsystem is thoroughly optimized. The current work complements and also proves the validity of the already published approach.

Keywords: fuel cell; TEG; heat recovery; heat exchanger; selection; power conditioning; optimization

1. Introduction

Thermoelectric generators (TEGs) have large advantages in low quality heat recovery among other techniques [1]. To recover the exhaust heat for power and further boost the efficiency of a high temperature polymer electrolyte membrane (HT-PEM) fuel cell power system, a thermoelectric

exhaust heat recovery subsystem has already been designed, modeled and optimized in previous studies [2,3,4,5].

Initially in [2], the potential contribution of TEG heat recovery to the HT-PEM fuel cell power system was preliminarily assessed. The design of the TEG subsystem was schemed and explained. Then in [3], a finite-element model of the subsystem was developed and presented. It is a model aiming to answer both design and operation requests, in turn to benefit the subsystem fabrication. A library of types of compact heat exchangers, therefore, is also integrated in the model. It includes 59 types of plate-fin heat exchanger surfaces, of which the performance data are highly trustworthy from experiments [6]. The model was then solved by a discretized ε-NTU method. In this way, the accuracy and flexibility of the subsystem model can both be assured. Equations are listed in Table 1.

Table 1 - Main equations [2,3].

Description	Equations
TEG properties	$\sum_{}^{n_{x,TE}}\sum_{}^{n_{y,TE}}\alpha_i=\alpha_{TE},\ \sum_{}^{n_{x,TE}}\sum_{}^{n_{y,TE}}R_{e,i}=R_{TE,e},\ \sum_{}^{n_{x,TE}}\sum_{}^{n_{y,TE}}R_{t,i}=R_{TE,t}$
TEG power output	$I_i=0.5(\alpha_i)(\overline{T}_{h,TE}(i)-\overline{T}_{c,TE}(i))/R_{e,i}$
	$w(i)=\alpha_i I_i\left(\overline{T}_{h,TE}(i)-\overline{T}_{c,TE}(i)\right)-I_i^{\,2}R_{e,i},\ P_{TEA}=\sum_{}^{n_x}\sum_{}^{n_y}w(i)$
Heat transfer	$\dot{q}_{h,TE}(i)=\dot{q}_{gas}(i)=\dot{m}_{gas}\left(h_{gas,i}-h_{gas,i+1}\right)$
	$\dot{q}_{gas}(i)=\varepsilon_{ctf}(i)\dot{m}_{gas}\left(h_{gas,i}-h_{gas,i}^{cw}\right)$
	$\dot{q}_{h,TE}(i)=UA_{hx}(i)(\overline{T}_{gas}(i)-\overline{T}_{h,TE}(i)),\ \overline{T}_{gas}(i)=(T_{gas}(i)+T_{gas}(i+1))/2$
	$\eta_{fin}(i)=1-A_{fin}^{A}(1-n_{fin}(i)),\ n_{fin}(i)=\tanh(ml_i)/ml_i$
	$ml_i=b_1/2\cdot sqrt(2\cdot h_{hx}(i)/(k\cdot fin_{thk}))$
Pressure drop	$\Delta p_{hx}=(u_{gas}^2/(2\rho_{gas,in}))[4f_{hx}L_{hx}\rho_{gas,in}/\left(D_h\overline{\rho}_{gas}\right)+\left(1+\sigma^2\right)\left(\left(\rho_{gas,in}/\rho_{gas,out}\right)-1\right)]$
Pumping power [7]	$P_{comp}=\dot{m}_{gas}R_{gas}T_{in}\ln\left(p_{out}/p_{in}\right)/M_{gas}\eta_{comp}$

By the model, 4 heat exchanger surfaces were identified of promising performances under fixed heat exchanger housing dimensions, which are directly decided by the subsystem size. Later on in [4], studies were carried out on the 4 surfaces. The superior one was pinpointed. Accordingly, the optimal subsystem size was figured out, which is mainly determined by the number of TEG modules crossing

the exhaust gas flow (n_{cro}) and the number of modules along the gas flow (n_{run}). Afterwards, TEG power conditioning was optimized to both on-design and off-design working conditions. Generally speaking, TEG power conditioning for maximum subsystem power output includes 3 scenarios: 1) Standalone mode: all TEG segments (fragments of the TEG modules in the finite-element model [3,4]) in the subsystem electrically stay in their dedicated circuits; 2) In-series mode: all TEG segments are electrically in-series; and 3) Maximum power point tracking technique (MPPT) mode: all TEG modules are evenly divided into several electrical branches and there is an ideal MPPT unit per each branch. Also, in this paper, the approach of choosing the heat exchanger type and optimizing the subsystem was formed. In brief, it has three tasks: I) selecting heat exchanger surface, II) determining subsystem size and III) power conditioning. In detail, there are the following 6 steps [3,4]:

1) Preliminary selection: pick out the promising heat exchanger surfaces among all the surfaces in the prepared heat exchanger library. These surfaces should guarantee higher subsystem power output and lower pressure drop than the rest. They are assessed under a fixed pre-optimized subsystem size. The criterion is that their subsystem pressure drop cannot exceed 900Pa. All TEG segments are in standalone mode.
2) Identify an adequate n_{run} for all the promising surfaces; all TEG segments are in standalone mode in this step.
3) Figure out all the feasible candidates of n_{cro} for each surface, under the adequate n_{run}; all TEG segments are still in standalone mode.
4) Choose the optimum n_{cro} for each surface under the adequate n_{run} when all TEG segments are in standalone mode, and then the corresponding optimum n_{run} while all TEG segments are in-series.
5) Identify the superior heat exchanger surface, with which the subsystem has the highest power output and low pressure drop. The optimized subsystem size is also identified.
6) Power conditioning: all the TEG modules are set to work in MPPT mode. The MPPT mode is tuned in detail. The optimum n_{run} is further fine-tuned in this step.

In this work, the above steps are rearranged. Preliminary selection is cancelled. TEG power conditioning is reconsidered from the beginning of the entire heat exchanger selection and subsystem

optimization process. Additionally, the 900Pa criterion is removed and all the available plate-fin heat exchanger surfaces in the library are evaluated. The three key factors, heat exchanger surface type, its housing dimensions and TEG power conditioning, are now freely combined. All the combinations are assessed on the subsystem power output and pressure drop. Finally, the superior surface in the whole library is found out. The corresponding subsystem configuration is optimized, thermally and electrically. In the end, the approach of designing and optimizing the TEG subsystem is updated and summarized.

2. Heat exchanger surface selection

The previous studies have emphasized the importance of heat exchanger surface selection. To assess the performances of each plate-fin surface, subsystem size should be specified beforehand, which is determined by n_{cro} and n_{run}. Then during the performance assessment, the subsystem size would be either kept invariant as the way identifying the four promising heat exchanger surfaces in [3,4] which saves the computational cost, or adjusted correspondingly which is of better theoretical integrity but is much more time-consuming. In this work, the latter method is used. Another factor re-examined in this study is the feasible ranges of n_{cro} and n_{run}. Previously, there were no limits on them. However, in practice the subsystem size is not recommended to exceed the fuel cell stack size, which is approximately 178 mm x 159 mm x 523 mm [8]. Confined by this, n_{cro} can only be chosen among 2, 4, 6, and 8; n_{run} is only available from 1 to 13. n_{run} is further restrained in the range from 5 to 13 regarding its practical meaning. To pinpoint the heat exchanger surface with superior performances, the whole library is then screened under all possible combinations of feasible n_{cro} and n_{run} values. Results are presented as follows.

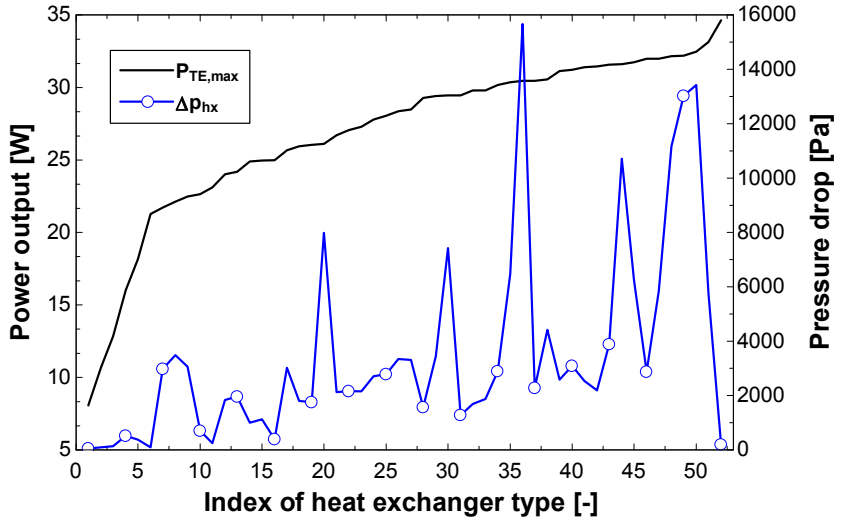

Fig. 1 – Peak performances of all applicable heat exchanger surfaces in the whole library, $n_{run} = 13$.

Calculations on $n_{run} = 13$ are taken as illustration. For each surface type, there is an efficient Reynolds-number interval [6]. Ruled out by this, there are 206 combinations left calculable. Among them, for each surface only the combination with peak subsystem power output is kept. As a total, there are 52 combinations corresponding to 52 surfaces left to assess. The subsystem power output and pressure drop for each combination are plotted in Fig. 1.

Data in Fig. 1 are sorted ascendingly by the subsystem power output. It can be seen the curves are similar as in [3]. With the power output increasing gradually, the pressure drop fluctuates significantly between heat exchanger surfaces. The largest difference is as high as 15610.9Pa! In principle, higher pressure drop consumes more pumping power and they are proportional [7]. Moreover, in this case a larger pressure drop from the TEG subsystem causes a higher back pressure of the fuel cell stack, which has been proved of no observable profit to the stack performance [9]. So the superior heat exchanger surface in the whole library must hold the highest subsystem power output and lowest pressure drop. It is 'Pin-fin plate-fin, surface PF-4(F)', No. 52 in Fig. 1. Details of it are given in Fig. 2 and [6]. The above conclusion is also corroborated by all the other n_{run} values in its range.

By now, the aforementioned task I has been improved and conducted. It is heat exchanger surface selection under correspondingly optimized TEG subsystem size. Throughout, all the TEG segments in

the subsystem are electrically in standalone mode. This mode indicates the ideal maximum subsystem power output, although it is lack of feasibility in practice.

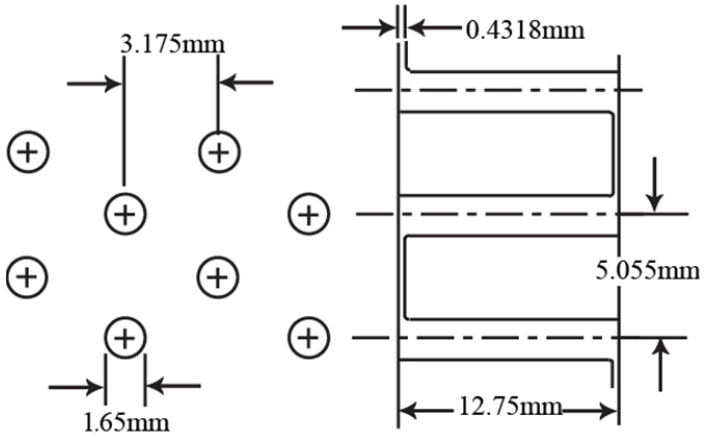

Fig. 2 - Detailed geometry of 'Pin-fin plate-fin, surface PF-4(F)' [6].

3. Optimal subsystem size and power conditioning

This section covers the above-mentioned task II and task III. It has already been proved in [4] that power conditioning affects the optimal subsystem size; they are interwoven with each other. In this section, the effects of power conditioning are combined and discussed throughout the optimization process, instead of solely discussed afterwards as in [4]. In the following calculations, n_{cro} is further confined among 4, 6, and 8, to avoid the possible whistle issues of 'Pin-fin plate-fin, surface PF-4(F)' when $n_{cro} = 2$ [4,6]. n_{run} is still constantly available from 5 to 13.

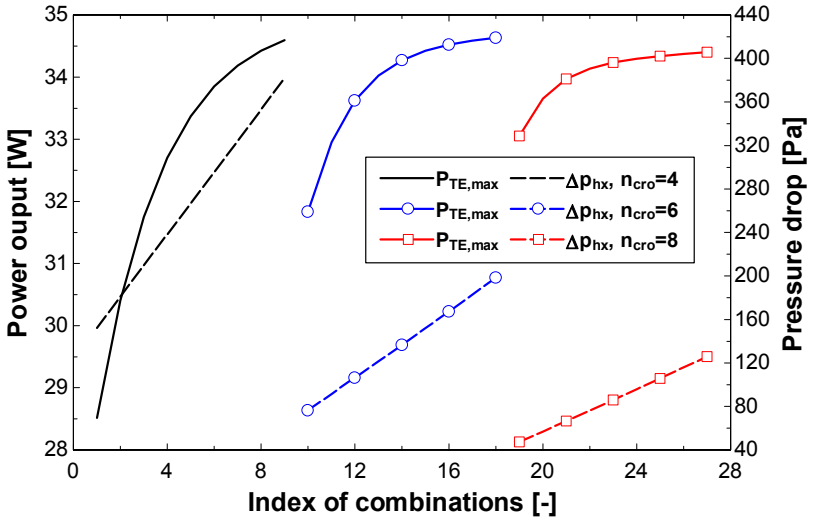

Fig. 3 - Subsystem performances under all possible subsystem sizes with all TEG segments in standalone mode.

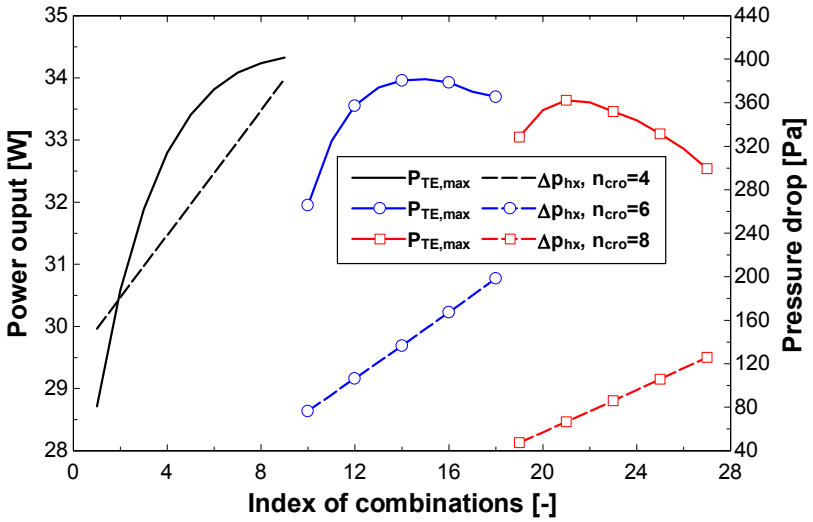

Fig. 4 - Subsystem performances with all TEG modules in 4 branches.

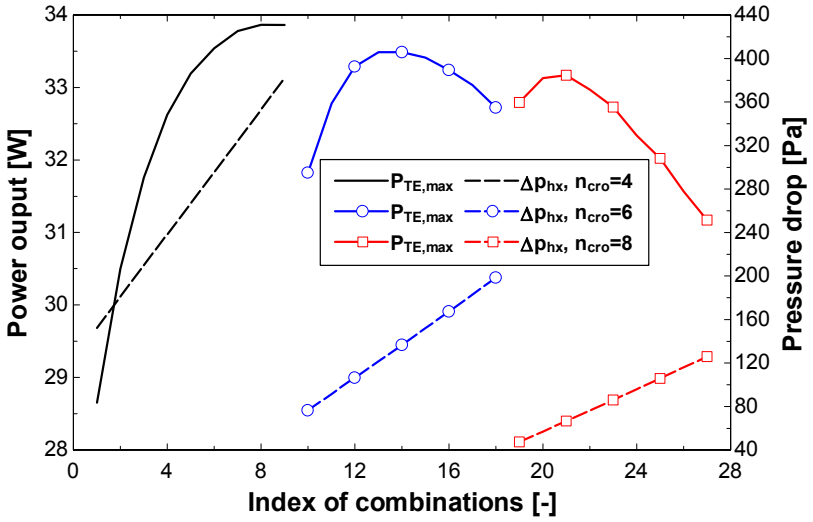

Fig. 5 - Subsystem performances with all TEG modules in 3 branches.

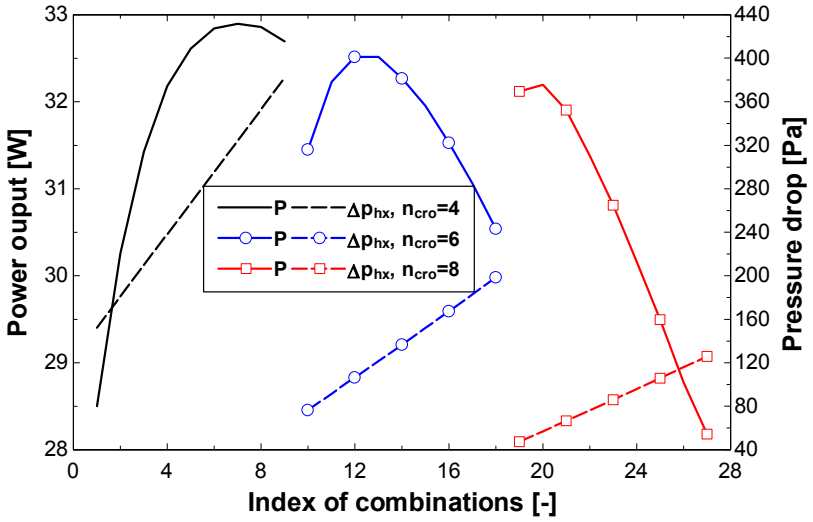

Fig. 6 - Subsystem performances with all TEG modules in 2 branches.

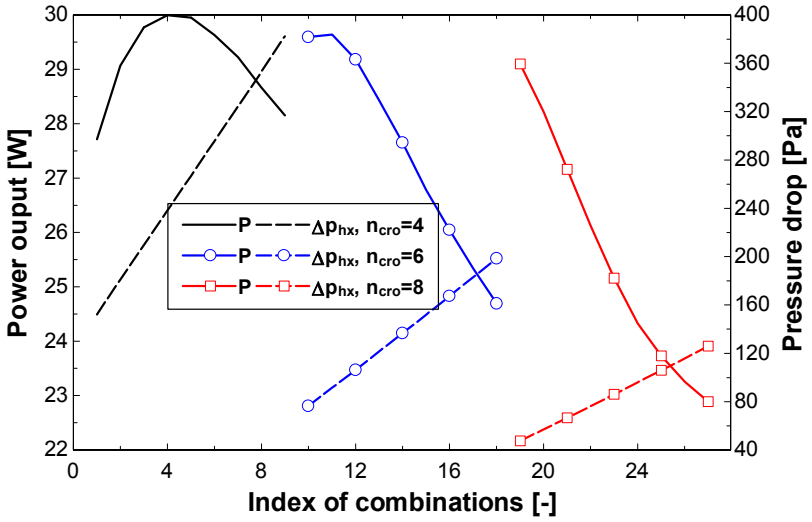

Fig. 7 - Subsystem performances with all TEG modules in series.

All three TEG power conditioning scenarios are discussed in this section. In detail, they are standalone mode, in series and ideal MPPT mode, which further has 4-branch mode, 3-branch mode and 2-branch mode [4]. As explained above, there is an ideal MPPT unit on each branch. The subsystem power output and pressure drop under every mode and every possible combination of n_{cro} and n_{run} are plotted in Fig. 3, Fig. 4, Fig. 6 and Fig. 7. The results are sorted by each n_{cro} value with n_{run} increasing through its range. The standalone mode of Fig. 3 gives the theoretical roof of the subsystem power output and helps scale the effects of power conditioning. It can be seen that increasing n_{run} initially contributes significantly to the subsystem power output but then this effect fades away, under any of the three n_{cro} values. The only difference lies that the subsystem power output is more sensitive to smaller n_{cro} values. It can also be noticed that although the subsystem size under $n_{cro}=6$ or $n_{cro}=8$ is 1.5 or 2 times as it is under $n_{cro}=4$, the maximum power output yet still remains nearly the same. Apparently, $n_{cro}=4$ is preferable since it saves material even though the subsystem pressure drop hereof is 1 to 3 times higher than the other two cases. It can be calculated from the equation in Table 1 that the pumping power differences are less than 3%, only several watts. They are almost negligible.

Apart from the standalone mode, the remaining connection styles give more realistic subsystem performances and are more feasible in practice. It is clear from Fig. 4 to Fig. 7 the subsystem power output decreases gradually with dividing all the TEG modules into fewer branches along the exhaust gas flow, under any subsystem size. Electrically dividing into branches, with the help of the MPPT, can improve the subsystem power output significantly [4]. It can also be noticed when dividing into fewer branches the subsystem peak power output point comes out earlier with smaller n_{run}, i.e., dividing into more branches encourages a larger n_{run}. There is a tradeoff between the subsystem performance, its structural complexity and its material cost. The final choice in this work is still the 3-branch mode. In this mode, the optimal subsystem configuration under each n_{cro} is listed in Table 2. It is notable that under $n_{cro}=4$ and $n_{run}=12$ the subsystem has the highest power output and the least total number of TEG modules. Consistent with [4], $n_{cro}=4$ and $n_{run}=12$ probably is still the final subsystem size although the pressure drop in this case is higher.

Table 2 - The optimal subsystem configurations in the 3-branch mode.

Index	n_{cro}	n_{run}	Power output [W]	Pressure drop [Pa]	Heat exchanger surface
1	4	12	33.86	353.25	
2	6	9	33.49	136.67	'Pin-fin plate-fin, surface PF-4(F)'
3	8	7	33.17	66.56	

By now, the subsystem size and power conditioning are optimized to the nominal working point of the fuel cell stack. In brief, it is called the on-design performance optimization of the TEG subsystem [4]. Then, on the whole operational range of the fuel cell stack, the off-design characteristics of the three optimized subsystem configurations listed above are analyzed and compared.

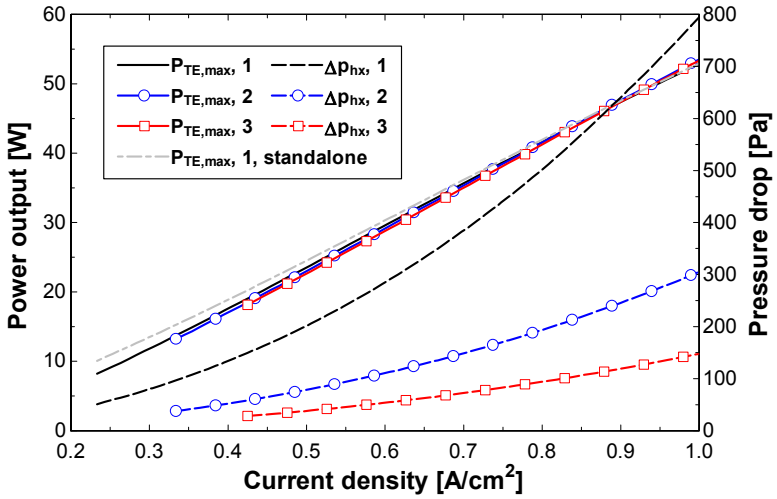

Fig. 8 - The off-design performances of the 3 configurations in Table 2.

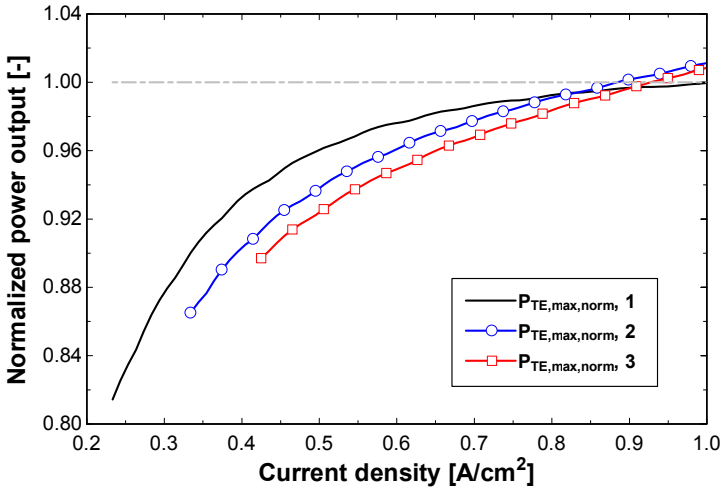

Fig. 9 - The normalized off-design power output of the 3 configurations in Table 2.

The subsystem power output and pressure drop under the three configurations are plotted in Fig. 8. Fig. 9 gives the normalized power output by the subsystem power output under the same size as configuration No. 1 but electrically in standalone mode. It can be concluded that configuration No. 1 almost dominates the whole operational range, referring to the subsystem power output. Only in the niche high current density region, it has around 1% lower power output than the other two configurations. However, the fuel cell stack is not recommended to work continuously in the region above the nominal working point 0.67 A/cm2, since its lifetime will be significantly shortened. It can

also be noticed that configuration No. 1 has a wider efficient Reynolds-number range, which starts from 0.23A/cm2, compared to 0.33 A/cm2 and 0.43 A/cm2 of the other two. In contrast, the subsystem pressure drop under configuration No. 1 is much higher than the other two. However, the differences are negligible for the same reason as analyzed above. In the end, it can be safely concluded that configuration No. 1 is still the final optimal configuration of this TEG subsystem, on the current whole compact heat exchanger library. The configuration is illustrated below in Fig. 10.

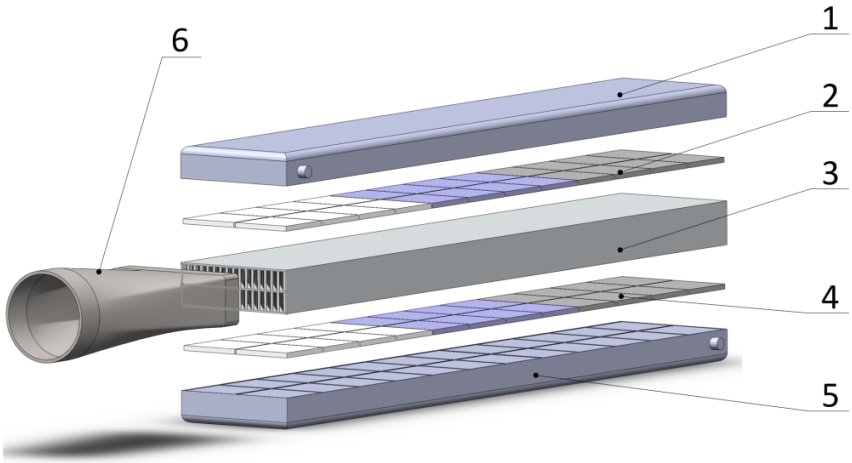

Fig. 10 - The final optimal architecture of the TEG subsystem [4]. (1,5 - Water jackets; 2,4 - TEG module assembly; 3 - Compact heat exchanger housing; 6 - Diffuser).

4. Conclusions

The superior heat exchanger surface for the TEG subsystem in the current entire compact plate-fin heat exchanger library is still 'Pin-fin plate-fin, surface PF-4(F)', after the 900 Pa criterion is unsealed.

The optimal configuration of the TEG subsystem determined by the approach proposed in this work is consistent with the previous studies. This work validates the already published approach and complements the methodology of designing and optimizing a TEG subsystem.

From this work, another approach of selecting the right heat exchanger surface and optimizing the TEG subsystem is as follows:

1) Heat exchanger selection under all possible combinations of n_{cro} and n_{run}. All TEG segments are in standalone mode.

2) Subsystem size and TEG power conditioning optimization: find out the optimum n_{cro}, n_{run} and power conditioning scenario, among all possible combinations of them.

5. Acknowledgements

The authors gratefully acknowledge financial support from Aalborg University and China Scholarship Council. The authors would like to acknowledge the help from Vincenzo Liso.

References

[1] Rowe DM. Thermoelectric generators as alternative sources of low power. Renewable Energy 1994; 5(2):1470-8.

[2] Xin Gao, Min Chen, Søren Juhl Andreasen, Søren Knudsen Kær. Potential Usage of Thermoelectric Devices in a High-Temperature Polymer Electrolyte Membrane (PEM) Fuel Cell System: Two Case Studies. Journal of Electronic Materials 2012; 41(6): 1838-1844.

[3] Xin Gao, Søren Juhl Andreasen, Min Chen, Søren Knudsen Kær. Numerical model of a thermoelectric generator with compact plate-fin heat exchanger for high temperature PEM fuel cell exhaust heat recovery. International journal of Hydrogen Energy 2012; 37: 8490-8498.

[4] Xin Gao, Søren Juhl Andreasen, Søren Knudsen Kær, Lasse Aistrup Rosendahl. Optimization of a thermoelectric generator subsystem for high temperature PEM fuel cell exhaust heat recovery. International Journal of Hydrogen Energy 2014. In press; DOI: 10.1016/j.ijhydene.2014.01.193.

[5] Xin Gao, Min Chen, G. Jeffrey Snyder, Søren Juhl Andreasen & Søren Knudsen Kær. Thermal Management Optimization of a Thermoelectric-Integrated Methanol Evaporator Using a Compact CFD Modeling Approach. DOI: 10.1007/s11664-013-2514-2.

[6] Kays WM, London AL. Compact heat exchangers. 3rd ed. New York: McGraw Hill; 1984.

[7] Kolb G. Fuel processing: for fuel cells. Weinheim, Germany: Wiley-VCH; 2008.

[8] Serenus 166/390 AirC Datasheet. http://www.serenergy.com/Downloads.htm. [Accessed: 22-Oct-2012].

[9] Alexandros Arsalis, Mads Pagh Nielsen, and Søren Knudsen Kær, Energy 36, 993 (2011).

Paper 5

Thermal Management Optimization of a Thermoelectric-Integrated Methanol Evaporator Using a Compact CFD Modeling Approach

Gao, Xin; Chen, Min; Snyder, G. Jeffrey; Andreasen, Søren Juhl; Kær, Søren Knudsen

Journal of Electronic Materials, 42(7), 2013, p. 2035-2042.